THE
PHYSICAL REVIEW

A journal of experimental and theoretical physics established by E. L. Nichols in 1893

SECOND SERIES, VOL. 72, No. 1 JULY 1, 1947

On the Production of Mesotrons by Nuclear Bombardment

W. G. McMILLAN† AND E. TELLER
University of Chicago, Chicago, Illinois
(Received March 27, 1947)

Mesotron production by nuclear bombardment with fast, heavy particles has been investigated theoretically in a semi-quantitative way to determine the expected threshold energies, the cross sections, and their energy dependence. Whereas a treatment in which the target nucleons are assumed to be at rest predicts a requisite incident energy of ~210 Mev, the present treatment, based on the Fermi degenerate gas model, finds the threshold incident energy as ~95 Mev. The threshold is somewhat higher for positive than for negative mesotrons. The cross section for single mesotron production, evaluated from the accessible volume in momentum space, is found to vary with the fractional excess energy, ϵ, as $\epsilon^{2.5}$ in the scalar or axial-vector theories; at low values of ϵ, a small difference in the energy dependence for negative and positive mesotrons arises from the necessity of giving the former a non-zero initial kinetic energy. For the pseudo-scalar and the polar-vector theories, the matrix element for mesotron emission is proportional to the momentum of the mesotron. This changes the power law to $\epsilon^{4.5}$.

INTRODUCTION

IN treatments of collisions between nuclei and high energy incident particles, it is often assumed as a first approximation that the constituent nucleons of the target nucleus may be considered as essentially free. For the case in which the desired result of the collision is the production of a mesotron (having rest-mass μ), the energy of the incident particle relative to the particular nucleon with which it collides must be at least μc^2. If the nucleon has only the small velocity of the nucleus as a whole, nearly all the relative energy must be supplied by the incident particle; in the limit of zero-nucleon velocity this predicts for an incident proton or neutron a requisite energy just twice the rest-mass of the mesotron,[1] or about 210 Mev.

A more refined calculation should take account of a possible contribution of the target-nucleon velocity to the relative energy, of any change in potential energy for the over-all process, and possibly also the effect of the inter-nucleonic forces. At least the first two of these refinements may be made rather easily. We shall use as our nuclear model the usual[2] degenerate Fermi gas mixture of protons and neutrons at zero temperature. Such a model is admittedly very crude, but will serve to determine orders of magnitude.

The limiting energy—the so-called "Fermi energy," E_F—of the degenerate gas sets an approximate upper limit, p_F, to the permissible momenta of the target nucleons. Using this maximum momentum, directed anti-parallel to the path of the incident particle, it is readily seen that a lowering of the required incident energy is obtained. Furthermore, if the incident particle is captured without ejection of other nucleons its binding energy is released. However, since all the lowest states within the degenerate gas are filled

† Guggenheim Fellow, 1946–1947.

[1] We shall employ the value $\mu = 202$ electron masses ($\equiv 103$ Mev), as recently determined by W. B. Fretter, Phys. Rev. 70, 625 (1946); see also D. J. Hughes, Phys. Rev. 71, 387 (1947).

[2] H. A. Bethe, Rev. Mod. Phys. 9, 82 (1937), ¶53A.

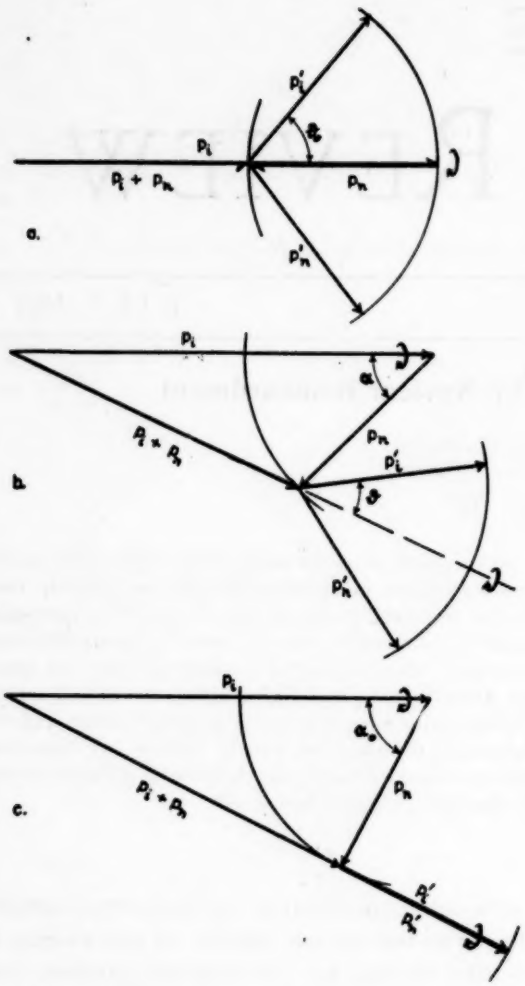

FIG. 1. Possible arrangements of the momentum vectors at the threshold energy with zero-mesotron velocity: (a) and (c) are the two extrema, (b) an intermediate case. Subscripts i and n refer to the incident particle and the nucleon, respectively; primes refer to post-collision conditions. The short curved arrows indicate rotations which leave the total energy unchanged. Here $p_n = p_n' = p_i' = p_F$, the radius of the Fermi sphere.

initially, both colliding particles must end in states of energy equal to, or greater than the Fermi energy. The program, then, will be: (1) to determine the minimum energy, E_{i0}, of the incident particle necessary to produce a mesotron; (2) to calculate from the accessible volumes in phase space the dependence of the cross section, σ, for mesotron production on the excess incident energy, ϵE_{i0}, above the threshold energy, E_{i0}; and (3), to fix the coefficient of the expression so obtained by considering collisions at energies much greater than E_{i0}.

DETERMINATION OF THE THRESHOLD ENERGY

In evaluating the minimum incident energy required to produce a single mesotron, it is necessary to consider the effect of the charge in some detail. When one compares the energy of the nucleus-mesotron couple at infinite separation (i.e., at the zero of potential energy) with that corresponding to a point in the nucleus, it is evident that for a *negative* mesotron to be observable it must be provided initially with at least the kinetic energy equivalent to the electrostatic potential energy, $-eV_0$, at the position of creation. The minimum observable end state is one in which the mesotron is at rest at infinity, and its corresponding relativistic energy is thus μc^2. On the other hand, a *neutral* mesotron retains any initial kinetic energy it may have had as well as its rest energy μc^2, while a *positive* mesotron at infinite distance has, in addition, the kinetic energy gained in being expelled from the nucleus.

Aside from these effects of the electrostatic potential, a natural permissible lower limit on the initial kinetic energy of the mesotron would seem to be set by the requirement that it have sufficient velocity to traverse a distance of the order of the nuclear radius within a "nuclear period," i.e., in $\sim 10^{-22}$ second. Depending upon the depth within the nucleus at which the creation occurs, the initial kinetic energy might have to be ~ 10 Mev for heavy nuclei. However, since there is no apparent reason why mesotrons should only be produced deep in the nucleus, the minimum initial kinetic energy may well be much less than this figure, especially for the lighter elements, and this factor will be neglected in the subsequent treatment. We will therefore assume[3] that the smallest total energy (including the rest energy) which may be given a negative or neutral

[3] At this point one might inquire as to the "binding energy" of the mesotron to the nucleon and its surrounding mesotron field, i.e., over and above its rest mass and the electrostatic effects. The essential question concerns the existence of a "mesotronic potential" analogous to the electrostatic potential. If such exists, either a potential barrier must be overcome, or the required initial kinetic energy of the mesotron will be raised, depending upon whether the force is a repulsion or an attraction. For lack of sufficient knowledge of this force we only mention the possibility, and hereafter neglect it. However, because of its necessarily short-range character and the comparatively long wave-length of the created mesotron, such a "mesotronic potential barrier" might well have a much smaller effect than would at first be supposed.

mesotron is μc^2, whereas the positive mesotron requires μc^2+eV_c. However, because of the tunnel effect[4] and the fact that the term eV_c is large ($\approx$15 Mev) only for the heavy elements, the effective difference in the threshold energies will generally be small.

Having decided on the minimum mesotron energies, a knowledge of the maximum energies of the target nucleons would permit the calculation of the necessary incident energy. The Fermi energy of the degenerate gas is given by the equation

$$E_F=[(\pi\hbar)^2/2M](3N/\pi v)^{\frac{1}{3}}, \tag{1}$$

where N is the number of neutrons or of protons, each of mass M, in the nuclear volume v. As an example, we consider the uranium nucleus and use for its radius the value $1.0\cdot10^{-12}$ cm. We find for the neutron and proton gases, respectively,

$$E_{FN}=22.3 \text{ Mev}; \quad E_{FP}=16.4 \text{ Mev}. \tag{2}$$

For a case in which the mesotron may have zero initial kinetic energy, Figs. 1a, c show in cross section the two extremes of the possible orientations of the four momentum vectors representing the two colliding particles before and after collision. All intermediate values of $\theta(0\leq\theta\leq\theta_0)$ and the associated values of $\alpha(0\leq\alpha\leq\alpha_0)$, such as the case shown in Fig. 1b, correspond to the same total energy, the difference being in the relative energy only. Besides these limited variations of θ (and α), the curved arrows indicate other (unrestricted) rotations which do not alter the total energy. These will be of importance in the next section in evaluating the accessible volume in phase space.

For the general collision process (in which the mesotron is given an initial momentum) the energy-conservation law reads

$$\frac{p_i^2+p_n^2}{2M}=\mu c^2+V+\frac{p_i'^2+p_n'^2}{2M}+\frac{p_\mu'^2}{2\mu}+zeV_c, \tag{3}$$

where $-(E_F+V)$ is the binding energy of the incident particle; subscripts i and n refer to the incident and nucleon particles, respectively, μ refers to the mesotron, and primes denote the post-collision state. In the last term V_c is the electrostatic potential at the point where the mesotron is born, and ze is the charge of the mesotron. If we neglect for the moment the last two terms on the right-hand side of Eq. (3), and recall that on the basis of the assumed nuclear model

$$p_n^2\leq 2ME_F\begin{cases}\leq p_i'^2\\ \leq p_n'^2,\end{cases} \tag{4}$$

evidently

$$p_i^2/2M\geq\mu c^2+V+E_F. \tag{5}$$

This expression means that the incident energy $p_i^2/2M$ must be greater than, or equal to the rest energy of the mesotron minus the binding energy of the incident particle. However, we are permitted to use the equality only if momentum can be conserved, which in turn implies the possibility of a construction as in Fig. 1. From part b of this figure we obtain the relation[5]

$$(2p_F\cos\theta)^2=(\mathbf{p}_i+\mathbf{p}_n)^2$$
$$=p_i^2+p_F^2-2p_ip_F\cos\alpha. \tag{6}$$

The desired construction will therefore be possible if there exist values of α for which $\cos\theta$, calculated from Eq. (6), is not greater than unity. Since $\cos\theta$ has its minimum value for $\alpha=0$, we require that

$$\cos\theta=(p_i-p_F)/2p_F\leq 1,$$

or

$$p_i=3p_F. \tag{7}$$

Using this result in Eq. (5), we see that momentum conservation will be possible provided that

$$E_F\geq(\mu c^2+V)/8. \tag{8}$$

Since $V\approx-25$ Mev, values of $E_F\approx10$ Mev will permit the momentum conservation corresponding to the minimal energy of Eq. (5). With a binding energy of 8 Mev we get from Eq. (5) 95 Mev for the threshold energy. For positive mesotrons the effective threshold is a few Mev higher. This result is radically different from the estimate of 210 Mev mentioned in the introduction.

THE ENERGY DEPENDENCE OF σ

When the minimal incident energy, E_{i0}, is exceeded, we have some latitude of choice in the magnitudes of the initial and final nucleon momenta and the mesotron momentum, as well as in their directions (cf. the discussion of Fig. 1

[4] There will, of course, be a finite probability for the positive mesotron to penetrate the Coulomb potential barrier when its energy lies between μc^2 and μc^2+eV_c.

[5] Vector quantities are symbolized in **bold-face** type; their absolute magnitudes by the same letters in *italics*.

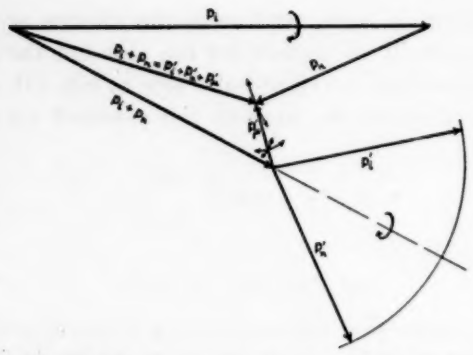

FIG. 2. A possible arrangement of the momentum vectors at the threshold energy for the case in which the minimal mesotron momentum p_μ' is not zero. Other symbols are the same as in Fig. 1. (*Note added in proof:* the vector colinear with the dashed line should be labeled $p_i'+p_n'$.)

above). In order to determine the dependence of the mesotron-production cross section σ on the fractional excess energy ϵ, we shall investigate the total volume in momentum space which corresponds to a successful collision. In this we should allow for the possibility that the minimum mesotron momentum is not zero; such a case is illustrated in Fig. 2. Starting from such an initial orientation of the momentum vectors appropriate to the minimal energy, and denoting increment vectors away from this orientation by π's with corresponding subscripts, we obtain

$$\epsilon E_{i0}=\left(\frac{\mathbf{p}_i'\cdot\boldsymbol{\pi}_i'}{M}\right)+\left(\frac{\mathbf{p}_n'\cdot\boldsymbol{\pi}_n'}{M}\right)+\left(\frac{\mathbf{p}_\mu'\cdot\boldsymbol{\pi}_\mu'}{\mu}\right)+\left(-\frac{\mathbf{p}_n\cdot\boldsymbol{\pi}_n}{M}-\frac{\pi_n^2}{2M}\right)+\left(\frac{\pi_i'^2}{2M}\right)+\left(\frac{\pi_n'^2}{2M}\right)+\left(\frac{\pi_\mu'^2}{2\mu}\right), \quad (9)$$

in which the (minimal) mesotron momentum $\mathbf{p}_\mu'$, and its increment $\boldsymbol{\pi}_\mu'$, are determined by momentum conservation:

$$\mathbf{p}_\mu'=\mathbf{p}_i+\mathbf{p}_n-\mathbf{p}_i'-\mathbf{p}_n', \quad (10a)$$

$$\boldsymbol{\pi}_\mu'=\boldsymbol{\pi}_i+\boldsymbol{\pi}_n-\boldsymbol{\pi}_i'-\boldsymbol{\pi}_n'. \quad (10b)$$

Each term in parentheses in Eq. (9) is intrinsically positive, as may be easily demonstrated with the help of Eq. (4) and the additional restriction that $|\mathbf{p}_\mu'+\boldsymbol{\pi}_\mu'|\geq p_\mu'$.

Since $\boldsymbol{\pi}_i$ is set by the initial conditions, Eq. (10b) gives three relations between the twelve components of $\boldsymbol{\pi}_i'$, $\boldsymbol{\pi}_n'$, $\boldsymbol{\pi}_n$, and $\boldsymbol{\pi}_\mu'$. From the remaining nine independent variables we eliminate from consideration those whose range is not appreciably altered by the excess energy. Such variations in momenta give rise to a practically constant factor in the volume of momentum space, and do not affect the energy dependence of the cross section. One such degree of freedom is the rotation of $\mathbf{p}_i'$ and $\mathbf{p}_n'$ about the dashed line, as indicated in Figs. 1b and 2; other possibilities are indicated by the curved arrows.

For simplicity we take first the case in which $p_\mu'=0$. We should consider only such variations of the π's for which

$$\mathbf{p}_n\times\boldsymbol{\pi}_n=0, \quad (11a)$$

and

$$(\mathbf{p}_i'\times\mathbf{p}_n')\cdot(\boldsymbol{\pi}_i'-\boldsymbol{\pi}_n')=0. \quad (11b)$$

Of the nine independent variables these relations eliminate three. One of the six remaining variables is evidently to be chosen parallel to $\mathbf{p}_n$, and by Eq. (9) will be of the order ϵ. Of the six coordinates of $\boldsymbol{\pi}_i'$ and $\boldsymbol{\pi}_n'$, Eq. (11b) eliminates only the one corresponding to a pure rotation. We are, therefore, left with three degrees of freedom in directions perpendicular to $\mathbf{p}_n'$ and $\mathbf{p}_i'$, and two parallel. By Eq. (9) the maximum value of each perpendicular component is of the order $\epsilon^{\frac{1}{2}}$, and of each parallel component, of order ϵ. These conditions do not violate momentum conservation since the largest mesotron momentum is of the order $\epsilon^{\frac{1}{2}}$, the same as the largest nucleon-momentum increment. The volume in momentum space corresponding to a successful collision for all energies below $(1+\epsilon)E_{i0}$ is thus proportional to the $1+3\cdot\frac{1}{2}+2=4.5$ power of ϵ. Differentiating with respect to ϵ, the volume per unit energy range, and therefore the cross section for the process, is proportional to $\epsilon^{3.5}$. This is the expected energy dependence for positive and neutral mesotrons.

For the case in which $p_\mu'\neq 0$, the additional condition

$$\mathbf{p}_\mu'\times\boldsymbol{\pi}_\mu'=0 \quad (11c)$$

restricts the vector $\mathbf{p}_\mu'+\boldsymbol{\pi}_\mu'$ to a spherical shell of thickness $\sim\epsilon$. An argument similar to that above now finds the total volume in momentum space proportional to ϵ^4, and the volume per unit-energy-interval proportional to ϵ^3. This is the case for negative mesotrons.[6]

[6] It is to be noted, however, that this result holds only as long as $\pi_\mu'\ll p_\mu'$. Since this condition will be violated

MULTIPLE MESOTRON PRODUCTION

For multiple production, the minimal requisite incident energy is approximately proportional to the number n of mesotrons produced. If the condition analogous to Eq. (8), namely,

$$E_F \geq (n\mu c^2 + V)/8, \tag{8'}$$

is satisfied, a generalization of Eq. (5) gives for the threshold energy

$$E_{i0} = (s+t)\mu c^2 + (V + E_F) + teV_c, \tag{12a}$$

where s is the number of negative plus neutral mesotrons, and t is the number of positive mesotrons produced. If Eq. (8') does not hold, E_{i0} is to be determined from the condition for conservation of the *relative* energy:

$$\tfrac{1}{2}(E_{i0}^{\frac{1}{2}} + E_F^{\frac{1}{2}})^2 = (s+t)\mu c^2 + V + teV_c. \tag{12b}$$

Comparison of the values of E_F obtained from Eq. (8') with the actual values of Eq. (2), shows that Eq. (12b) must be used for $n = s+t > 2$. The case $n=2$ is borderline, so neither (12a) nor (12b) applies exactly; the threshold by either equation, however, is not far from 200 Mev. The energy dependence of the production cross section for n mesotrons (in case $n>2$) is found to be $\epsilon^{(3n+5)/2}$. For $n=2$ the ambiguity as to whether (12a) or (12b) applies leads to a power law between ϵ^5 and $\epsilon^{5.5}$, with the threshold $\sim$200 Mev. This is mentioned since recent considerations[7-9] suggest that the creation of a *single* charged mesotron may be forbidden.

So far we have dealt only with the energy dependence of the density of energy states in phase space, and have calculated the cross sections with the tacit assumption that the square of the matrix element between initial and final states (i.e., before and after collision) is independent of the momentum of the mesotron. Such an assumption is justified only in the case of the scalar and axial-vector theories of mesotron forces.[10] However, in order to explain the existence of a nuclear quadrupole moment, it has been necessary in the mesotron theory to introduce the first derivative of the mesotron field into the interaction terms (pseudo-scalar and polar-vector theories). When the initial mesotron kinetic energy is zero, the matrix element is proportional to $\epsilon^{\frac{1}{2}}$, and thus for each mesotron produced an additional factor of ϵ is introduced into the expression for the cross section.

THE ABSOLUTE MAGNITUDE OF σ

We may carry the discussion one step further and determine the order of magnitude of the absolute cross sections for mesotron production. For high energies the above restrictions on the accessible volume of momentum space are less important, and at $\epsilon=1$ can be considered to be absent.[11] At this energy ($E_i \sim 200$ Mev for single mesotron production), the energy E relative to an *average* target nucleon is about 100 Mev; the corresponding wave-length, $\lambda = \hbar/(2mE)^{\frac{1}{2}} \approx 0.45 \cdot 10^{-13}$ cm, is evidently smaller than the range of nuclear forces, $\hbar/\mu c = 2 \cdot 10^{-13}$. This fact justifies a consideration of the collision in terms of a particle picture.

For two nucleons to interact strongly the distance of closest approach must, of course, be less than the range of nuclear forces. A closer collision is actually necessary for the following reason. In order to produce a "quantum" of rest-mass μ, the relative frequency ω of the two particles during collision must be equivalent to at least an energy μc^2; thus for $E = \mu c^2$,

$$\omega \geq E/\hbar. \tag{13}$$

With the collision parameter b (the distance of closest approach) the predominant angular frequency will be of the order of u/b, where u is the relative velocity. This gives

$$u/b \geq E/\hbar, \quad \text{or} \quad b \leq \hbar u/E = 2\hbar/p = 2\lambda, \tag{14}$$

and there will be a high enough frequency only if the collision parameter is less than twice the relative wave-length λ. The corresponding creation cross section, σ, for a single nucleon is therefore

$$\sigma = \pi b^2 = 4\pi\lambda^2 = 4\pi\hbar^2/2mE.$$

even at relatively low values of $\epsilon(\sim 0.1)$, the cross section for negative mesotrons will have essentially the same energy dependence as that given for positive mesotrons. Other approximations vitiate these results very near the threshold, and it is thus questionable if the indicated behavior difference caused by the charge would be experimentally significant.

[7] J. A. Wheeler, Phys. Rev. **71**, 462 A (1947).

[8] E. Fermi, E. Teller, and V. Weisskopf, Phys. Rev. **71**, 314 (1947).

[9] M. Conversi, E. Pancini, and O. Piccioni, Phys. Rev. **71**, 209 (1947).

[10] W. Pauli, *Meson Theory* (Interscience Publishers, Inc., New York, 1946), Chap. 1.

[11] The fact that the mesotron has only one-tenth the mass of a nucleon has the consequence that at $\epsilon=1$ the restrictions have not yet vanished completely. Thus the cross sections to be given for $\epsilon=1$ are somewhat overestimated.

With $E\sim 100$ Mev we find $\sigma=0.025$ barn per nucleon; this sets an approximate upper limit on the cross section.

Since the *scattering* of neutrons by protons presumably corresponds to the emission and reabsorption of a mesotron, one would not expect the cross section for mesotron production to be of an order of magnitude lower than that for scattering. Estimates of the scattering cross section at these energies give a result comparable with the value of σ obtained above. The total cross section for an intermediate element of mass number A will thus be simply 0.025A barn. For the heavier elements this may give a figure larger than the geometrical area of the nucleus, and correspondingly must be corrected downwards.

For the sake of definiteness, the total cross section for the creation of a single mesotron (in the pseudo-scalar or polar-vector theories) will be given approximately by

$$\Sigma\sim 0.025A\epsilon^{4.5}\text{ barn}, \tag{15a}$$

with

$$\epsilon\approx(E_i-100)/100, \tag{15b}$$

while that for mesotron pair creation (again in the pseudo-scalar theory) is

$$\Sigma\sim 0.025A\epsilon^{7.5}, \tag{16a}$$

with

$$\epsilon\approx(E_i-200)/200. \tag{16b}$$

CONCLUDING REMARKS

In determining the probable relation of the estimates given above to the true cross sections, we distinguish between two different types of errors: (1) those which are introduced through the approximate character of the assumed nuclear model and of the calculations employed; and (2) those which enter through failure to take account of all relevant factors in the domain of nuclear forces, as was for example suggested in reference 3. This second category merely reflects the lack of conclusive knowledge concerning nuclear forces, and it is impossible at this stage to estimate the over-all effect of these errors.

In the first group, the nature and magnitudes of the approximations are more evident. The assumption of a continuum of energy levels at all energies above the threshold leads to a dependence on a higher power of ϵ than would have been obtained at low energies by using the correct, discrete spectrum. This means that the cross sections obtained from Eqs. (15) and (16) have been decreased (from their values at $\epsilon=1$) by too high a power of ϵ, and are therefore underestimated. Furthermore, the fluctuations in the target-nucleon momenta, whose terminae nominally lie in the surface of the Fermi sphere, cause the volume in momentum space to be underestimated for small ϵ, again indicating that the cross sections given above are, if anything, too low.

Other complications, possibly having opposite effects, would enter if, for example, there were an unfavorable radial distribution of energy among the nucleons such that fast internal particles were shielded by slower external ones. However, with such high energies the incident particle will be only slightly deflected in scattering collisions and the corresponding energy loss will be small. Even with the generous estimate of several Mev per scattering process, the effect on the mesotron-production cross section would not be very noticeable when the incident energy is, say, 20 Mev above the threshold. The assumption that at $\epsilon=1$ no restrictions apply to the momentum volume also gives rise to an overestimate of σ. As mentioned in reference 11, the small mass of the mesotron is likely to cause some restrictions in the region of $\epsilon=1$.

When these approximations are considered, it seems a reasonable estimate that at $\epsilon=0.1$ the probable error of the cross sections given above is of the order of magnitude of a factor 10, although an unfavorable accumulation of errors might raise this figure.[12] It should be borne in mind, however, that this does not include those inaccuracies which may be introduced through ignorance of the correct form of the interaction to be used in the mesotron field, and of the selection rules which specify the number and kind of mesotrons which can be produced.

ACKNOWLEDGMENT

One of the authors (W. G. M.) wishes to thank the John Simon Guggenheim Memorial Foundation which made this investigation possible.

[12] *Note added in proof:* Messrs. W. Horning and M. Weinstein have kindly communicated to us their manuscript on "Meson materialization," to appear in the *Physical Review*, in which they confirm our result for the energy dependence of the cross section for single mesotron production (for the scalar theory) but obtain a significantly lower value for the coefficient.

On the Division of Nuclear Charge in Fission*

R. D. PRESENT
University of Tennessee, Knoxville, Tennessee
(Received February 3, 1947)

The theory of the most probable charge number of a fission fragment of given mass number is examined. Two hypotheses previously suggested are (1) that the charges divide in the same ratio as the masses and (2) that the most probable charges correspond to minimum energy of two droplets in contact. These hypotheses predict results at variance with each other and with preliminary experiments. In this paper the actual division of charge is calculated for the final configuration of spheres in contact on the basis of a general nuclear model in which the charge distribution in the nucleus is non-uniform. The tendency of the protons to spread outward results in the smaller fragment of an asymmetric fission having a greater proton-neutron ratio than the larger fragment. In the most probable division (mass ratio 2:3) the most probable partners (of odd mass number) should both have chain lengths equal to 3.6. In the case of a 1:2 mass ratio, the probable chain lengths of the light and heavy partners should be 2.5 and 4.1, respectively. Data on the independent fractional yields of particular chain members are found to lie near a smooth (error) curve when plotted with the aid of the theoretical results.

1. INTRODUCTION

THE division of nuclear charge in fission depends on the extent to which the proton and neutron densities and spatial distributions are altered during the fission process.

Feenberg[1] and Wigner[2] independently have studied the effect of electrostatic repulsion of the protons on the nuclear particle density for normal nuclei. The tendency of the protons to spread outward is accompanied by a tendency of the neutrons to follow the protons because of the exclusion principle and well-known properties of nuclear forces. Whether the neutron density at the surface of the nucleus is greater or less than at the center depends on the compressibility of nuclear matter. Wigner has made the "liquid-drop" assumption of incompressibility or uniform total density, and in the case of uranium his method gives the result that the proton-neutron ratio at the surface exceeds the same ratio at the center by 36 percent. Feenberg obtains a lower result (21 percent for uranium) by a more elaborate calculation in which the nuclear compressibility is taken explicitly into account. While in the former method the proton density is 21 percent larger at the surface than at the center, the latter method gives a 49 percent increase in proton density accompanied by a 23 percent increase in neutron density in going to the surface. The associated corrections to the binding energy are small, and the corrections to the nuclear radius are negligible. So far there has appeared to be no way in which to verify the existence of these effects. It is suggested here that there must be a small but possibly observable effect on the nuclear charge distribution of the primary fission fragments and the most probable number of β-decays of a fragment of given mass number.

If the proton density were uniform throughout the nucleus, the charges of the fragments would be in the same ratio as the masses. However, if the proton density is greater at the surface, the smaller fragment of an asymmetric fission must have a greater proton-neutron ratio than the larger fragment. This effect is enhanced in the Wigner model by the decrease in neutron density from center to surface. On the Feenberg model where the neutron density varies in the opposite fashion, the effect is a differential one caused by the proton density varying more steeply than the neutron density. Since the effect depends on the relative shift of the proton spatial distribution with respect to the neutron distribution, the method of Wigner will give somewhat larger results.

A rough estimate of the size of the effect can be made as follows: The critical shape of a dividing uranium nucleus, corresponding to the saddle

* This document is based on work performed under Contract No. W-35-058-eng-71 for the Manhattan Project, and the information covered therein will appear in Division IV of the MPTS as part of the contribution of the Clinton Laboratories. References 8 and 11 are to Plutonium Project Reports.

[1] E. Feenberg, Phys. Rev. 59, 593 (1941).

[2] E. Wigner, University of Pennsylvania Bicentennial Conference (1941).

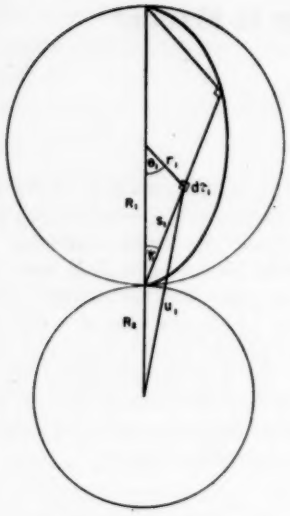

FIG. 1. Diagram of the coordinate system employed.

point of the potential energy *versus* deformation parameter hypersurface, is not very different from a prolate spheroid of eccentricity $\sqrt{3}/2$ with a slight flattening at the equator preliminary to "pinching-in."[3] We assume that the proton and neutron densities vary only with the distance from the center, and use a parabolic fit to the radial dependence of the density computed by Feenberg, the total charge being normalized to that of the undeformed nucleus. The spheroid is sliced into two unequal parts, and the charge on each fragment computed. The calculation is an elementary one and, in view of the more precise calculation to be described in the next section, no details will be given here. The results can be expressed in terms of the charge numbers, Z_1 and Z_2, of the light and heavy fragments and their mass numbers, A_1 and A_2, before neutron emission. Setting γ equal to $[Z_1/(Z_1+Z_2)]/[A_1/(A_1+A_2)]$, one finds that for a 2:3 ratio of the fragment masses, γ is 1.010, and for a 1:2 division, γ is 1.020. Somewhat larger values are obtained if Wigner's densities are used, γ being 1.014 and 1.023 in the two cases, respectively. These results cannot be very accurate in view of (1) our use of the density variation appropriate to the sphere for the critical spheroid and (2) the further elongation of the drop beyond the critical shape accompanied by a further spreading of charge.

[3] R. D. Present, F. Reines, and J. K. Knipp, Phys. Rev. **70**, 557 (1946).

2. ASSUMPTIONS AND FORMULATION

In this section we calculate the charge distribution in the deformed nucleus just before scission into two unequal fragments. This configuration is approximated by two spheres in contact, and the proton and neutron densities are taken to be functions of the distance from the point of contact and of the angle with the axis of symmetry. The nuclear model is that already described by Wigner.[2] We outline the principal assumptions of the calculation:

(A) The charge redistributes itself rapidly during the deformation time for fission so that the charge density has its equilibrium value for every shape of the dividing drop. This follows if the redistribution of the charge is accomplished via the meson field and requires no redistribution of the heavy particles (nucleons).

(B) The total particle density is assumed to be uniform throughout the volume of the deformed nucleus. This is the liquid-drop assumption of incompressibility of nuclear matter.

(C) The decrease of electrostatic energy when the charge goes to the surface is counterpoised by an increase in the "isotopic spin energy." The isotopic spin energy arises from the exclusion principle and the character of nuclear forces and is represented in the mass defect formula by the term or terms in $N-Z$. (The isotopic spin $T_z=(N-Z)/2$.) The mass defect formula proposed by Weizsäcker and employed by Bethe and Bacher, Bohr and Wheeler, and others, contains a term in $(N-Z)^2$. Wigner[4] has shown that the potential energy of the nucleus computed from the symmetrical Hamiltonian contains a term in $(N-Z)/A$ and has included both linear and quadratic terms in $N-Z$ in his mass defect formula. The presence of the linear term considerably reduces the magnitude of the quadratic term. Wigner's mass defect formula is used in the following.

(D) It is assumed that the isotopic spin energy is a "volume energy," i.e., that it can be expressed as an energy density, depending on the local difference in proton and neutron density, integrated over the volume of the nucleus. The numerical coefficient of this energy density is obtained from the empirical coefficients of the

[4] E. Wigner, Phys. Rev. **51**, 947 (1937).

$(N-Z)$ and $(N-Z)^2$ terms in the mass defect formula. Since these coefficients are approximately independent of nuclear size, it is assumed that the same numerical coefficient can be used for the configuration of spheres in contact as for normal separated nuclei.[5]

Figure 1 shows the coordinate system used. Spherical polar coordinates with origin at the point of tangency and polar axis along the axis of symmetry are denoted by s, ψ, and φ; the same coordinates with origin taken at the center of one of the spheres are denoted by r, θ, and φ. R_1 and R_2 are the radii of the two spheres in contact and R the radius of the original nucleus. The ratio R_1/R is denoted by λ_1; hence $\lambda_1^3+\lambda_2^3=1$. Let $\rho_Z(s,\psi)$ be the proton density, $\rho_N(s,\psi)$ the neutron density, and ρ the uniform total particle density. Z, N, and A represent as usual the total numbers of protons, neutrons and nucleons; and Z_1, N_1, and A_1 refer to the numbers in sphere 1. Since the effects to be calculated depend on the difference in proton and neutron densities, we introduce the "local isotopic spin" $t(s,\psi)$ defined by $t=(\rho_N-\rho_Z)/2\rho$. The average values $\bar{\rho}_Z$, $\bar{\rho}_N$, and $\bar{t}$ are the values appropriate to a uniform charge distribution. We have

$$T_t=A\bar{t}=\rho\iiint_{1+2}t\,d\tau=\rho\iiint t(s_1,\psi_1)d\tau_1+\rho\iiint t(s_2,\psi_2)d\tau_2, \quad (1)$$

whence

$$\iiint_{1+2}(t-\bar{t})d\tau=0. \quad (2)$$

It is necessary to evaluate the change in the electrostatic self-energy of each sphere and in the mutual electrostatic energy of the two in going from uniform to non-uniform charge density. Since the deviation from uniform density is small, second-order terms in $\epsilon=\rho_Z-\bar{\rho}_Z=\rho(\bar{t}-t)$ will be neglected. Then the change in the self-energy of each sphere is given by

$$\Delta E_i^e=\frac{e^2}{2}\iiint\iiint\left\{\frac{\rho_Z(\mathbf{r}_a)\rho_Z(\mathbf{r}_b)-\bar{\rho}_Z^2}{r_{ab}}\right\}d\tau_a d\tau_b \quad i=1,2$$

$$=\frac{e^2}{2}\iiint\iiint\frac{\bar{\rho}_Z\epsilon(\mathbf{r}_a)}{r_{ab}}d\tau_a d\tau_b+\frac{e^2}{2}\iiint\iiint\frac{\bar{\rho}_Z\epsilon(\mathbf{r}_b)}{r_{ab}}d\tau_a d\tau_b$$

$$=e^2\iiint\iiint\frac{\bar{\rho}_Z\epsilon(\mathbf{r}_a)}{r_{ab}}d\tau_a d\tau_b=e\iiint\epsilon(\mathbf{r}_a)V_0(r_a)d\tau_a,$$

where $V_0(\mathbf{r}_a)$ is the potential of a uniform distribution. Hence,

$$\Delta E_i^e=\frac{Z_i^{(0)}e^2\rho}{R_i}\iiint\left\{\frac{3}{2}-\frac{1}{2}\frac{r_i^2}{R_i^2}\right\}\cdot(\bar{t}-t_i)d\tau_i. \quad (3)$$

Similarly, the change in the mutual electrostatic energy is

$$\Delta E_{12}^e=e^2\iiint d\tau_1\iiint d\tau_2\left\{\frac{\rho_Z(\mathbf{r}_1)\rho_Z(\mathbf{r}_2)-\bar{\rho}_Z^2}{r_{12}}\right\}$$

$$=e^2\iiint d\tau_1\iiint d\tau_2\left\{\frac{\bar{\rho}_Z\epsilon(\mathbf{r}_1)+\bar{\rho}_Z\epsilon(\mathbf{r}_2)}{r_{12}}\right\}$$

$$=e\iiint d\tau_1\epsilon(\mathbf{r}_1)V_2^{(0)}(\mathbf{r}_1)+e\iiint d\tau_2\epsilon(\mathbf{r}_2)V_1^{(0)}(\mathbf{r}_2)$$

$$=Z_2^{(0)}e^2\rho\iiint\frac{(\bar{t}-t_1)d\tau_1}{u_1}+Z_1^{(0)}e^2\rho\iiint\frac{(\bar{t}-t_2)d\tau_2}{u_2}, \quad (4)$$

[5] A further assumption is that the kinetic energy correction terms arising from the gradients of proton and neutron densities (Weizsäcker terms) can be neglected. Feenberg has included these terms explicitly. However, the effect

where $V_2^{(0)}(\mathbf{r}_1)$ is the potential at $\mathbf{r}_1$ because of a uniform distribution over sphere 2, and $u_1 = (s_1^2+R_2^2+2R_2 s_1\cos\psi_1)^{\frac{1}{2}}$ is the distance to $\mathbf{r}_1$ from the center of sphere 2.

We next consider the evaluation of the isotopic spin energy from the mass defect formula. The latter involves the partition quantum numbers $(PP'P'')$ of the ground state, where P is equal to the isotopic spin T_f, and P' and P'' are of the order of unity.[2,4,6] Neglecting[7] the terms in P' and P'', the mass defect formula is found to contain two terms depending on the isotopic spin of the form: $c_1(N-Z)/A+c_2(N-Z)^2/A$. These correspond to an energy density g_T given by

$$g_T=\frac{c_1\rho}{A}\cdot\left(\frac{N-Z}{A}\right)+\frac{c_2\rho}{A}\cdot\frac{(N-Z)^2}{A}$$

$$=\frac{c_1\rho}{A}\cdot\frac{\rho_N-\rho_Z}{\rho}+c_2\rho\cdot\left(\frac{\rho_N-\rho_Z}{\rho}\right)^2$$

$$=(2c_1\rho/A)t+4c_2\rho t^2. \qquad (5)$$

The relation (5) is now assumed to hold when g_T and t are functions of position in the deformed nucleus. The difference in isotopic spin energy between the non-uniform and uniform charge distributions is then given by

$$\Delta E_T=\int\!\!\int\!\!\int_{1+2} g_T d\tau-\int\!\!\int\!\!\int_{1+2}\bar{g}_T d\tau$$

$$=(2c_1\rho/A)\int\!\!\int\!\!\int_{1+2}(t-\bar{t})d\tau$$

$$+4c_2\rho\int\!\!\int\!\!\int_{1+2}(t^2-\bar{t}^2)d\tau$$

$$=4c_2\rho\int\!\!\int\!\!\int_{1+2} t(t-\bar{t})d\tau \qquad (6)$$

in view of Eq. (2). The term $c_1(N-Z)/A$ makes no contribution to the energy difference. The indirect effect of this term is very considerable, however, since its omission from the mass-defect formula leads to a larger value for c_2. In the Weizsäcker-Bethe formula which contains no term in $(N-Z)/A$, the coefficient c_2 is approximately 20 Mev. The value of c_2 in Wigner's formula is about 12.5 Mev.

The spatial variation of t throughout the two spheres is determined by minimizing the energy difference ΔE between the non-uniform and uniform charge distributions where

$$\Delta E=\Delta E_T+\Delta E_C$$

$$=\Delta E_T+\Delta E_1{}^C+\Delta E_2{}^C+\Delta E_{12}{}^C. \qquad (7)$$

We develop $t(s,\psi)$ in a power series in s and $\cos\psi$ and, because of the smallness of the effect, use only the first terms. Assuming continuity of the densities and their derivatives at the point of contact of the spheres, one omits linear terms. Hence

$$t_i(s_i,\psi_i)=\bar{t}+\delta-\alpha_i(s_i/R)^2+\beta_i(s_i/R)^2\cos\psi_i,$$

$$i=1,2. \qquad (8)$$

The parameter δ is expressed in terms of α_1, α_2, β_1, and β_2 by means of Eq. (2), and the latter are determined from the minimizing conditions

$$\frac{\partial\Delta E}{\partial\alpha_1}=\frac{\partial\Delta E}{\partial\alpha_2}=\frac{\partial\Delta E}{\partial\beta_1}=\frac{\partial\Delta E}{\partial\beta_2}=0. \qquad (9)$$

The charge number of sphere 1 is altered from $Z_1^{(0)}=Z\lambda_1{}^3$ for uniform density to Z_1 when the density is not uniform. Thus

$$Z_1-Z\lambda_1{}^3=\int\!\!\int\!\!\int_1(\rho_Z-\bar{\rho}_Z)d\tau$$

$$=\rho\int\!\!\int\!\!\int_1(\bar{t}-t_1)d\tau_1 \qquad (10)$$

gives the distribution of charge between the fragments. Equations (1) through (10) suffice for the calculation of $\gamma=[Z_1/(Z_1+Z_2)]/[A_1/(A_1+A_2)]$ for any ratio of fragment sizes (provided that α_i and β_i are not too large).

3. PRELIMINARY ESTIMATE

A preliminary estimate of the size of the effects can be simply obtained by replacing Eqs. (8) and (9) by

$$t_i=\bar{t}+\delta_i,\quad \frac{\partial\Delta E}{\partial\delta_i}=0,\quad i=1,2, \qquad (8'\text{–}9')$$

of these terms is partly taken into account when the isotopic spin energy is taken from the mass defect formula with its empirically determined coefficient. One can regard the Weizsäcker terms as expanded in powers of $(N-Z)/A$ and thus partly included in the other terms when empirical coefficients are used.

[6] E. Feenberg and E. Wigner, "Reports on progress in physics," Phys. Soc. London 8, 274 (1941).

[7] One neglects P', P'^2, and $P'P''$ compared to P^2. In the case of an even-even nucleus $P'=P''=0$ in the ground state.

corresponding to uniform but different charge densities for the two spheres. Equations (2), (3), (4), and (6) reduce to

$$\delta_1\lambda_1^3+\delta_2\lambda_2^3=0, \tag{11}$$

$$\Delta E_i^c=-(8/5)\pi R^2\cdot Ze^2\rho\cdot\delta_i\lambda_i^5, \tag{12}$$

$$\Delta E_{12}^c=-(4/3)\pi R^2\cdot Ze^2\rho\cdot(\delta_1+\delta_2)\cdot[\lambda_1^3\lambda_2^3/(\lambda_1+\lambda_2)], \tag{13}$$

$$\Delta E_T=4c_2\rho\cdot(4/3)\pi R^3\cdot(\delta_1^2\lambda_1^3+\delta_2^2\lambda_2^3). \tag{14}$$

In the case of the uranium and plutonium isotopes the quantity $Ze^2\rho\cdot 4\pi R^2\cdot A^{-1}$ is slightly less than 50 mMU (milli-mass units). The coefficient $4c_2$ is slightly greater than 50 mMU. In the following we take both quantities equal to 50 mMU. Then,

$$\frac{\Delta E}{100A}=\frac{\delta_1^2\lambda_1^3+\delta_2^2\lambda_2^3}{2}-\frac{\delta_1\lambda_1^5+\delta_2\lambda_2^5}{5}-\frac{\delta_1+\delta_2}{6}\cdot\frac{\lambda_1^3\lambda_2^3}{\lambda_1+\lambda_2} \tag{15}$$

which is to be minimized subject to (11). The charges are then computed from

$$Z_1=Z\lambda_1^3-\delta_1\lambda_1^3A, \tag{16}$$

giving the following results:

$$\begin{aligned}\lambda_1^3:\lambda_2^3=2:3 &\qquad \gamma=1.0194\\ =1:2 &\qquad =1.0360\\ =1:3 &\qquad =1.0607\end{aligned} \tag{17}$$

For the 1:2 division of uranium $\Delta E=-1.16$ mMU. This simple calculation gives values of γ slightly larger than those obtained from the more accurate calculation described below.

4. DETAILED ESTIMATE

The detailed estimate of the effect is based on the use of (8) to represent the departure from uniform charge distribution. On substituting (8) into (2), (3), (4), and (6) we find

$$\delta=(3/4\pi R^3)\cdot\{(\alpha_1L_1+\alpha_2L_2)-(\beta_1A_1+\beta_2A_2)\}, \tag{18}$$

$$\Delta E_i^c=(Ze^2\rho/2R^3)\cdot\{-(16/5)\pi\delta\lambda_i^5R^5+3\alpha_iL_i\lambda_i^2-\alpha_iN_iR^{-2}-3\beta_iA_i\lambda_i^2+\beta_iD_iR^{-3}\}, \tag{19}$$

$$\Delta E_{12}^c=Ze^2\rho R^2\cdot\{-(8\pi\delta/3)\cdot[\lambda_1^3\lambda_2^3/(\lambda_1+\lambda_2)]+(\alpha_2\lambda_1^3P_2+\alpha_1\lambda_2^3P_1)R^{-4}-(\beta_2\lambda_1^3Q_2+\beta_1\lambda_2^3Q_1)R^{-4}\}, \tag{20}$$

$$\Delta E_T=-4c_2\rho\delta R^{-2}\cdot\{(\alpha_1L_1+\alpha_2L_2)-(\beta_1A_1+\beta_2A_2)\}+4c_2\rho R^{-4}\cdot\{(\alpha_1^2M_1+\alpha_2^2M_2)-2(\alpha_1\beta_1B_1+\alpha_2\beta_2B_2)+(\beta_1^2C_1+\beta_2^2C_2)\}, \tag{21}$$

where

$$\begin{aligned}
L_1&=\int\int\int s_1^2d\tau_1=2\pi(16/15)R_1^5,\\
M_1&=\int\int\int s_1^4d\tau_1=2\pi(16/7)R_1^7,\\
N_1&=\int\int\int r_1^2s_1^2d\tau_1=2\pi(24/35)R_1^7,\\
A_1&=\int\int\int s_1^2\cos\psi_1d\tau_1=2\pi(32/35)R_1^5,\\
B_1&=\int\int\int s_1^4\cos\psi_1d\tau_1=2\pi(128/63)R_1^7,\\
C_1&=\int\int\int s_1^4\cos^2\psi_1d\tau_1=2\pi(64/35)R_1^7,\\
D_1&=\int\int\int r_1^2s_1^2\cos\psi_1d\tau_1=2\pi(544/3^3\cdot5\cdot7)R_1^7,\\
P_2&=\int\int\int(s_2^2/u_2)d\tau_2=2\pi R_1^4K(\lambda), \qquad P_1=2\pi R_2^4K(\lambda^{-1}),\\
Q_2&=\int\int\int(s_2^2/u_2)\cos\psi_2d\tau_2=2\pi R_1^4W(\lambda), \quad Q_1=2\pi R_2^4W(\lambda^{-1}).
\end{aligned} \tag{22}$$

TABLE I. Calculated numerical values.

$\lambda_1^3:\lambda_2^3$	α_1	α_2	δ	$\gamma-1$	$\Delta E/100A$
2:3	0.0364	0.0187	0.0254	0.0158	−.000127
1:2	0.0465	0.0153	0.0244	0.0290	−.000145
1:3	0.0658	0.0122	0.0225	0.0493	−.000169

The integrals $K(\lambda)$ and $W(\lambda)$ with $\lambda=\lambda_1/\lambda_2$ are given by

$$K(\lambda)=\int_0^{2/\lambda} dyy^4\int_{\lambda y/2}^1 \frac{dx}{(2yx+y^2+1)^{\frac{1}{2}}}$$

$$=4\lambda^{-4}+\frac{32}{5}\lambda^{-5}-\frac{2}{15(1+\lambda)^2}\cdot\left\{\left(\frac{\lambda+2}{\lambda}\right)^3\cdot\left(\frac{6+6\lambda-\lambda^2}{\lambda^2}\right)+1\right\}, \tag{23}$$

$$W(\lambda)=\int_0^{2/\lambda} dyy^4\int_{\lambda y/2}^1 \frac{xdx}{(2yx+y^2+1)^{\frac{1}{2}}}$$

$$=-\frac{32}{9}\lambda^{-6}-\frac{8}{9}\lambda^{-3}+\frac{2(2-\lambda)m^3}{9(1+\lambda)\lambda^3}+\frac{1+(5\lambda/2)}{48(1+\lambda)^{5/2}}\cdot\{2nm^3-nm-\log(n+m)\}, \tag{24}$$

where $m=(\lambda+2)/\lambda$ and $n=2\lambda^{-1}(1+\lambda)^{\frac{1}{2}}$. The evaluated integrals are substituted into (18), (19), (20), and (21) to give

$$\delta=(8/5)(\alpha_1\lambda_1^5+\alpha_2\lambda_2^5)-(48/35)(\beta_1\lambda_1^5+\beta_2\lambda_2^5), \tag{25}$$

$$\Delta E/100A=-\delta^2/2-(\delta/5)(\lambda_1^5+\lambda_2^5)-(\delta/3)(\lambda_1^3\lambda_2^3/\lambda_1+\lambda_2)+(12/7)(\lambda_1^7\alpha_1^2+\lambda_2^7\alpha_2^2)$$
$$+(11/35)(\lambda_1^7\alpha_1+\lambda_2^7\alpha_2)+(1/4)(K(\lambda)\lambda_1^7\alpha_2+K(\lambda^{-1})\lambda_2^7\alpha_1)$$
$$-(64/21)(\lambda_1^7\alpha_1\beta_1+\lambda_2^7\alpha_2\beta_2)+(48/35)(\lambda_1^7\beta_1^2+\lambda_2^7\beta_2^2)-(256/3^3\cdot5\cdot7)(\lambda_1^7\beta_1+\lambda_2^7\beta_2)$$
$$-(1/4)(W(\lambda)\lambda_1^7\beta_2+W(\lambda^{-1})\lambda_2^7\beta_1). \tag{26}$$

Numerical values are inserted in (25) and (26) and the minimizing conditions (9) give four simultaneous equations for α_1, α_2, β_1, and β_2. Since the determinants are close to vanishing, greater accuracy is obtained by solving these equations by the method of elimination. When $\lambda_1^3:\lambda_2^3=1:2$ the minimum energy occurs at: $\alpha_1=0.184$, $\alpha_2=0.099$, $\beta_1=0.140$, $\beta_2=0.085$, $\delta=0.0377$, and $\Delta E=-4.7$ mMU for uranium. The signs of the α's and β's correspond to a charge density increasing with distance s from the point of contact and with increasing angle ψ with the symmetry axis. The charges on the fragments are obtained from (10) and (22) which give

$$Z_1-Z\lambda_1^3=-\rho\delta\cdot(4/3)\pi R_1^3+\rho L_1\alpha_1/R^2-\rho A_1\beta_1/R^2$$
$$=(4/3)\pi R^3\rho\cdot\{-\lambda_1^3\delta+(8/5)\lambda_1^5\alpha_1-(48/35)\lambda_1^5\beta_1\}. \tag{27}$$

When $\lambda_1^3=\frac{1}{3}$ we find from the numbers given above that $\gamma=1.029$. This is to be compared with the value of 1.036 of the preliminary estimate. If the angular variation of charge density is neglected (i.e., if $\beta_1=\beta_2=0$), the results are changed to: $\alpha_1=0.0466$, $\alpha_2=0.0153$, $\delta=0.0244$, $\Delta E=-3.4$ mMU, and $\gamma=1.029$. As would be expected, the angular variation has a negligible effect on the division of charge but leads to an appreciable lowering of the energy. For our present purposes it is sufficiently accurate to omit all terms in β_1 and β_2 from the preceding formulae. Figure 2 is a plot of $(\gamma-1)$ *vs.* λ_1^3 obtained in this way, and Table I gives some of the numerical results.

DISCUSSION OF RESULTS

The theoretical results are represented in Fig. 2 which enables one to calculate the division of nuclear charge between fragments of given sizes. For the range of sizes shown, the higher order terms in α_1 and α_2 are negligible, as has previously been assumed.

The principal sources of uncertainty in these results are (1) the assumption of uniform total particle density and (2) the use of Wigner's mass defect formula with the large term in $(N-Z)/A$. In both respects our calculation gives an upper limit for $(\gamma-1)$. Since no definite knowledge of the compressibility of nuclear matter is at hand, the first assumption is reasonable. However, Feenberg's method, in which a roughly estimated value of the compressibility is used, would give smaller results probably closer to the truth. No definite confirmation of Wigner's term in $(N-Z)/A$ for heavy nuclei is yet at hand. The size of this term relative to the conventional term in $(N-Z)^2/A$ is a consequence of the symmetrical Hamiltonian. If this term should prove to be small or absent (as in the Weizsäcker-Bethe formula) the value of $(\gamma-1)$ would be considerably reduced. It is possible but unlikely that the calculated values of $(\gamma-1)$ are too large by as much as 50 percent.

Figure 2 enables one to predict the most probable initial charge of a fission fragment of given mass. We distinguish the primary fission fragment nucleus of mass number A_i from the fission product nucleus of mass number A_i' where $A_i'=A_i-1$. Experimental measurements deal with the product nucleus formed from the fragment nucleus by neutron emission. Since the fraction of fragment nuclei emitting more than one neutron apiece is small, this possibility will be neglected. Figure 3 represents the charge number Z_i of the fragment or of the product nucleus plotted against the mass number A_i' of the product nucleus. The charge numbers $Z_i^{(0)}$ following from the hypothesis of uniform charge distribution $(\gamma=1)$ are shown for comparison. In a very asymmetric division the Z_i and $Z_i^{(0)}$ curves differ by as much as one charge number, the smaller fragment having a higher, and the larger a lower, charge than would be expected if the charges divided in the same ratio as the masses. Still greater differences would be obtained for divisions more asymmetric than those shown in Fig. 3. The dots in Fig. 3 represent stable isotopes of odd mass number. A fairly well defined curve can be drawn through these points; such a curve would be nearly identical with a plot of Z_A *vs.* A in the notation of Bohr and Wheeler. The periodicities of the dots or of the Z_A curve are of course not reflected in the theoretical curve for Z_i (the finer details of nuclear binding represented by the terms in the Hamiltonian which depend on the partition quantum numbers P' and P'' have been neglected). Because of this and also because the theoretical curve gives fractional rather than integral charge numbers, no exact predictions for particular isotopes can be made. Nevertheless, some predictions are possible concerning the average behavior of the number ν of β-decays of a fragment of given mass and most probable charge for that mass. Fragments of the same mass but different charge are formed independently in the fission process, and their yield as primary fission products can be measured in a few instances. It is thus possible to estimate ν for several neighboring odd masses and

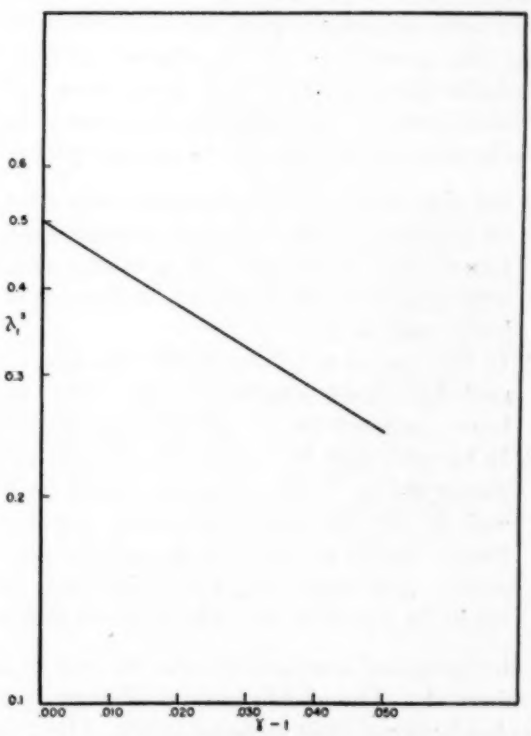

FIG. 2. Calculated curve of $(\gamma-1)$ *vs.* λ_1^3.

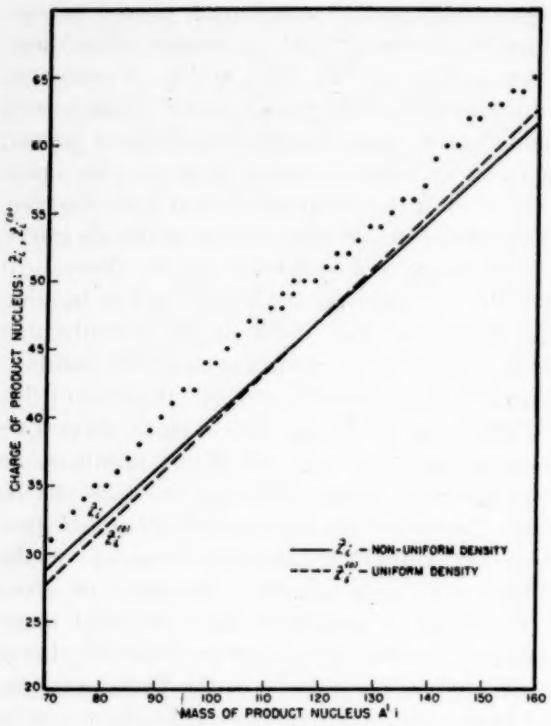

FIG. 3. Charge *vs.* mass of the product nuclei.

compare the result with Fig. 3 where ν is the mean vertical distance from the Z_i curve to the dots. The quantity ν will be referred to as the "probable chain length" for a given mass ratio of the fragments. The following conclusions can then be drawn from the theoretical curve for Z_i:

(1) For that mass ratio which occurs with greatest frequency in slow neutron uranium fission (about 2:3 or 93:141) the probable chain lengths of the complementary fragments are both equal to 3.6.
(2) In the case of a 1:2 or 78:156 division, the probable chain lengths for the light and heavy partners are 2.5 and 4.1, respectively.
(3) In the case of a 1:3 or 58:176 division (not shown in Fig. 3), the values of ν would be 2.4 and 3.5 for the light and heavy partners. Decay chains for such an extremely asymmetric split have not been observed but might be found in very fast neutron fission.

The foregoing conclusions refer to odd mass numbers A_i'. The stable isobars of even mass number have not been included in Fig. 3 because the dots would scatter so widely that the probable chain length ν would undergo large fluctuations from one mass number to the next. The probable chain lengths for the even mass numbers are on the average appreciably smaller than for the odd mass numbers, since the even mass dots lie mostly below a curve through the odd mass dots. Data on even masses will be utilized below.

The energy correction ΔE caused by spreading of the charge is small for all observed modes of division (cf. Table I), and the difference between the values of ΔE for symmetric and the most probable (2:3) asymmetric fission is of the order of one Mev. Hence the considerations of this paper make no appreciable change in fission calculations involving the energy of two spheres in contact or a deformed ellipsoidal nucleus.

Wigner and Way[8] have suggested that the charge might divide in such a way that the total decay energy of the two chains would be a minimum. Extending this idea to take into account the electrostatic repulsion of the fragment nuclei, Way[9] has calculated the division of charge by assuming that the most probable division is that in which the energy of the two product nuclei in contact is a minimum. While this assumption is a reasonable one, it can hardly be expected to be accurate, particularly in view of the fact that the most probable mass ratio of the fragments observed in the division of various fissionable nuclei does not in general correspond to minimum energy of the product nuclei in contact.[9,10] The results obtained by Way, after minimizing the total decay plus electrostatic energy using the Bohr-Wheeler mass defect formula, are nearly the same as ours for the 1:2 mode but are significantly different for the 2:3 mode (the probable chain length for 93 is 3.1 compared to our value of 3.6).

Some confirmation of these results is provided by the chemical investigation of fission product decay chains. It appears from the work of Glendenin, Coryell, and others[11] that the known facts about decay chains, with mass numbers corre-

[8] E. Wigner and K. Way, Report CC-3032 (1945); Plutonium Project Reports 9B, 6.4 (1946).
[9] K. Way, private communication.
[10] S. Flügge and G. v. Droste, Zeits f. physik. Chemie [B], 42, 274 (1939).
[11] Summarized in Glendenin, Coryell, Edwards, and Feldman, CL-LEG-No. 1 (1946). Most of the data have been published in the J. Am. Chem. Soc. 68, 2411 (1946).

sponding to the most likely modes of fission, are consistent with the result of equal probable chain lengths (3.6) for the complementary fragments. Insufficient data are available, however, to draw conclusions about the chain lengths in a 1:2 division. In the case of a few mass numbers, it has been found possible to measure the independent yield of a particular member of the decay chain, formed directly from the fission process. This is possible when the preceding member of the chain has a long half-life or is stable (belonging to a pair of stable isobars). Assume that the total yield of the chain is known. Then the fraction of the chain of a given mass formed with a particular charge is determined in a few instances. If these fractions are plotted against $Z-Z_P$, where Z_P is the most probable charge for a fission fragment of the given mass, it is reasonable to expect the points to lie near a smooth (error) curve symmetrical about $Z=Z_P$. Such a plot has been made by Glendenin, Coryell, Edwards, and Feldman;[11] they find that if Z_P is determined either from unchanged charge distribution ($Z_i^{(0)}$), or from minimum energy of nuclei in contact (Way's method), the resulting points show systematic deviations from a symmetrical error curve, the lighter mass points (Br^{82} and Rb^{88}), and the heavier mass points (Xe^{135} and Cs^{136}) appearing to lie on separate curves displaced by about one unit of charge in both cases. On the other hand, if the values of Z_P are obtained by an empirical postulate of equal probable chain lengths for complementary fragments, all points appear to lie near a smooth curve. We have replotted their data taking Z_P equal to the theoretical value Z_i from Fig. 3. The resulting points lie reasonably close to a single error curve with some scatter but no systematic deviation, i.e., there is no evidence of separate curves for the lighter and heavier fission products. Some scatter is to be expected in view of the neglect of finer details of nuclear binding in the theoretical treatment; however, all the points lie within one-fifth of a charge unit of the best drawn error curve symmetrical about $Z=Z_i$. This can be considered as a preliminary check on the theory; evidently more experimental points, corresponding to a greater range of mass numbers, are needed to provide definitive confirmation.

Method for Measuring Neutron-Absorption Cross Sections by the Effect on the Reactivity of a Chain-Reacting Pile

H. L. Anderson, E. Fermi, A. Wattenberg, G. L. Weil, and W. H. Zinn
Argonne Laboratory, University of Chicago, Chicago, Illinois

(Received March 14, 1947)

This paper describes a method for measuring neutron-absorption cross sections based on the following principle: Introduction of a neutron-absorbing substance into a pile decreases the reactivity and in order to keep the power level constant the control rods must be displaced. By proper calibration this displacement may be used as a precision measure of the absorption cross section.

1. INTRODUCTION

THE reactivity of a chain-reacting pile depends critically on the balance of neutron production, absorption, and leakage. A small change in the absorption of neutrons taking place in the pile produces a drift in the intensity at which the pile is operating. This effect has been utilized for measuring neutron-absorption cross sectons.

This method was particularly useful in the development of piles since it gives directly the effect of the neutron absorption of various materials in the operation of a pile. The method measures the absorption directly while effects of scattering usually enter in a minor way. This has an advantage over methods which obtain the absorption as the difference between the total and the scattering cross section, especially where the difference is small.

2. NEUTRON REPRODUCTION

In the first two chain-reacting piles which were constructed at the Metallurgical Project, neutrons were reproduced in a structure consisting of a lattice of uranium lumps embedded in a pile of graphite bricks. In this structure neutrons are reproduced in a cycle in which fast neutrons are slowed down to thermal energies by elastic collisions with carbon. Upon reaching thermal energies, the neutrons continue to diffuse without further loss in energy, on the average, until they are either absorbed in the pile or escape the pile by leakage. A fraction of the neutrons which are absorbed produce fission in uranium with the liberation of new fast neutrons. The average number of neutrons produced from one original neutron in such a cycle is called the reproduction factor, k. The value of k depends on the balance of neutron production, absorption, and leakage.

When the pile is operated at sufficiently high intensity, the neutron production is predominantly that from neutron-induced fission and the contribution from spontaneous fission (α, n) reactions, (γ, n) reactions, and cosmic rays becomes vanishingly small. The pile is said to be in the critical condition when the neutron intensity remains constant. The value of k is then just slightly less than unity, the deviation from unity measuring just the amount of neutron production which is contributed by other neutron sources than the neutron-induced fission. In the piles used in our work, the critical condition could be obtained by the adjustment of a cadmium control rod. Insertion of more or less cadmium in the pile served to increase or decrease the amount of neutron absorption with consequent decrease or increase in the value of k. In what follows, the neutron intensity at which the pile is operated will be taken to be high enough so that the value of k at the critical condition may be considered to be unity with sufficient accuracy.

When the value of k is slightly larger than unity, the neutron intensity will drift upwards, while with k slightly less than unity, the neutron intensity will drift downward. The reactivity is a measure of the excess of k over unity. For $k-1=2.5\times10^{-5}$, the neutron intensity will increase with a period of about 1 hour. For pile periods very long compared to the longest delayed neutron period (78 sec.), $(k-1)$ is inversely proportional to the period.

3. CONTROL ROD CALIBRATION

In this work, we have measured the effect of the insertion of an absorber in the pile by ob-

serving the displacement of the control rod which was required to return the pile to the critical condition. It was found, however, that for a given change in reactivity, the displacement required, if measured in centimeters, was not always the same but depended on the position of the control rod in the pile. It was convenient to introduce a new unit of rod position such that displacements measured in the new units would always be proportional to $(k-1)$. In order to provide a precise definition of such a unit, use was made of the property of the pile that its period is proportional to $1/(k-1)$ in the limit of long periods. Accordingly, the unit of rod position was given the name *inhour* (from "inverse hour," symbol: ih), with the significance that when the control rod is displaced from the critical position by 1 inhour, the pile will have a period of (very nearly) 1 hour. (See Appendix I.)

4. NEUTRON ABSORPTION

The introduction of a neutron-absorbing substance into a pile reduces the value of k. To compensate for this loss of k, it is necessary to move the control rod out of the pile. The change in the critical position of the rod measured in inhours is a measure of the absorption of the substance.

The absorption of two substances may be compared by comparing the change in critical position which they produce. However, the number of neutrons absorbed by the substance depends on the way in which its cross section varies with energy, and on the energy distribution of the neutrons in the pile. It is clear that our measurement is a measure of the average value of the cross section for the particular energy distribution which obtains in the pile used. In the graphite piles which were used for this work, the contribution of the thermal neutrons predominates except in a few instances for those substances which have strong, low lying resonance levels. For most substances, the effect of scattering on the value of the reproduction factor enters in a relatively minor way. In most cases, then, a comparison of the effect on k of two substances is a comparison mainly of their thermal-neutron-absorption cross section.

5. INTENSITY MEASUREMENT

The intensity of operation of the pile was measured by observing the ionization current produced in a large BF_3 ionization chamber connected to a high sensitivity galvanometer. Small drifts were observed with a differential galvanometer, which was connected so as to measure the difference between the ionization current and that provided by a battery and potentiometer. By adjusting the neutron intensity to give an ionization current of 10^{-5} ampere, it was easy to observe drifts of 1/1000 in intensity, using a differential galvanometer with a sensitivity of 10^{-9} ampere for 1-mm deflection at 1 meter. Thus a displacement of 0.01 inhour from criticality would produce a drift of 5 mm in 3 minutes. This was ample sensitivity for most measurements, as will be discussed later.

6. BORON STANDARD

A standard absorber was prepared using known amounts of boron, the cross section of which is accurately known. The value of the absorption cross section for boron has been measured[1] by the transmission method for slow neutrons using a mechanical velocity selector. Such a measurement gives an absolute and accurate measure of the absorption cross section, because in boron the scattering cross section is very small compared to the absorption cross section, and it is easy to analyze the results obtained at different neutron velocities in terms of a part proportional to $1/v$ which is caused by the absorption, and a constant part which is caused by the scattering. At 2200 meters per second, these authors give 703×10^{-24} cm^2 for the absorption cross section of boron.

In carrying out an absorption comparison, it is important that every atom of the sample have the same chance to capture a neutron; or failing this exactly, it is sufficient if the unknown and the standard samples are conditioned in such a way that the situation is the same for both. In order to minimize the effects of self-absorption and yet obtain an easily measured effect, an arrangement was used which distributed the absorber over a fairly wide area. In the case of the

[1] E. Bragdon, E. Fermi, J. Marshall, and L. Marshall, Phys. Rev. (to be published).

TABLE I. Standardization of absorption measurements.

Critical position in inhours		
Blank	Borax	Cadmium
105.127	99.806	98.926
105.144	99.806	98.902
105.163	99.821	
105.145	99.862	
105.190		
105.153	99.823	98.914

boron standard, in some measurements we used BF_3 gas, in others we used borax for which we provided a graphite holder, $10\times10\times120$ cm³ which could contain 92 aluminum dishes for the borax about 1 inch in diameter each, and distributed inside the graphite. This holder could be reproducibly inserted near the center of the pile, in a position symmetrically disposed with respect to the neighboring uranium lumps. (See Appendix II.)

The boron standard was made by preparing a solution of borax and depositing one milliliter of this solution on a disk of filter paper in each of a set of 92 aluminum dishes. This solution, when evaporated, had the appearance of having distributed itself quite uniformly over the filter-paper disk. In making a comparison with an unknown absorber, equal filter-paper disks and equal aluminum dishes were always used to make the standard and the unknown identical in every respect except for the borax in the one and the material of the unknown in the other. The total absorption cross section of the borax for the average pile neutrons was about 9 cm²; and since this was distributed over a total area of 460 cm², the effect of self-absorption was of the order of 2 percent. If the size of the unknown is adjusted to give the same absorption cross section over the same area, no error resulting from self-absorption occurs in the comparison. The error in the relative absorption cross section occurs as the difference in the self-absorption effects.

The borax solution was analyzed for boron by first standardizing a solution of sodium hydroxide with potassium hydrogen tartrate. The borax was converted to boric acid with HCl, using a methyl orange indicator, and a titration was then carried out with the NaOH in the presence of mannitol. The method is that given in Treadway and Hall, *Analytical Chemistry 2*, 502. Two sets of three measurements each were carried out in our borax solution, one by Mr. W. Sturm of the Argonne Laboratory, and the other, independently, by Mr. D. Revinson of the Analytical Chemistry Group of the Metallurgical Laboratory. The average of the first series gave 2.816×10^{-4} mole of boron per ml, and for the second set, 2.793×10^{-4} mole of boron per ml. The agreement was considered satisfactory and the average of these results, 2.804×10^{-4} mole per ml was used in determining the cross sections. To the cross section per atom of boron, which at 2200 meters per second is 703×10^{-24} cm², we added 1×10^{-24} cm² to take into account the contribution of the sodium and hydrogen, and used 704×10^{-24} cm² at 2200 meters/second for the atomic-absorption cross section of borax. The total cross section of 92 borax disks was thus 10.94 cm² at 2200 meters/second.

7. CRITICAL POSITION MEASUREMENTS

The effect of this boron standard on the reactivity of the pile was studied by comparing the critical position obtained with a blank set of aluminum dishes, and filter-paper disks with that obtained with the 92 borax absorbers. Since the absorption was distributed among 22 neighboring cells, only a minor perturbation in the neutron intensity distribution was produced. Measurements of the critical position were made by setting the control rod to produce first a slow drift in one direction and then in the other, and interpolating between the two settings in inverse proportion to the period of drift observed.

The critical position may be altered during the course of the measurement because of changes in temperature and barometric pressure which may take place. It is always necessary to make corrections for these effects during the course of a

TABLE II. Analysis of columbium pentoxide.

Spectrochemical analysis Sample No. (old sample)		Mfg. spectrochemical analysis Sample No. 2 (new sample)	
	99→ Cb		
Ce	50 ppm	Ta_2O_5	None
Gd	10 ppm	TiO_2	Less than 0.001%
Hf	50 ppm	Fe_2S	None
Mo	20 ppm	ZnCuMg	Very weak
Sc	5 ppm	SiO_2	0.03%
Pr	5 ppm		
S	20 ppm		
Zr	100 ppm		

measurement. In the Argonne graphite pile, the temperature effect amounted to -0.814 ih/°C while the pressure effect, which was caused by the change in the amount of air nitrogen in the pile, amounted to -3.23 ih/cm Hg. There was also a humidity effect caused by the change in water content of the air on the pile which amounted to -2.85 ih/cm H_2O vapor. Of these, the most serious was the pressure effect, and it was always necessary to read the barometric pressure to 0.01 mm of Hg using a special mercury or aneroid barometer. Barometric pressure changes rapidly and in a spurious way, and over the short interval of time of such a change the pressure may not have had a chance to equilibrate over all the pile structure. The limiting sensitivity of the method is imposed by the pressure effect and amounts to ~ 0.01 ih.

The temperature effect is less troublesome because the temperature of the pile changed slowly and in a regular way, so that by arranging a series of measurements in a cyclic time sequence of the form *ABBA* the slow drift in critical position caused by temperature change would be automatically eliminated in the averages.

In Table I is listed a series of measurements of critical position expressed in inhours with, and without the borax standard. The effect of pressure has already been corrected for in these values.

From these data, the sensitivity of the method is seen to be 2.052 cm² (at 2200 m/s) per inhour of rod displacement, with a precision measure of about ± 0.03 cm².

As an example of the method, the measurement of the absorption cross section of columbium is of interest. Columbium has only one isotope, and it was to be expected that the absorption of a neutron would give rise to a radioactive isotope so that the absorption cross section could be measured by observing the *B* emissions. Early activation cross section measurements by L. Seren, H. Friedlander, and S. Turkel at the Argonne Laboratory gave an apparent result of about 0.02×10^{-24} cm².

A high purity sample of Cb_2O_5 was obtained from the Fansteel Company. A preliminary measurement showed an absorption cross section of 1.4×10^{-24} cm², almost 100 times larger than that found by the activation method. A new sample was then obtained from the Fansteel Company which was reported to have even higher purity than the first. Spectroscopic analyses made on the two samples are given in Table II.

TABLE III. Absorption of columbium.

	Critical position in inhours			
	Blank	Cb No. 1	Boron (std.)	Cb No. 2
Run A	117.66	115.14	115.39	115.14
Run B	117.67	115.17	115.39	115.15
			115.40	
	117.66	115.15	115.39	115.14

Change in critical position

Due to Cb No. 1 ih = 2.51
Cb No. 2 ih = 2.52
Boron std. ih = 2.27

Absorption cross section of Cb (referred to 2200 m/s) = 1.44×10^{-24} cm²

The Cb_2O_5 was pressed into pellets which were placed in the aluminum sample dishes covered with a disk of filter paper. In order to obtain approximately the same control-rod displacement, 46 of the standard boron dishes were used. These were uniformly distributed in the graphite holder. The no-absorber critical position was obtained with empty aluminum dishes and blank filter-paper disks. The first sample contained 931.45 grams of Cb_2O_5, the second sample 934.31 grams, while there was 0.1395 gram of boron in the standard. Measurements of critical position of the rod in inhours are given in Table III. Corrections for changes in pressure during the measurement are already included in the numbers given.

With very good agreement for both samples, the experiment yielded for the ratio of the average absorption cross section, for pile neutrons, of columbium to that of boron the value 0.00204. On the assumption that the absorption cross section obeys the same law of variation with neutron velocity as does the boron (the $1/v$ law) the columbium-absorption cross section may be given the value of 1.4×10^{-24} cm² at 2200 m/s.

8. CADMIUM STANDARD ABSORBER

In a large part of the work it was found convenient to use cadmium as a standard absorber rather than boron. A wire of cadmium has the property that practically all neutrons with energy less than about 0.3 ev which strike it will be

TABLE IV. Measurement of the beryllium cross section.

Sample	Change in inhours
7296 grams Be	−0.11
12960 grams C	0.00
8 cm² Cd	−3.80

absorbed. Since most of the neutrons in the pile are below 0.3 ev, cadmium serves as a convenient standard absorber, whose neutron cross section may be obtained from its geometrical dimensions.

Cylindrical cadmium wires of diameter D and length l have a geometrical cross section for isotropically distributed neutrons

$$A = \tfrac{1}{4}\pi D l$$

neglecting end effects.

In comparing the effect of cadmium to that of the standard borax absorbers, we used wires which had an average diameter of 0.1006 cm and a total length of 128.25 cm, giving a neutron cross section of 10.14 cm². These wires were distributed uniformly over the graphite holder together with blank aluminum dishes and blank filter-paper disks. Control-rod displacements resulting from the cadmium and compared to the borax are given in inhours in Table I. The effect of the cadmium is seen to be 6.239 ih or 1.625 cm²/ih.

The neutron cross section of cadmium may be converted to that of a $1/v$ absorber at 2200 meters per second by multiplying by the factor $2.052/1.625 = 1.26$.

9. TEMPERATURE OF PILE NEUTRONS

Since the boron absorption of neutrons varies according to the $1/v$ law, the number of neutrons which are absorbed by thin absorbers is proportional to the neutron density, and is independent of the neutron velocity distribution. Thick cadmium, however, captures every thermal neutron which strikes it, hence the absorption by cadmium depends also on the average velocity of neutrons.

A comparison of the effect of the absorption of these two substances gives information about the average velocity of pile neutrons. In making the comparison it is necessary to subtract that part of the effect of boron which is caused by absorption of neutrons above the cadmium limit. This was done by means of a BF_3 counter placed above a hole extending into the center of the pile. Using boron carbide collimation, the counter could not see neutrons which might be reflected by the pile shield, but only those emerging directly from near the bottom of the hole. Such neutrons have a distribution quite close to that which is present inside the pile. With no cadmium in the beam we observed 5200 counts per minute; with cadmium, 112 counts per minute; and with 3 inches of B_4C powder in the beam, 4 counts per minute. The contribution of the neutrons above the cadmium limit is thus 2.08 percent. Thus, an absorber whose cross section is 2.095 cm² at 2200 m/s, and which absorbs according to the $1/v$ law up to the cadmium limit and not at all above, changes the critical position by 1 inhour. For an absorber which absorbs all neutrons up to the cadmium limit with equal probability the same change in critical position is produced by 1.625 cm² of cross section. It follows that the average velocity of the neutrons which are in the center of the pile and below the cadmium limit is 2836 meters per second. This corresponds to a neutron temperature of 383° Kelvin.

10. EFFECT OF SCATTERING

A neutron scatterer may affect the reactivity of a pile either by altering the spatial, or the energy distribution of neutrons in the pile. A scatterer placed near a uranium lump may reduce the number of neutrons which can diffuse into the lump and thereby diminish the reactivity. An increase in the reactivity may be obtained if the scatterer is placed near the edge of the pile so that the neutron leakage is reduced. A pure scatterer can, however, produce no change in the spatial distribution if it is placed in a region where the gradient of the neutron density is zero. For this reason, absorption measurements are always made with the sample symmetrically disposed with respect to the uranium lump, and near the center of the pile.

With a scatterer in this position, its effect on the energy distribution does alter the reactivity of the pile in a non-negligible way. By increasing the slowing-down power of the moderator, the resonance absorption in uranium is decreased and the result is an increase in the reactivity.

11. ABSORPTION CROSS SECTION OF BERYLLIUM

For certain light elements with very small neutron absorption, the increase in the reactivity due to slowing down (see Appendix III) may be comparable to the decrease due to absorption and must be taken into account. We describe, as an example, a determination of the absorption cross section of beryllium. Beryllium metal blocks were placed in the Argonne pile distributed in 16 cells, 456 grams per cell. The results of the inhour measurements are given in Table IV.

The measurement with cadmium wires standardizes the geometry used for absorption. As discussed above, the cadmium standardization may be reduced to that of a $1/v$ absorber at 2200 meters per second by multiplying its cross section by the factor 1.26. Thus the cadmium standardization gives: $3.80/8\times1.26=0.377$ ih/cm².

The measurement with graphite shows that the effect of slowing down on the reactivity of the graphite we used is equal to the effect of its absorption. The absorption cross section of our graphite as measured by a diffusion method was known to be 0.0049×10^{-24} cm² at 2200 m/s. The effect of the slowing down is proportional to $\sigma_s\xi$, where σ_s is the cross section for scattering for resonance neutrons, and ξ is the average logarithmic loss of energy per collision (see Appendix III). For graphite $\sigma_s=4.8\times10^{-24}$ cm² per atom and $\xi=0.158$ while for beryllium $\sigma_s=6.1\times10^{-24}$ cm² per atom and $\xi=0.202$ so the effect of slowing down in beryllium is:

$$\frac{6.1\times0.202}{4.8\times0.158}\times0.377\times4.9\times10^{-27}\times\frac{7296}{9}\times6.02\xi\times10^{23}=1.46 \text{ ih}.$$

Subtracting this from the total effect -0.11 ih we have for the effect of absorption -1.57 ih. Thus, the absorption cross section of beryllium at 2200 m/s is:

$$\frac{1.57}{0.377}\,\frac{9}{7296\times6.02\times10^{23}}=8.5\times10^{-27} \text{ cm}^2/\text{atom}.$$

Since an accurate chemical analysis for the beryllium blocks we used was not available this result represents an upper limit of the capture cross section of beryllium. We have reason to believe, however, that the material was of high purity.

TABLE V. Calibration of control rod of Argonne pile.

x cm	$di\text{n}/dx$	ih
0	.000	0
50	.023	.7
100	.067	2.7
150	.158	8.2
200	.299	19.5
250	.418	37.8
300	.492	60.7
350	.520	86.0
400	.490	111.5
450	.402	133.7
500	.281	151.2
550	.142	161.3

APPENDIX I

The Inhour

The inhour is proportional to $k-1$, thus,

$$\text{ih}=C(k-1)$$

where the value of C is given by

$$C=\lim_{k\to1}\frac{1}{T(k-1)},$$

and T is the period of the pile in hours.

The relation between the displacement from criticality in inhours and the period of the pile may be obtained from the intensities and periods of the delayed neutron emission. For the uranium-graphite pile, the following formula has been used in our work:

$$\text{ih(crit)}-\text{ih}=\frac{64}{T}+\frac{245}{T+3.57}+\frac{688}{T+10.1}+\frac{1938}{T+34.5}+\frac{665}{T+83},$$

where T is the period of the pile in seconds. The numbers in the denominators are the periods of the various delayed neutron emissions in seconds. The contribution of some shorter periods has been disregarded. It is to be noted that because of the way in which the inhour has been defined, the accuracy with which this formula gives the period becomes greater and greater for larger and larger values of the period. According to the above formula, the pile has a period of 1 hour when

$$\text{ih(crit)}-\text{ih}=0.990.$$

Calibrations of the control rod may always be effected with the use of this formula by observing the period of the pile for a given displacement of the control rod from the critical position. The value of the inhour is measured from its zero value corresponding to control rod out of the pile. Table V gives the sensitivity of the control rod $di\text{h}/dx$ as a function of the position of the rod in the pile in centimeters. The integral of this curve is also given.

The inhour is useful as a measure of rod displacement

because it is a measure of pile reactivity which is independent of the position of the control rod, so that linear interpolations are accurate in comparing the effects of different absorbers. Moreover, its value has an almost unambiguous significance for all graphite-uranium piles.

The value of the constant C is known for uranium-graphite piles to be

$$C=2.5\times10^{-5}\ \text{hours}^{-1}$$

with an accuracy of about 20 percent.

APPENDIX II

Effect of Position

The effect of a given absorber on the reproduction factor depends on its position in the pile. Because of the inhomogeneous character of the structure the general variation of neutron density has superimposed on it a strong local variation. Thus the density n of neutrons at the position x, y, z may be represented by

$$n(x, y, z)=\alpha(x, y, z)\beta(x, y, z),$$

where α is a smooth function, and β has the same periodicity as the cells and describes the local variations of intensity. For small absorbers which do not perturb the neutron distribution appreciably, the effect on the reactivity is proportional to the square of α and depends also in a complicated way on the position of the absorber within the cell.

In order to minimize the variations caused by this last factor it is preferable to place the absorbers not too close to the uranium lumps. For the graphite-uranium piles, the variation of α may be obtained with sufficient accuracy from the solutions of the diffusion equation

$$\nabla^2\alpha+B^2\alpha=0$$

subject to appropriate boundary conditions. In a uniform cubic structure of side a, α may be expected to vanish near the boundary so that the solution is

$$\alpha(x, y, z)=\alpha(0, 0, 0)\cos(\pi x/a)\cos(\pi y/a)\cos(\pi z/a),$$

in which the origin of the coordinates is taken at the center of the pile. Thus, the effect on k of an absorber added to the central cell is 8 times greater than if it were added to the average cell. The number of neutrons which it absorbs is only $\pi^3/8$ times greater.

In the Argonne pile used in this work, the design of the cell was such that an absorber having a cross section for pile neutrons of 1 cm² placed midway between two lumps would absorb about 1/28 of the neutrons absorbed by the cell itself. Thus, inappreciable perturbations of the neutron distribution would be caused in general if the amount of absorber added per cell had less than 1 cm² of absorption.

APPENDIX III

Energy Distribution of Pile Neutrons

It is convenient to distinguish two groups of neutrons in the pile, in consideration of the property of cadmium, in quite thin sheets, which absorbs completely one of these with only a minor effect on the other. Cadmium has a fairly sharp absorption limit between 0.3 and 0.5 ev depending on its thickness. Neutrons whose energy is below this limit are cadmium-absorbable and sometimes are termed C-neutrons. The neutrons of higher energy are not appreciably absorbed by cadmium and are sometimes termed epicadmium neutrons.

Because of the nature of the slowing-down process, the number of neutrons in a logarithmic energy interval is proportional to dE/E. Since the distance for slowing down is large compared with the spacing of the uranium lumps, but small compared with the dimensions of the pile, the distribution of sources may be taken to be uniform and the loss by leakage and absorption (which amounts to about 10 percent down to 1 ev) may be neglected in general. It is thus appropriate to speak of the slowing-down density $q(E)$ which is the number of neutrons per cm³ which is slowed from above to below the energy E within one second. This quantity is conserved in the pile except for losses caused by leakage and absorption, as mentioned. The relation to the density of neutrons $n(E)$ per unit energy interval is generally

$$n(E)=Q(E)\frac{1}{vE}\frac{1}{\xi_s\sigma_s}.$$

Here v is the neutron velocity, and σ_s is the reciprocal mean free path for collision with the moderator (carbon), and ξ_s is the average logarithmic loss of energy per collision.

The value of ξ for elastic collisions and isotropic scattering for a moderator of mass M of atomic weight A is:

$$\xi=1-\frac{(A-1)^2}{2A}\log\frac{A-1}{A-1},$$

which for not too small A reduces to $\xi\approx2/A$. For carbon ξ has the value 0.158, for oxygen it is 0.121, while for hydrogen its value is unity. The product $\xi_s\sigma_s$ is the slowing-down power per cm³ of the moderator.

Once the neutrons fall below the cadmium limit, the mechanism of the slowing down is greatly altered. The neutron energy becomes comparable to the energy of crystal binding of the atoms with which they collide, and to the energy of thermal agitation. The slowing down proceeds more slowly, and indeed, because of the preferential absorption of neutrons having lower energies, thermal equilibrium is never established exactly. For most purposes, it is sufficiently accurate to consider the C-neutrons in the pile as a group of neutrons having a Maxwellian energy distribution with a temperature somewhat higher than the true temperature of the pile, as discussed in the text.

Neglecting the variation of $q(E)$ and σ_s with neutron energy, the number of epicadmium neutrons which are absorbed per second by a substance with absorption cross section $\sigma_a(E)$ is

$$A_{\text{res}}=\int_{E\text{Cd}}^{\infty}\sigma_a(E)n(E)v\,dE=\frac{q}{\xi\sigma_s}\int_{E\text{Cd}}^{\infty}\sigma_a(E)\frac{dE}{E},$$

where the upper limit has been extended to infinity because the contribution to the absorption at high energies is usually quite small. The integral has been called the resonance-absorption integral, and in general its principal contributions come from the low energy neutrons.

Below the cadmium threshold, the neutrons have approximately the Maxwellian distribution as was pointed out above. This is a rather narrow energy range and the chance that a resonance occurs in it is fairly rare. Except for those cases where a resonance below 0.3 ev is known to occur, it is reasonable to suppose that the absorption has a $1/v$ dependence so that the thermal activation is given by:

$$A_{th} = n\vartheta\sigma(\vartheta).$$

Here ϑ is the average velocity of the C-neutrons, and n is their density. The ratio of the activations is given by:

$$\frac{A_{res}}{A_{th}} = \frac{q}{n\vartheta}\int_{E_{Cd}}^{\infty}\sigma_a(E)\frac{dE}{E}\Big/\xi\sigma_s\sigma(\vartheta).$$

The quantity $(q/nv)\cdot(1/\xi\sigma_s)$ can be determined from the measurements described above in which a BF_3 counter was exposed to the neutrons from a hole in the pile. These data gave

$$\left(\frac{A_{th}}{A_{res}}\right)(\text{boron}) = 47.1.$$

Since the boron absorption follows the $1/v$ law, we have

$$\sigma(\vartheta)\Big/\int_{E_{Cd}}^{\infty}\sigma(\vartheta)\left(\frac{E(\vartheta)}{E}\right)^{\frac{1}{2}}\frac{dE}{E}\left(\frac{E_{Cd}}{2E(\vartheta)}\right)^{\frac{1}{2}}$$

for 0.90 gm/cm^2 of Cd we may take $E_{Cd}=0.4$ ev, while for $E(\vartheta)$ we take 0.042 ev and obtain, thereby, the general expression

$$\frac{A_{res}}{A_{th}} = \frac{0.045}{\sigma(\vartheta)}\int_{E_{Cd}}^{\infty}\sigma(E)\frac{dE}{E}$$

with an uncertainty of about 10 percent resulting from the uncertainty in E_{Cd}. The coefficient 0.045 is in good agreement with the value obtained from an independent method of obtaining this number based on the use of a calibration of indium foils in a "standard graphite pile" which is described elsewhere. This relation is useful in determining the value of $\int\sigma_a(E)dE/E$ from a comparison of the activations induced in a substance with and without cadmium protection.

The work reported here was done in 1943–44. It was carried out under contract between the University of Chicago and the Manhattan District Corps of Engineers, War Department.

PHYSICAL REVIEW VOLUME 72, NUMBER 1 JULY 1, 1947

Evidence for, and Cross Section of 115 Day Se^{75} *

H. N. FRIEDLANDER, L. SEREN, AND S. H. TURKEL**
Argonne National Laboratory, Chicago, Illinois

(Received March 8, 1947)

Evidence has been given to show that the 115-day activity produced in selenium by thermal neutrons is due to Se^{75} which decays by K electron capture to As^{75}, accompanied by a 0.4 Mev γ-ray. A value for the cross section of Se^{74} for radiative capture of a thermal neutron has been given.

SEABORG'S tables[1] report as a K-capture process a 48-day and a 160-day activity for Se^{75} produced from As^{75} by a (p, n) and $(d, 2n)$ reaction, respectively. However, we have found a K-capture activity with a half-life of 115 ± 5 days produced by an (n, γ) reaction on selenium irradiated in the Argonne pile. The remainder of this paper will give evidence for this activity and for a value of the activation cross section for its production from Se^{74}.

The 115-day activity was established by counting samples mounted on scotch tape foils with an aluminum-walled cylindrical Geiger counter. One sample was counted for over six months.

Possibility of an arsenic activity produced by an (n, p) reaction on the selenium was ruled out by chemical separations from the selenium using an arsenic carrier. No activity was found in the arsenic fractions. The chemical separation was checked by adding 27-hour As^{76} to non-activated selenium and separating the two elements. No arsenic activity was found in the selenium por-

* Work completed July 1944 and submitted for clearance December 1946. This document is based on work performed under Contract No. W-7401-eng-37 for the Manhattan Project at the Argonne National Laboratory. The information covered in this document will appear in Division IV of the Manhattan Project Technical Series as part of a contribution of the Argonne National Laboratory.

** Present addresses of authors: H. Friedlander, Department of Chemistry, University of Chicago; L. Seren, General Electric Research Laboratory, Schenectady, New York; S. Turkel, Nuclear Engineering Powered Aircraft Department, Fairchild Engine and Airplane Corporation, P.O. Box 415, Oak Ridge, Tennessee.

[1] G. T. Seaborg, Rev. Mod. Phys. **16**, 1 (1944).

TABLE I.

Element	K-absorption edge
Zn	1.2805A
Ga	1.1902A
Ge	1.1164A
As	1.0426A

TABLE II.

Element	$K-\alpha_1$	$K-\alpha_2$
$_{34}$Se	1.10248A	1.10652A
$_{33}$As	1.17344A	1.17743A
$_{32}$Ge	1.25130A	1.25521A

tions. Similar separations with germanium ruled out the possibility of an (n, α) reaction on the selenium to produce germanium. The possibility of the activity being due to impurities in the selenium was ruled out by using a sample of Hilger spectroscopically standardized selenium reported to be 99.9964 percent pure. Samples of selenium of doubtful purity showed this activity to be fully as strong as did the Hilger sample. The only other elements exhibiting half-lives of this order of magnitude, having large cross sections, and which could be impurities (since they have similar chemical properties with selenium), were tellurium and tantalum. Both of these were eliminated by spectroscopic analysis of the Hilger sample.

It then remained to determine the selenium isotope responsible. Since a possible reaction was an (n, γ) reaction on Se^{82} to produce Se^{83} with subsequent beta decay to Br^{83}, which has a 140-minute half-life, a search for a bromine daughter was undertaken. A bromide ion carrier was added to a selenium solution in hydrochloric acid. After allowing 24 hours for the possible bromine daughter to grow, the bromide ion was separated from the selenium ion. No activity was found in the bromine fraction, thus eliminating Se^{83}. The only other possibilities were Se^{75}, Se^{79}, and Se^{81}. The two latter would be negative beta-emitters, whereas the first would be a positron emitter or produce arsenic K x-rays by K-capture. Cloud chamber studies showed that very few beta-particles (positive or negative) were emitted, as will be discussed below. Further evidence for Se^{75} was obtained by bombarding arsenic, which consists of only the one stable isotope As^{75}, with 12 Mev deuterons from the cyclotron at Washington University in St. Louis. The only possible selenium isotope which could be produced (this by a $(d, 2n)$ reaction) for which no stable isotope was known was Se^{75}. The selenium thus produced was then separated from the arsenic. The decay of the sample also gave a 115 ± 5 day half-life and the mass absorption coefficients for this sample were the same as those for the sample produced by the pile neutrons on selenium.

A study of the radiation emitted showed a γ-ray of about 0.4 Mev, as determined by an absorption curve taken with lead absorbers after electrons and x-rays were absorbed by one centimeter of Lucite. An absorption curve taken on the main radiation with aluminum absorbers gave a mass absorption coefficient of 42 cm^2/g. This is roughly the value to be expected for x-rays from elements like arsenic or selenium. If K-electron capture were the mode of decay of Se^{75}, arsenic K x-rays would be expected. However, if positron emission were the mode of decay, any x-rays accompanying them would be selenium x-rays. Table I gives the values of the K-critical absorption wave-lengths for several absorbers.[2] X-rays of wave-lengths slightly shorter than the K-critical values for an absorber are strongly absorbed by it. Table II gives the main K x-ray lines[3] for arsenic, selenium, and germanium. We see that if selenium x-rays are present they would be more strongly absorbed by germanium or gallium absorbers than by arsenic absorbers, whereas arsenic x-rays would be more strongly absorbed in gallium or zinc absorbers than in germanium absorbers. If germanium x-rays are present, they would be more strongly absorbed in zinc than in gallium absorbers. Table III gives the values of the mass absorption coefficients for

TABLE III.

Absorber	μ/ρ in cm^2/g
$_{13}$Al	42
$_{30}$Zn	115
$_{31}$Ga	102
$_{32}$Ge	56
$_{33}$As	56

[2] A. H. Compton and S. K. Allison, *X-Rays in Theory and Experiment* (D. Van Nostrand Company, Inc., New York, 1935), second edition, p. 792.
[3] Reference 2, p. 784.

various absorbers, as measured by us. Since gallium shows stronger absorption than germanium we must conclude that arsenic x-rays are present due to K-capture in Se^{75}.

In order to verify completely the presence of x-rays and the absence of β-particle decay, a foil of the active selenium was placed in a cloud chamber.[4] With argon gas in the chamber many short tracks of photoelectrons, having a range about one millimeter and *originating in the gas*, were observed, but few longer electrons (above the background) originated *at the foil*, as is shown in Fig. 1. With helium gas in the chamber, only a few photoelectrons were seen in the gas, and an upper limit on the number of electrons starting from the foil could be fixed. These results showed that only a few percent of the disintegrations could be by positron emission, whereas the major portion is by K-electron capture with subsequent emission of As K x-rays.

The activation cross section[5] for the production of Se^{75} from Se^{74} by a thermal neutron (n, γ) process was calculated on the basis of the cloud-chamber tracks, on an estimation of the counter efficiency for the arsenic K x-rays, and on an estimation of the counter efficiency for the γ-rays produced. The calculations by the three methods checked fairly well, and a weighted average is 22×10^{-24} cm^2/isotopic atom, or 0.2×10^{-24} cm^2/natural atom, since the natural abundance of Se^{74} is 0.9 percent. The probable error is estimated to be about ± 40 percent.

The chemical procedures of separation used were the following. A solution of selenium was prepared by dissolving selenium metal powder in concentrated nitric acid, evaporating to dryness, and redissolving in a minimum of concentrated HCl. Arsenous oxide or germanium oxide carrier was then added and the selenium precipitated by reduction to the metal with sulfur dioxide. The precipitated metal was washed with water, and then with ethyl alcohol, and dried at 110°C. The arsenic or germanium was then precipitated from the acid solution as a sulfide by use of hydrogen sulfide.

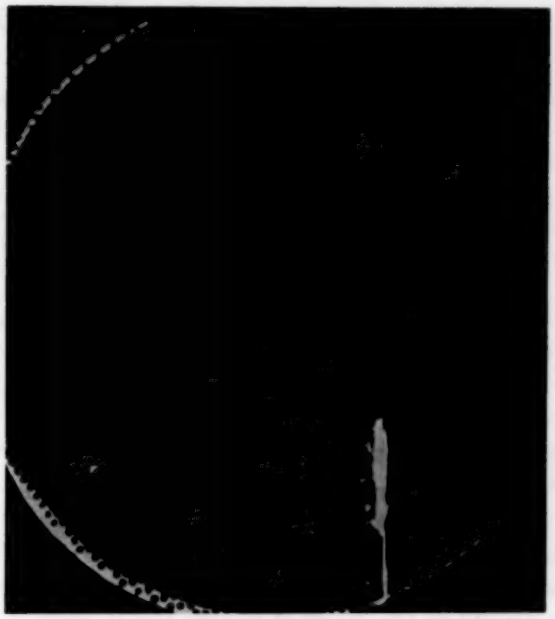

FIG. 1. Cloud-chamber photograph (by D. Hughes and C. Eggler) of 115-day Se^{75}. The many small blobs are due to photoelectrons produced in the argon gas from the x-rays. A few beta-rays originating at the foil can also be seen.

In the case of the cyclotron bombardment, the arsenous oxide was dissolved in concentrated HCl, selenous oxide carrier was added and the selenium was precipitated by reduction with sulfur dioxide.

To look for the possible bromine daughter, selenium was dissolved and the bromine was allowed to grow for 24 hours in the presence of added sodium bromide carrier. Then silver nitrate was added, precipitating silver selenide and bromide which were then redissolved in concentrated aqueous ammonia. The silver bromide was then reprecipitated from hot nitric acid solution in which silver selenide remains soluble.

The mass absorption coefficients were obtained by placing foils of known thickness of the suitable element between the sample and a bell-type, thin mica-window Geiger counter. The absorbers of gallium, germanium, and arsenic were prepared by placing known amounts of the powdered oxides on scotch tape.

[4] The cloud-chamber work was done by D. Hughes and C. Eggler.

[5] For a fuller discussion of cross-section procedure see a paper on "Thermal neutron activation cross sections," by the same authors (to be published).

Ionization Yield of Radiations. II. The Fluctuations of the Number of Ions

U. FANO
X-Ray Section, National Bureau of Standards, Washington, D. C.
(Received March 7, 1947)

The ionization produced by individual fast charged particles is frequently used as a measure of their initial energy; fluctuation effects set a theoretical limit to the accuracy of this method. Formulas are derived here to estimate the statistical fluctuations of the number of ions produced by constant amounts of radiation energy. The variance of the number of ionizations is found to be two or three times smaller than if this number were governed by a Poisson distribution. An improved understanding is gained of the statistical treatment of fluctuation phenomena.

1. INTRODUCTION

THE number of ion pairs J produced in a volume of gas following the absorption of ionizing radiation is closely proportional to the amount V of energy absorbed. The ratio V/J is generally of the order of magnitude of 30 to 35 ev; it depends very little on the quality of the ionizing radiation and comparatively little on the nature of the gas. This question has been discussed in a recent paper,[1] which will be referred to as (I).

The constancy of the ratio V/J is frequently relied upon to obtain an experimental estimate of V by measuring J and multiplying it by a factor ϵ. This factor is equal to the ratio of the mean values of V and J obtained from a large number of experiments carried out under comparable conditions.

Even when all pertinent physical factors, including V, are kept constant, the number J is subject to statistical fluctuations. Knowledge of the extent of these fluctuations, which set an upper limit to the accuracy of experimental techniques, is of interest, e.g., when the ionization produced by individual particles serves as a measure of their initial energy; this was kindly pointed out to the author by Dr. R. G. Sachs. A rough theoretical estimate of this effect is derived in the present paper. Specifically, it is proposed to estimate the variance of J under the condition that the energy loss V has a fixed value V_0, i.e., to calculate the expected value of $(J-J_0)$,[2] where $J_0=V_0/\epsilon$ is the expected value of J under the stated condition.

2. STATISTICAL TREATMENT

The production of a measurable number of ionizations involves a large number of elementary processes. Hence, the first objective is to express the variance of J in terms of quantities pertaining to individual elementary processes. For example, one may consider as an elementary process the impact of a fast charged particle against a gas molecule.

The probability that J assumes any given value after a *fixed number of impacts* has taken place, or after a particle has covered a *fixed length of track*, can be easily obtained; under these conditions the total *energy loss* V would be subject to *fluctuations*, just as is J. We are interested, however, in the opposite case of a *fixed energy loss*, $V=V_0$, with *fluctuating length of track* and *number of impacts*; in this case the probability distribution of J requires further investigation.

This problem is analogous to that of the straggling in range of α-particles[2] which is solved through the following consideration: If a particle happens to lose an amount of energy V instead of the expected amount V_0 along a length of track l, it is expected to lose the amount V_0 along a length of $l+\Delta l$, where $\Delta l=l(V_0-V)/V_0$. The fluctuation of energy loss along Δl is disregarded here, but this fluctuation tends to average out since Δl may be positive or negative. Similarly, if the particle happens to have produced J ionizations along l while losing the energy V, it will produce $\Delta J=(V_0-V)/\epsilon$ ionizations along Δl. Thus the eventual fluctuation of J for fixed V_0, namely, $(J+\Delta J)-J_0$ turns out to be equal, at least approximately, to the fluctuation $J-V/\epsilon$

[1] U. Fano, Phys. Rev. **70**, 44 (1946).

[2] N. Bohr, Phil. Mag. **30**, 581 (1915).

for fixed l; the probability of the latter can be easily calculated. The essential point is that the quantity $J-V/\epsilon$:

(a) Coincides with $J-J_0$ when $V=V_0$.

(b) Has the *mean value zero* and hence its variation over short sections of track can be disregarded so that its mean square should have, at least approximately, the same value for fixed l (or for fixed number of impacts) as for fixed $V=V_0$.

If n_p and E_p are the number of ionizations and the energy loss resulting from the pth impact within a group of N impacts occurring under the same conditions, then the mean values $\bar{n}_p=\bar{n}$ and $\bar{E}_p=\bar{E}$ are independent of p and:

$$J=\sum_{p=1}^{N} n_p, \quad V=\sum_{p=1}^{N} E_p, \quad \epsilon=\bar{E}/\bar{n}. \tag{1}$$

Since the results of successive impacts are independent of one another, the mean of $(J-V/\epsilon)^2=[\sum_p (n_p-E_p/\epsilon)]^2$ is obtained by adding the mean of $(n_p-E_p/\epsilon)^2$ in each impact, and this is also independent of p. Hence, for a fixed $N=V_0/\bar{E}=J_0/\bar{n}$, the desired variance is given by:

$$\langle (J-V/\epsilon)^2\rangle_{Av}=N\langle (n-E/\epsilon)^2\rangle_{Av}=FJ_0, \tag{2}$$

where:

$$F=\langle (n-E/\epsilon)^2\rangle_{Av}/\bar{n}. \tag{3}$$

Independent mathematical investigation[3] of a quantity

$$X=\sum_{p=1}^{N} x_p,$$

where the x_p's are independent random variables governed by the same probability distribution *and* $\bar{x}_p=0$, has actually shown that $\bar{X}=0$ and $\langle X^2\rangle_{Av}=\bar{N}\langle x^2\rangle_{Av}$ *even though* N *is not fixed but subject to fluctuations*, provided only that $\bar{N}$ and $\langle N^2\rangle_{Av}$ are finite. This confirms that the variance of J for $V=V_0$ is given by Eq. (2) *exactly*, even when the number of elementary processes involved is not large. It also shows that Bohr's formula for the straggling in range has a similarly large range of application and can be derived directly by taking the variance of the quantity $l-V/B$ (B=stopping power) whose mean is zero.

[3] M. A. Gershick and D. Blackwell, Ann. Math. Statistics (to be published).

3. TREATMENT OF SECONDARY IONIZATION

The method introduced in (I), Section 4, is to consider every inelastic impact undergone by gas molecules as an elementary process, independently of whether the impinging particle is fast or slow, a "primary" or a "secondary."[4] The approximation involved is to assume that the ratios among the cross sections for different types of impact are independent of the speed and nature of the impinging particle. This assumption is not closely fulfilled but offers a convenient basis for discussion.

Call s_j the cross section for an impact which sends the molecule to its jth excited state; E_j is the energy absorbed by the molecule inclusive of all its electrons. Following the notation of (I), the state j is classified as:

(e) if $E_j<I$, where I is the first ionization potential (simple excitation);

($i1$) if $I\leqslant E_j<2I$ (an electron is ejected which is incapable of further ionization);

($i2$) if $E_j\geqslant 2I$ (an electron is ejected with energy E_j-I, and is capable of further ionization).

The treatment in the preceding section can now be applied considering that:

(a) The number of ionizations per impact is $n_j=0$ in case (e), $n_j=1$ in cases ($i1$) and ($i2$).

(b) The energy actually lost by the ionizing radiation in case ($i2$) is only I, since E_j-I can be utilized again.

Then:

$$F=[\Sigma_j^{(e)}s_j(E_j/\epsilon)^2+\Sigma_j^{(i1)}s_j(1-E_j/\epsilon)^2 +\Sigma_j^{(i2)}s_j(1-I/\epsilon)^2]/\Sigma_j^{(i1,\,i2)}s_j. \tag{3'}$$

4. DISCUSSION

For purposes of comparison it is pointed out that if the number of ionizations were governed by a Poisson distribution, then $\langle (J-J_0)^2\rangle_{Av}=J_0$, that is $F=1$.

Formula (3') is easier to evaluate numerically than (3). Experimental or theoretical data on the ratios among the s_j's can be used. The nature of the formula is such that the result is rather insensitive to moderate errors in the s_j's.

[4] The method might be extended to cover the impacts of ionizing (primary or secondary) photons against molecules. Another case which is not covered by the present theory is the double ionization caused, for example, by removal of an internal electron followed by an Auger process. These phenomena appear to involve only a small fraction of the ionized molecules.

In the case of atomic H, available theoretical numerical data[5] have been used with the result:

$F\sim 0.46$ for 100 kv impinging electrons
$F\sim 0.42$ for 1 kv impinging electrons. (4)

The calculation has been repeated using the same simplified theory of impacts as in (I), Section 4, namely, by taking (with notation similar to that in (I)):

$$s_j = s_j^{(g)} + s_j^{(h)}, \quad s_j^{(g)} = (k x_{j0}^2 \log r)/\mathrm{Ry},$$
$$s_j^{(h)} = 0 \text{ for } E_j < I, \quad s_j^{(h)} = k/E_j^2 \text{ for } E_j \gtrsim I \qquad (5)$$

where x_{j0} is the dipole matrix element for the transition from the normal to the jth state and $r = 2mv^2/I$. Hence:

$$F = \{\Sigma_j^{(e)}(x_{0j}^2/x_i^2)(E_j/\epsilon)^2 + \Sigma_j^{(i1)}(x_{0j}^2/x_i^2)(1-E_{0j}/\epsilon)^2 + (x_{i2}^2/x_i^2)(1-I/\epsilon)^2 + (\epsilon_1/I\log r) \times [1-(1+2\log 2)I/\epsilon + 3I^2/2\epsilon^2]\}/[1+(\epsilon_1/I\log r)] \qquad (3'')$$

with

$$x_i^2 = x_{i1}^2 + x_{i2}^2 = \Sigma_j^{(i1,\,i2)} x_{0j}^2, \quad \epsilon_1 = \mathrm{Ry}/x_i^2,$$

Ry = Rydberg's energy. This formula holds for any substance; experimental or theoretical values of x_{0j} can be used. The results for H are:

$F\sim 0.47$ for 100 kv impinging electrons
$F\sim 0.43$ for 1 kv impinging electrons. (4′)

The agreement between (4) and (4′), even though it may be partly accidental, parallels the agreement obtained in (I) under the same circumstances and encourages the application of the simplified theory of impacts.

There remains to be discussed the effect of the assumption that the ratios among the s_j's are independent of the speed and nature of the impinging particles. This assumption was taken as a basis in (I), Section 4, as well as in Section 3 of this paper. The correct procedure in both cases should have been:

(a) To classify all impacts undergone by individual molecules according to the nature and speed of the radiation impinging on that molecule (e.g., "secondary electron of 47 ev");

(b) To calculate ϵ and F (as defined by (1) and (3), the former being equivalent to (3) of (I)) for each "kind" of impinging radiation;

(c) To calculate the final average values of ϵ and F, giving to each "kind" of impinging radiation a weight proportional to the number of ionizations that are expected to be produced *directly* by it.

From this standpoint it appears that the values of ϵ and F calculated in (I) and above in this paper should be intended, strictly speaking, to apply *only* to the ionization produced *directly* by electrons of the stated energy *excluding* that produced by secondaries or by the same electrons after considerable slowing down. In practice, however, since ϵ and F do not depend very greatly upon the kind of impinging radiation, the corrections required are not too large.

It is of particular interest to evaluate ϵ and F for the slow secondary electrons which produce a large fraction of the total ionization. To do this properly, experimental data on impact cross sections might be used, as it is difficult to obtain theoretical data owing to the lack of suitable approximation methods. However, the theory applicable to fast electrons indicates that the frequency of excitations decreases with decreasing energy as compared to that of ionizations. This has the effect of decreasing the theoretical estimate of F as well as that of ϵ. A crude estimate may be hazarded by extrapolating the results of the simplified theory down to $\log r = 2$, which would correspond to slow electrons not quite able to produce further ionizations. This yields (still for atomic H) $F\sim 0.33$. Since approximately equal numbers of ionizations are produced in H by primary and by secondary electrons, the over-all value for H might be expected to be $F\sim 0.4$. If the same method of crude estimation is applied to correct the second approximation value $\epsilon_2 = 36$ ev obtained in (I) for H, a new estimate ~ 32 ev is obtained.

No attempt has been made to calculate F for substances other than H, the purpose of the paper being simply to estimate its order of magnitude. It appears, in view of the considerations presented in (I), that the influence of the factor s_j in the sum $\sum_j^{(e)}$ in (3′) or (3″) should decrease sharply as I increases, the factor $(E_j/\epsilon)^2$ in the same summation should, however, counteract this effect strongly. The factors $(1-E_j/\epsilon)^2$ and

[5] Geiger-Scheel, *Handbuch der Physik* (Julius Springer, Berlin, 1933), Vol. 24/1, pp. 517, 519.

$(1-I/\epsilon)^2$ in the remaining summations should act to reduce the value of F as I increases.

In conclusion, it seems rather likely that F should generally be of the order of magnitude of $\frac{1}{3}$ to $\frac{1}{2}$.[6]

[6] The ionizing action of comparatively energy-rich but slow ions, of velocity close to that of molecular valence electrons, constitutes an exceptional case for the determination of both ϵ and F; ϵ may become much larger than 30–35 ev, and F may approach 1.

I wish to thank Dr. J. H. Curtiss and Dr. C. Eisenhart for helpful discussions and advice on the statistical treatment and Dr. D. Blackwell for discussing his results with me prior to publication.

PHYSICAL REVIEW VOLUME 72, NUMBER 1 JULY 1, 1947

Higher Angular Momenta and Long Range Interaction in Resonance Reactions

E. P. WIGNER AND L. EISENBUD
Clinton Laboratories, Oak Ridge, Tennessee

(Received March 20, 1947)

The results of two preceding articles on the energy dependence of the reaction and scattering cross sections are generalized. As before, the configuration space is divided into two parts. In the internal region or reaction zone there is no restriction on the type of interaction between the particles. In the external region, on the other hand, the interaction takes place between the colliding or separating particles without changing their structure (wave function). The present article deals with a more general situation than the preceding ones, first by allowing for an interaction, although only of a restricted type, outside the reaction zone. The most common type of interaction which plays a role outside the reaction zone is the electrostatic interaction of the colliding or separating particles. In addition, the present article does not restrict the angular momentum of the particles to zero, but permits the treatment of arbitrary angular momenta. The cross sections are expressed in well-known fashion in terms of the collision matrix $\mathfrak{U}$ which is, of course, independent of the size of the internal region. $\mathfrak{U}$, in its turn, is expressed by the $\mathfrak{R}$ matrix ((35) and (38)) and the quantities ω, $\mathfrak{B}$, and $\mathfrak{C}$ describing the interaction in the external region. $\mathfrak{R}$ as function of energy is given by (24), and a number of properties of this function are enumerated. None of the quantities $\mathfrak{R}$, ω, $\mathfrak{B}$, and $\mathfrak{C}$ are strictly independent of the size of the internal region, although the combination (38), i.e., the collision matrix, of course, is.

I. INTRODUCTION AND SUMMARY

THE present treatment of the representation of the scattering and reaction cross sections differs from that given in two previous papers[1a, b] in that it divides the problem of finding a stationary solution of the quantum-mechanical equations into two steps. The first step is taken in Section III; Section II is devoted to the introduction of several definitions and a few mathematical preliminaries. In Section III an expression is obtained for the value which the wave function assumes on the surface S separating the internal and external regions,[2] in terms of the normal derivative of the wave function on that surface. The essential content of this section may be described as follows. A complete set of orthonormal functions X_λ is defined in the internal region by means of an Hermitean boundary value problem. The X_λ are those solutions of the wave equation which satisfy the boundary condition that their normal derivatives vanish at the boundary S of the internal region. If an arbitrary stationary-state wave function, φ, associated with the energy E, is expanded in terms of the X_λ the expansion coefficients are found to be $\gamma_\lambda/(E_\lambda-E)$ where $\gamma_\lambda=\int X_\lambda^*(\partial\varphi/\partial n)dS$. The E_λ is the characteristic value associated with X_λ, $\partial\varphi/\partial n$ denotes the normal derivative; the integral is to be extended over the boundary surface S. As a result, the value of φ is given by

$$\varphi=\sum_\lambda \frac{\gamma_\lambda}{E_\lambda-E}X_\lambda=\sum_\lambda \frac{\int X_\lambda^*(\partial\varphi/\partial n)dS}{E_\lambda-E}X_\lambda. \quad (1)$$

[1a] E. P. Wigner, Phys. Rev. **70**, 15 (1946).
[1b] E. P. Wigner, Phys. Rev. **70**, 606 (1946). Professors J. Schwinger and V. Weisskopf have kindly informed us that they have recently obtained results which closely parallel those of the present paper.
[2] Most of the notions (such as internal and external region, etc.) used in this paper were formulated by the writers in 1940 for a review article, the publication of which was postponed because of the war. It will appear shortly in another journal.

Since γ_λ depends only on the normal derivative of φ on S, Eq. (1) constitutes a relation between the value and the normal derivative of φ on S. If both φ and $\partial\varphi/\partial n$ are expanded into an orthogonal system, the integral operator defined by (1) goes over into the matrix $\mathfrak{R}$ which has the same significance as the $\mathfrak{R}$ of reference 1b. The expression obtained there for $\mathfrak{R}$ is rederived here, and it is shown that the constant matrix $\mathfrak{R}_\infty$ vanishes. The $\mathfrak{R}$ matrix plays a central role, and since its form is given implicitly by (1), this equation contains, in a sense, the essential content of the present paper.

Although the boundary condition on the X_λ, which is actually used in Section III, is somewhat more complicated than the one given above (vanishing normal derivative on S), the relation which is derived between value and normal derivative of φ is formally identical with (1). The reasons for the choice of the particular boundary conditions employed will become apparent later, but it should be emphasized here, perhaps, that there is a certain arbitrariness in the choice of these conditions (and hence of the X_λ and E_λ) and that the ones used may not always be the most suitable ones.

Section IV deals with the second step for obtaining an expression for the scattering and reaction cross sections. It consists in obtaining that consistent set of values and derivatives of the wave function on the surface S, the continuation of which into the external region gives the asymptotic form which corresponds to an experiment to determine the scattering and reaction cross sections. While Section III deals with the condition that the values and derivatives of the wave function on the surface dividing the internal and external regions be continuable into the internal region, Section IV gives the condition that the continuation into the external region give the correct asymptotic behavior. One can also say that Section IV gives Heisenberg's S matrix or Wheeler's collision matrix[3] in terms of the $\mathfrak{R}$ matrix obtained in Section III.

In Section V some general aspects of the results of the preceding sections are discussed. Also the form of the one-level resonance formula, which follows when all terms of Eq. (1), excepting one, can be assumed to be independent of energy, is derived.

II. THE INTERNAL AND EXTERNAL REGIONS OF CONFIGURATION SPACE

Qualitatively, the internal region of the configuration space is characterized by the condition that all particles are relatively close together, the external region by the requirement that the system is well separated into two sub-systems. The forces between these sub-systems are either entirely absent or, if present, of such a nature that the internal structure of the sub-systems is not affected. The boundary between the internal and external regions will be called S.

For a more exact and quantitative formulation we must start with a few preliminaries.[4] Let us consider a typical nuclear reaction

$$\mathrm{Li^7+H^1}\rightarrow\begin{cases}\mathrm{Li^7+H^1}\\ \mathrm{Be^7}+n\\ \mathrm{Li^6+H^2}\\ \mathrm{He^4+He^4}\end{cases}\qquad(A)$$

The various reaction products which appear on the right side will be called "alternatives." Thus $\mathrm{He^4+He^4}$ is an alternative of the reaction (A). The pair $\mathrm{Li^6+H^2}$ represents not one but several alternatives, corresponding to the different possible states of polarization of the spins of $\mathrm{Li^6}$ and of $\mathrm{H^2}$. Since both these spins are 1, the total possible number of polarizations is $3\times3=9$, and the third pair of (A) represents 9 alternatives. The pair $\mathrm{Li^7+H^1}$ can be formed so that $\mathrm{Li^7}$ is in the normal state or in the first excited state. In the former case, the spin is $\frac{3}{2}$, giving $4\times2=8$ alternatives, in the latter case probably $\frac{1}{2}$, giving $2\times2=4$ alternatives. The same holds of the $\mathrm{Be^7}+n$ pair. Altogether, the reaction (A) is, in the energy region in which the above described end products are possible, an $(8+4)+(8+4)+9+1=34$ alternative reaction. It is desirable, furthermore, to consider, along with the reactions (A), all the reactions in which any of the end products of (A) is the initial state. These are, in the present instance, 34×34 reactions.

[3] J. A. Wheeler, Phys. Rev. **52**, 1107 (1937); W. Heisenberg, Zeits, f. Physik **120**, 513, 673 (1943); C. Moller, I. D. Kgl. Danske Vid. Sels. Mat. Phys. Med. **23**, 1 (1945).

[4] The definition of "alternatives" which follows is not quite the same as that used in Proc. Nat. Acad. **32**, 302 (1946).

Some of these are, of course, not real reactions but scattering processes.

There is a certain arbitrariness in the definition of the states of polarization of the pair Li^6+H^2, for instance. We shall use the following convention: From the spin wave functions of the pair we build such a linear combination that the composite angular momentum of the pair is definite. Similarly, the component of this angular momentum in a given direction (usually the Z direction) shall have a definite value. The different alternatives will be distinguished by two indices, s and ν. The former determines the nature and state of excitation of the pair together with the angular momentum resulting from the spins of the pair. The magnitude of this resultant angular momentum will be denoted by j_s. The index ν gives the component of this angular momentum in the Z direction. Neither $j_s\hbar$ nor $\nu\hbar$ is necessarily the total angular momentum or the Z component of total angular momentum of the system because they do not include the angular momentum of the motion of the nuclei, which forms the pair s, with respect to their common center of mass. This is, to be sure, zero in a head-on collision, but is finite in general.

The product of the normalized wave functions of the two nuclei He^4+He^4 will be denoted by ψ_ν if s designates the pair He^4+He^4. In general, the $\psi_{s\nu}$ will not be a simple product but a linear combination of such products, which will be assumed, in all cases, to be normalized:

$$\int |\psi_{s\nu}|^2 di_s = 1, \tag{2}$$

where di_s denotes integration over the internal coordinates of the nuclei which make up the pair s. It is probably unnecessary to mention that $\psi_{s\nu}$ is independent of the energy with which these particles collide or separate. In addition to (2), one can assume[5] that $\psi_{s\nu}$ is real in the sense that

$$K\psi_{s\nu} = -i^{2\nu}\psi_{s-\nu}, \tag{3}$$

where K implies the transition to the conjugate imaginary and multiplication with the imaginary spin operator (σ_y) of all the elementary particles in the two nuclei. The point of the normalization (3) is that the scalar product of two functions, normalized by (3), is real. It is zero if the j value of the two functions is different, or if their ν values are different. If the two j and ν are the same, the scalar product is independent[6] of ν and one can argue[5]

$$(f_\nu, g_\nu) = (Kg_\nu, Kf_\nu) = (i^{2\nu}g_{-\nu}, i^{2\nu}f_{-\nu})$$
$$= (g_{-\nu}, f_{-\nu}) = (f_{-\nu}, g_{-\nu})^*, \tag{4}$$

However, because of the last statement (f_ν, g_ν) is also equal to $(f_{-\nu}, g_{-\nu})$; it is equal to its conjugate complex and hence real.

We now can state more accurately what we mean by external and internal parts of the configuration space. In the external part, the most general solutions of the quantum-mechanical equations with a definite energy are linear combinations of functions of the form

$$F_s(r_s, \Omega_s)\psi_{s\nu}(i_s). \tag{5}$$

In this, $\psi_{s\nu}$ is one of the functions described above, i_s denoting the internal coordinates of the nuclei which make up the pair s. The r_s and Ω_s denote length and direction of the vector connecting the nuclei of the pair s. In other words, the system is in one of the alternate states (A) which the reaction can yield. The F_s is a solution of the Schrödinger equation in three-dimensional space with the potential which acts between the pair s. The external region is so defined that the interaction of the nuclei which make up the different pairs can already be represented by a potential. Clearly, F_s is independent of ν. The internal region is the remaining part of configuration space.

It may be well to remark here that the size of the internal region is not defined; the above gives it only a minimum size. It is always possible to add to the internal region part of the configuration space which could be in the external region. One will try, however, for reasons which will become clear later, to make the internal region as small as possible. It should be noted, furthermore, that the size of the internal region is a

[5] E. P. Wigner, Göttinger Nachr. **31**, 546 (1932). Actually, the normalization used in this paper is somewhat awkward since (3) implies that a function ψ_{s0}, which is real in the sense (3), is imaginary in the usual sense. However, this is purely a matter of convention and plays, in fact, very little part in the following. The spins of the particles make the following derivation appear much more complicated than it actually is. If the spins of all the particles participating in the reaction were zero, all j_s would vanish; $s(j_s, l)_{Jm} = s(0, l)_{Jm} = \delta_{lJ}$ would hold, and all formulae would be considerably simplified.

[6] E. P. Wigner, *Gruppentheorie* (Edwards Brothers, Ann Arbor, 1944), Chapter XII.

function of the energy range which one considers. With increasing total energy of the system, the number of excited states of the product nuclei which one has to take into account will also increase, and so will the distance at which these excited nuclei interact intimately. At the energy at which three or more free product nuclei can be formed, the present considerations lose validity.

Since $F_s(r_s, \Omega_s)$ obeys a second-order partial differential equation in three-dimensional space, it is completely determined in that part of the three-dimensional space which corresponds to the external region, if its value and normal derivative at the surface S of that region are given. It is practical, therefore, to choose surfaces $r_s = a_s$ to form the boundary between these regions. Since, furthermore, the Schrödinger equation for F_s has a spherically symmetric potential, its general solution is a linear combination of functions of the form

$$r_s^{-1}\mathfrak{s}_{sl}(r_s)P_{lm}(\Omega_s) \quad \text{and} \quad r_s^{-1}\mathfrak{c}_{sl}(r_s)P_{lm}(\Omega_s). \tag{6}$$

The $P_{lm}(\Omega_s)$ are the well-known spherical harmonics giving, to the relative motion of the pair s, the value lh for the magnitude of the angular momentum and the value mh for its Z-component. We assume that the P_{lm} are normalized if integrated over the surface of the unit sphere, and that they obey a condition similar to (3):

$$P_{lm}(\Omega)^* = -(-)^m P_{l-m}(\Omega). \tag{7}$$

The $\mathfrak{s}_{sl}(r_s)$ and the $\mathfrak{c}_{sl}(r_s)$ are solutions of the radial Schrödinger equation which applies to F_s. These are chosen so that at $r_s = a_s$,

$$\mathfrak{s}_{sl}(a_s) = 0, \qquad \mathfrak{c}_{sl}(a_s) = (M_s/\hbar)^{\frac{1}{2}},$$
$$\frac{d}{dr_s}\mathfrak{s}_{sl}(a_s) = \left(\frac{M_s}{\hbar}\right)^{\frac{1}{2}}, \quad \frac{d}{dr}\mathfrak{c}_{sl}(a_s) = -\frac{l}{a_s}\left(\frac{M_s}{\hbar}\right)^{\frac{1}{2}}. \tag{8}$$

M_s is the reduced mass of the pair s. Evidently, $\mathfrak{s}$ and $\mathfrak{c}$ depend not only on the energy but also on the position $r_s = a_s$ of the boundary between internal and external regions; P_{lm} is independent of both. The notations $\mathfrak{s}$ and $\mathfrak{c}$ were chosen to manifest the analogy with the functions $(M/\hbar)^{\frac{1}{2}}k^{-1}\sin k(r-a)$, and $(M/\hbar)^{\frac{1}{2}}\cos k(r-a)$ into which $\mathfrak{s}$ and $\mathfrak{c}$ go over if the angular momentum $l=0$, and if there are no forces acting in the external region between the particles of the pair s.

The boundary conditions (8) were chosen with a view to making the behavior of $\mathfrak{s}$ and $\mathfrak{c}$ simple for small kr. For small kr, the two simplest solutions of the radial wave equation behave as r^{l+1} and r^{-l}. The latter satisfies the boundary condition for $\mathfrak{c}$. The corresponding boundary condition for $\mathfrak{s}$ would read $\mathfrak{s}_{sl}(a_s) = (M_s/\hbar)^{\frac{1}{2}}a_s/(l+1)$. Since this is a small quantity, it was replaced by 0, which also gave some formal simplifications.

The last preliminary step is the formation of wave functions which have definite total angular momenta which include both the spins of the particles of the pair s and the momentum of their relative motion. This can be done by the coefficients $s_{J\nu m}^{(jl)}$, well known from the vector-addition model[7]

$$\begin{aligned}\mathfrak{D}_{sl\mu}{}^J(r_s, \Omega_s, i_s) &= \textstyle\sum_m s(j_s, l)_{J\mu-m m} r_s^{-1} \\ &\quad \times \mathfrak{s}_{sl}(r_s)P_{lm}(\Omega_s)\psi_{s\mu-m}(i_s), \\ \mathfrak{V}_{sl\mu}{}^J(r_s, \Omega_s, i_s) &= \textstyle\sum_m s(j_s, l)_{J\mu-m m} r_s^{-1} \\ &\quad \times \mathfrak{c}_{sl}(r_s)P_{lm}(\Omega_s)\psi_{s\mu-m}(i_s).\end{aligned} \tag{9}$$

The symbols $\mathfrak{D}$ and $\mathfrak{V}$ were chosen because $\mathfrak{D}$ has a finite derivative, $\mathfrak{V}$ a finite value on the boundary of the internal and external regions. Both $\mathfrak{D}$ and $\mathfrak{V}$ are solutions of the quantum-mechanical equation in the external region for a stationary state with energy E. They represent states with a total angular momentum J, and a Z component μ (zero linear momentum), and they both are real in the sense that they satisfy the equations,

$$K\mathfrak{D}_{sl\mu} = -i^{2\mu}\mathfrak{D}_{sl-\mu}, \quad K\mathfrak{V}_{sl\mu} = -i^{2\mu}\mathfrak{V}_{sl-\mu}. \tag{10}$$

As a result of the normalization of $\mathfrak{s}_{sl}$ and $\mathfrak{c}_{sl}$ as given by (8), it follows that on the surface S

$$\frac{\partial \mathfrak{D}_{sl\mu}{}^J}{\partial r_s} = \mathfrak{V}_{sl\mu}{}^J \text{ (on } S). \tag{11}$$

A second relation which will be useful in the next section is

$$\int \mathfrak{V}_{sl\mu}{}^{J*}\mathfrak{V}_{s'l'\mu}{}^J dS = \delta_{ss'}\delta_{ll'}(M_s/\hbar), \tag{12}$$

which is a consequence of (8), the orthogonality

[7] Reference 6, Chapter XVII, Section 6. The number of alternatives, as defined in the paper of reference 4, is the number of different pairs s, l for a given J. It is also the number of dimensions of the matrix $\mathfrak{R}$ which will be defined in Section III.

of the P_{lm} and the ψ_{sv}, and the unitary character of the s-coefficients (Chapter XVII of reference 6).

It may be well to repeat that the $s(j,l)_{J\mu-mm}$, the P_{lm}, and the ψ_{sv} are independent both of the energy E and also of the location a_s of the boundary between external and internal regions. The δ_{sl} and $\mathfrak{C}_{sl}$ depend on both. This completes the preliminary work for the rest of the development.

III. THE $\mathfrak{R}$ MATRIX

The general solution of the quantum-mechanical equations in the external region is a linear combination of the $\mathfrak{D}$ and $\mathfrak{V}$ of (9) with arbitrary coefficients. The purpose of the present section is to derive relations between these coefficients which guarantee that the solution can be continued into the internal region to give a singularity-free solution of the equations in that region also. Since the coefficients of the $\mathfrak{D}$ determine the derivative of the wave function on the surface S which separates the external and internal regions, and since the coefficients of the $\mathfrak{V}$ do likewise for the value of the wave function, the relations between these coefficients give also the relations between derivative and value of the wave function which must hold on the surface S in order that the continuation of the wave function into the internal region be possible.

Since the quantum-mechanical equations are linear, it is sufficient to determine a set of basic solutions out of which the general solution, and in particular the one fitting the experimental conditions, can be obtained by superposition. We chose these wave functions so that they represent states with definite values of the total angular momentum J and its Z-component μ. These will be, in the external region, superpositions of the $\mathfrak{D}$ and $\mathfrak{V}$ with a single J and μ. We may drop, therefore, for this section, the superscript J.

There are as many linearly independent states with definite J and μ (and definite energy) as the indices s and l can assume values. (This is equal to the number of alternatives, as defined in reference 4. The index l can assume every integer value between $|J-j_s|$ and $J+j_s$.) We shall define our basic solutions so that they contain only one $\mathfrak{D}$; the coefficients of the $\mathfrak{V}$ are then determined:

$$\varphi_{sl\mu}=\mathfrak{D}_{sl\mu}+\sum_{s'l'}R_{sl;s'l'}\mathfrak{V}_{s'l'\mu}. \tag{13}$$

Equation (13) holds in the external region but φ can be continued into the internal region. $\mathfrak{R}$ depends on the energy and on J but is independent of μ. Applying K to (13) one obtains by (10)

$$-K\varphi_{sl\mu}=i^{2\mu}\mathfrak{D}_{sl-\mu}+\sum_{s'l'}R_{sl;s'l'}{}^{*}i^{2\mu}\mathfrak{V}_{s'l'-\mu}. \tag{14}$$

Since $K\varphi$ is also a solution of the quantum-mechanical equations,[5] (14) is evidently $i^{2\mu}\varphi_{sl-\mu}$, and since $\mathfrak{R}$ is independent of μ,

$$R_{sl;s'l'}{}^{*}=R_{sl;s'l'}, \tag{15}$$

i.e., the elements of $\mathfrak{R}$ are real.

The object of this section is to determine the coefficients R as functions of the energy. For this purpose we consider those solutions $X_{\lambda\mu}$ of the quantum-mechanical equations in the internal region which satisfy the boundary conditions at the surface S,

$$-\frac{l+1}{a_s}\int X_{\lambda\mu}{}^{*}P_{lm}(\Omega_s)\psi_{sv}dS = \int \mathrm{grad}_n X_{\lambda\mu}{}^{*}P_{lm}(\Omega_s)\psi_{sv}dS,$$

where grad_n is the component of the gradient normal to S. The $X_{\lambda\mu}$ thus satisfy the same boundary condition as the $\mathfrak{V}_{sl\mu}$. The characteristic value problem for the $X_{\lambda\mu}$ is Hermitean, and $X_{\lambda\mu}$ can be assumed to form a complete set of orthonormal functions. Furthermore, since the problem defining the $X_{\lambda\mu}$ does not prefer any direction in ordinary space, a J and μ can be defined and $X_{\lambda\mu}$ assumed to be real in the sense of (3). The characteristic value of $X_{\lambda\mu}$ will be denoted by[8] E_λ.

[8] It should be noted that this is a well-defined boundary value problem even though some of the E_λ fall outside the energy region in which the formulae are valid. That region applies to E and not to the E_λ. P. L. Kapur and R. Peierls, Proc. Roy. Soc. **A166**, 277 (1937) also introduce an orthogonal system to express the wave functions in what corresponds to our internal region. As a result, there are many common features between their treatment and ours. However, their boundary condition depends on the energy so that they use, in effect, a different set of expanding functions for every energy. As a result, the "constants" in their equations are only approximately independent of energy, and this dependence makes it quite difficult to derive e.g., the proportionality of the particle widths in the one-level formula to the velocity. The complicated nature of the relation of their constants to those used here is illustrated in Fig. 2 of reference 1b. On the other hand, their constants have a closer relation to the observable cross sections than ours.

If one applies Green's theorem to $\varphi_{sl\mu}$ and $X_{\lambda\mu}$, the terms in the surface integral which contain the $\mathfrak{U}$ drop out by virtue of the boundary condition imposed on the $X_{\lambda\mu}$, and one has

$$-\frac{\hbar^2}{2M_s}\int X_{\lambda\mu}^*\frac{\partial}{\partial r_s}\mathfrak{D}_{sl\mu}dS = (E-E_\lambda)\int X_{\lambda\mu}^*\varphi_{sl\mu}dI. \quad (16)$$

The last integral has to be extended over the internal region. The left side assumes[9] that only those $\mathfrak{D}$ and $\mathfrak{U}$ have to be considered on the part of S which is given by $r_{s'}=a_{s'}$ which have the first index s'.

Introducing (11) into (16) we obtain for its left side

$$-\frac{\hbar^2}{2M_s}\int X_{\lambda\mu}^*\mathfrak{U}_{sl\mu}dS=-\left(\frac{\hbar}{2}\right)^{\frac{1}{2}}\gamma_{\lambda sl}; \quad (17)$$

the right side defines the γ which is independent of E (and of μ) and, as the scalar product of two real functions, is also real because of (4). Since the $X_{\lambda\mu}$ form an orthonormal set, we can write for the internal region

$$\varphi_{sl\mu}=\sum_\lambda A_{sl\lambda}X_{\lambda\mu}, \quad (18)$$

whence (16) gives

$$A_{sl\lambda}=\left(\frac{\hbar}{2}\right)^{\frac{1}{2}}\frac{\gamma_{\lambda sl}}{E_\lambda-E}. \quad (19)$$

The energy dependence of the $\mathfrak{R}$-matrix could now be obtained by a development which closely parallels that of reference 1. In this method a second application of Green's theorem to the functions $\varphi_{sl\mu}$ and $\varphi_{s'l'\mu'}$, for the different energies E and E', is made. The evaluation of the surface integral involved is obtained by neglecting on that part of the surface which is given by $r_t=a_t$, all $\mathfrak{D}$ and $\mathfrak{U}$ terms the first index of which is not t. The result of this procedure,

$$R_{sl;s'l'}=\sum_\lambda\frac{\gamma_{\lambda sl}\gamma_{\lambda s'l'}}{E_\lambda-E}+R_{sl;s'l'}(\infty) \quad (20)$$

where $R_{sl;s'l'}(\infty)$ is an arbitrary real-symmetric matrix independent of the energy, is a generalization of Eq. (33a) of reference 1b.

The $\mathfrak{R}$-matrix may also be obtained by the requirement that $\varphi_{sl\mu}$ be continuous at the boundary S. This condition leads to the above equation with $R(\infty)=0$. Since $\mathfrak{D}$ is zero at the boundary we have as the condition for continuity from (13), (18), and (19)

$$\left(\frac{\hbar}{2}\right)^{\frac{1}{2}}\sum_\lambda\frac{\gamma_{\lambda sl}}{E_\lambda-E}X_{\lambda\mu}=\sum_{s''l''}R_{sl;s''l''}\mathfrak{U}_{s''l''\mu}. \quad (21)$$

If both sides are multiplied by $-(\hbar^2/2M_s)\mathfrak{U}_{s'l'\mu}^*$ and integrated over the boundary S we have, on making use of (17),

$$-\left(\frac{\hbar}{2}\right)\sum_\lambda\frac{\gamma_{\lambda sl}\gamma_{\lambda s'l'}}{E_\lambda-E}=-\frac{\hbar^2}{2M_{s'}}\sum_{s''l''}R_{sl;s''l''}\times\int\mathfrak{U}_{s''l''\mu}\mathfrak{U}_{s'l'\mu}^*dS. \quad (22)$$

The orthogonality properties of the $\mathfrak{U}_{sl\mu}$, (12), reduce this equation to

$$R_{sl;s'l'}=\sum_\lambda\frac{\gamma_{\lambda sl}\gamma_{\lambda s'l'}}{E_\lambda-E}. \quad (23)$$

Note that $\mathfrak{R}$ in addition to being real is symmetric. In the matrix notation used in reference 1 Eq. (23) becomes[10]

$$\mathfrak{R}(E)=\sum_\lambda\frac{\gamma_\lambda\times\gamma_\lambda}{E_\lambda-E}. \quad (24)$$

Although hardly any assumptions enter into (24), the class of functions which can be brought into the form (24) has some remarkable properties. Let us consider first the case of a single alternative reaction with spins zero in which case both the matrices $\mathfrak{R}$ and the vectors γ be-

[9] This is the condition which gives the effective lower limit to the size of the internal region. It shows, in particular, that the size of the internal region becomes increasingly large as one approaches the energy at which a new pair of reaction products is about to become energetically possible. This case needs, therefore, separate investigation.

[10] Concerning the derivation given above, which leads to the more specific formula (23) or (24), it is well to remark that it is based on the convergence of the series of (18) at the boundary S. One can prove the convergence of this series under certain simplifying restrictions, and we are convinced that (18) converges also in general. We point this out specifically because it is easy to see that the series of the normal derivatives of the right side of (18) does not converge to the derivative of the left side. In finding the present derivation the main difficulty was to realize that (18) is a correct equation even at the surface S but that the equation obtained by differentiating it term by term is incorrect.

come numbers. Then $\Re(E)$ has the following properties:[11]

(i) All its odd derivatives are positive wherever they exist (i.e., except at the points E_λ).

(ii) All its derivatives satisfy the inequality

$$(R^{(n+m)}/(n+m)!)^2 \leqslant R^{(2n+1)}R^{(2m-1)}/(2n+1)!(2m-1)!$$

except at the points E_λ.

It is not known whether every real function which satisfies these conditions can be brought into the form (24). If there are several alternatives, $\Re$ is a matrix and (i) and (ii) hold for the quadratic form of $\Re$ with any real energy-independent vector.

Although it may be a mere mathematical curiosity, it will be mentioned that if $\Re$ has the form (24), the function

$$\frac{\Re}{1+\alpha\Re} \tag{25}$$

also can be brought into that form. In addition, of course, any linear combination of functions of the form (24) with positive coefficients has again that form.

IV. CONNECTION BETWEEN $\Re$ AND THE COLLISION MATRIX

The last two equations, (23) and (24), contain the major result of the present article: they give in conjunction with (13) the connection between the derivative and the value of the wave function on the surface S which must hold if the wave function is to be continuable into the internal region. The real constants which appear in (23), i.e., the E_λ and the γ_λ, are energy independent although they differ for different total angular momenta J. In order to bring this out, the $\Re$ will be given an upper index J henceforth.

As far as the present derivation is concerned, it seems that the above constants can be entirely arbitrary. It is possible, however, that this is not the case and that there are relations between them (similar to the sum rules) which are always fulfilled.

The purpose of this section is to express the scattering and reaction cross sections in terms of $\Re^J$. For this purpose, we need the asymptotic behavior of the solutions $\mathfrak{D}$ and $\mathfrak{V}$ which are defined in (9) and occur in (13). Because of the real character of the $\mathfrak{s}$ and $\mathfrak{C}$ we can write

$$\begin{aligned}\mathfrak{s}_{sl}(r_s)&\rightarrow\tfrac{1}{2}i(A_{sl}v_s^{-\frac{1}{2}}\exp(-ik_sr_s)\\&\qquad-A_{sl}^*v_s^{-\frac{1}{2}}\exp(ik_sr_s)),\\ \mathfrak{C}_{sl}(r_s)&\rightarrow\tfrac{1}{2}(B_{sl}\omega_{sl}^*v_s^{-\frac{1}{2}}\exp(-ik_sr_s)\\&\qquad+B_{sl}\omega_{sl}v_s^{-\frac{1}{2}}\exp(ik_sr_s)).\end{aligned} \tag{26}$$

The A, B, and ω are energy-dependent constants; B and ω can be assumed to be positive real, and of modulus 1, respectively. A is complex in general. The reason for the notation adopted in (26) will be apparent later. The $v_s=\hbar k_s/M_s$ is the relative velocity of the particles of the pair s at infinity, so that the $v_s^{-\frac{1}{2}}\exp(\pm ik_sr_s)$ corresponds to unit flux. Since the $\mathfrak{s}_{sl}$ and $\mathfrak{C}_{sl}$ satisfy the same second-order differential equation, $\mathfrak{C}_{sl}d\mathfrak{s}_{sl}/dr_s-\mathfrak{s}_{sl}d\mathfrak{C}_{sl}/dr_s$ is independent of r_s. As the value of this expression is $M_s/\hbar$ at $r_s=a_s$ (Eq. (8)), it follows that

$$B_{sl}\omega_{sl}A_{sl}+B_{sl}\omega_{sl}^*A_{sl}^*=2. \tag{27}$$

The B_{sl}, ω_{sl}, and A_{sl} may be considered as diagonal elements of the diagonal matrices $\mathfrak{B}$, ω, and $\mathfrak{A}$. They will play roles similar to the various powers of k in earlier articles.[1] With this notation, (27) reads

$$\mathfrak{B}\omega\mathfrak{A}+\mathfrak{B}\omega^*\mathfrak{A}^*=2, \tag{28}$$

so that one can also write

$$\mathfrak{B}\omega\mathfrak{A}=1-i\mathfrak{C},\quad \mathfrak{B}\omega^*\mathfrak{A}^*=1+i\mathfrak{C}, \tag{29}$$

where $\mathfrak{C}$ is a real diagonal matrix. It will be assumed that the $\mathfrak{s}$ and $\mathfrak{C}$ are known functions of r. Hence the $\mathfrak{A}$, ω, and $\mathfrak{B}$ will be energy dependent but known quantities. We shall further use the abbreviations I_{srlm} and E_{srlm} for those solutions of the quantum-mechanical equations in the external region which correspond to incident and emerging waves. Their asymptotic behavior is given by

$$\begin{aligned}I_{srlm}&\rightarrow\psi_{sr}(i_s)P_{lm}(\Omega_s)v_s^{-\frac{1}{2}}r_s^{-1}\exp(-ik_sr_s),\\ E_{srlm}&\rightarrow\psi_{sr}(i_s)P_{lm}(\Omega_s)v_s^{-\frac{1}{2}}r_s^{-1}\exp(ik_sr_s).\end{aligned} \tag{30}$$

They are, of course, functions of the form (5).

The asymptotic form of the $\mathfrak{s}$ and $\mathfrak{C}$ is given by (26), the $\mathfrak{D}$ and $\mathfrak{V}$ are expressed in terms of

[11] The following is the third property which was referred to in reference 4.

the $\mathfrak{s}$ and $\mathfrak{C}$ in (9), and the φ are expressed in terms of the $\mathfrak{D}$ and $\mathfrak{V}$ in (13). One obtains by means of these equations, for the φ in terms of the incoming and outgoing waves I and E,

$$\varphi_{sl\mu}=\tfrac{1}{2}\sum_{s'l'm}(\mathfrak{R}^J\mathfrak{B}\omega^*+i\mathfrak{A})_{sl;s'l'}\times s(j_{s'},l')_{J\mu-mm}I_{s'\mu-ml'm}+\tfrac{1}{2}\sum_{s'l'm}(\mathfrak{R}^J\mathfrak{B}\omega-i\mathfrak{A}^*)_{sl;s'l'}\times s(j_{s'},l')_{J\mu-mm}E_{s'\mu-ml'm}. \quad (31)$$

One can obtain from (31), by linear combination, a solution in which only one type of incident wave is present:

$$2\sum_{s'l'}\{(\mathfrak{R}^J\mathfrak{B}\omega^*+i\mathfrak{A})^{-1}\}_{sl;s'l'}\varphi_{s'l'\mu}=\sum_m s(j_s,l)_{J\mu-mm}I_{s\mu-mlm}-\sum_{s'l'm}u_{sl;s'l'}{}^J s(j_{s'},l')_{J\mu-mm}E_{s'\mu-ml'm}, \quad (32)$$

where

$$u_{sl;s'l'}{}^J=-\{(\mathfrak{R}^J\mathfrak{B}\omega^*+i\mathfrak{A})^{-1}\times(\mathfrak{R}^J\mathfrak{B}\omega-i\mathfrak{A}^*)\}_{sl;s'l'}. \quad (33)$$

From this, one obtains by means of the orthogonality relation of the coefficients s (Eq. (28), Chapter XVII of reference 6) a solution in which only one incident beam occurs. This becomes, in the external region,

$$I_{svlm}-\sum_{s'v'l'm'}U_{svlm;s'v'l'm'}E_{s'v'l'm'}, \quad (34)$$

in which

$$U_{svlm;s'v'l'm'}=\sum_J s(j_s,l)_{Jvm}u_{sl;s'l'}{}^J\times s(j_{s'},l')_{Jv'm'}\delta_{m+v,\,m'+v'} \quad (35)$$

is the ordinary collision matrix. The last factor of (35) expresses the conservation law for the Z component of the angular momentum since v is the Z component of the spins, and m is the Z component of the angular momentum of the relative motion of the two particles. The conservation law for the absolute value of the angular momentum is not immediately evident from the form (35) but is included in the s factors.

The symmetric and unitary nature of the $\mathfrak{U}$ would follow at once from the orthogonality relations of the s coefficients if the symmetric unitary nature of the $\mathfrak{u}^J$ matrices were evident. If the spins of the particles are all zero, the $\mathfrak{U}$ matrix in fact becomes, in the sense of reference 5, identical with $\delta_{ll'}$ times the $\mathfrak{u}^l$ matrix. It is desirable, for these reasons, to bring the $\mathfrak{u}^J$ into a form in which their unitary and symmetric nature is at once apparent.

For this purpose we express $\mathfrak{A}$ and $\mathfrak{A}^*$, by means of (29), in terms of the $\mathfrak{B}$, ω, and $\mathfrak{C}$:

$$\mathfrak{u}=(\mathfrak{R}\mathfrak{B}\omega^*+\mathfrak{C}\mathfrak{B}^{-1}\omega^*+i\mathfrak{B}^{-1}\omega^*)^{-1}\times(-\mathfrak{R}\mathfrak{B}\omega-\mathfrak{C}\mathfrak{B}^{-1}\omega+i\mathfrak{B}^{-1}\omega). \quad (36)$$

The superscript J has been omitted on both sides. For the first factor one can write, since the $\mathfrak{B}$, ω, $\mathfrak{C}$ all commute,

$$[i\mathfrak{B}^{-1}(-i\mathfrak{B}\mathfrak{R}\mathfrak{B}-i\mathfrak{C}+1)\omega^*]^{-1}=-i\omega(1-i\mathfrak{B}\mathfrak{R}\mathfrak{B}-i\mathfrak{C})^{-1}\mathfrak{B}. \quad (37)$$

The second factor can be transformed in a similar way to give $i\mathfrak{B}^{-1}(i\mathfrak{B}\mathfrak{R}\mathfrak{B}+i\mathfrak{C}+1)\omega$. Hence

$$\mathfrak{u}^J=\omega\frac{1+i\mathfrak{B}\mathfrak{R}^J\mathfrak{B}+i\mathfrak{C}}{1-i\mathfrak{B}\mathfrak{R}^J\mathfrak{B}-i\mathfrak{C}}\omega. \quad (38)$$

It is permissible to use the fraction sign in (38) since both numerator and denominator depend on a single matrix: $\mathfrak{B}\mathfrak{R}^J\mathfrak{B}+\mathfrak{C}$. Since this matrix is evidently symmetric and Hermitean, the fraction is symmetric and unitary and it remains such if multiplied both in front and in back by the unitary matrix ω. Equations (35), (38), and (24) give the collision matrix in terms of real parameters. Although the values of these parameters are dependent on a_s, the collision matrix, which is a property of the physical system, must itself be independent of these quantities.

The wave function describing a collision experiment may be obtained by well-known procedures in terms of the collision matrix $\mathfrak{U}$. The plane wave representing particles of type s moving along the Z axis has the form

$$iv_s^{-\frac{1}{2}}\exp(ik_sz_s)\psi_{sv}(i_s)=\frac{\pi^{\frac{1}{2}}}{ik_s}\sum_l(2l+1)^{\frac{1}{2}}(E_{svl0}-(-)^lI_{svl0}). \quad (39)$$

This wave is normalized to unit current of the s particles per unit area normal to the beam. The normalization of the P_{l0}, which are used in the

definition of E and I, is given by

$$P_{l0}(\Omega_s)=i((2l+1)/4\pi)^{\frac{1}{2}}P_l(\cos\theta_s),$$

where the $P_l(\cos\theta_s)$ are the usual Legendre polynomials.

A continuable solution with the same incident waves as (39) may be formed by taking an appropriate linear combination of solutions of the type (34):

$$-\frac{\pi^{\frac{1}{2}}}{ik_s}\sum_l(-)^l(2l+1)^{\frac{1}{2}}\times\Big(I_{srl0}-\sum_{s'r'l'm'}U_{srl0;\,s'r'l'm'}E_{s'r'l'm'}\Big). \quad (40)$$

The continuable solution which satisfies the boundary conditions for an experiment involving collisions between the s particles, is obtained from (40) by adding and subtracting the emerging waves of (39). The wave function describing the collision system, therefore, is

$$iv_s^{-\frac{1}{2}}\exp(ik_sz_s)\psi_{sr}(i_s)+\frac{\pi^{\frac{1}{2}}}{ik_s}\sum_{ls'r'l'm'}(2l+1)^{\frac{1}{2}}\times((-)^lU_{srl0;\,s'r'l'm'}-\delta_{srl0;\,s'r'l'm})E_{s'r'l'm'}, \quad (41)$$

where

$$\delta_{srl0;\,s'r'l'm'}=\delta_{ss'}\delta_{rr'}\delta_{ll'}\delta_{0m'}.$$

The density of the s' systems resulting from the collision is obtained by squaring the part of the sum in (41) which refers to these systems and integrating over the internal coordinates $i_{s'}$. The number per second of s' systems crossing a surface subtending a solid angle $d\Omega_{s'}$ at the collision center, is obtained from the density by multiplying with $r_{s'}{}^2v_{s'}d\Omega_{s'}$. This is the differential cross section for the collision between the systems characterized by s with the polarization specified by j_s and ν. The differential cross section is obtained by averaging the cross sections for all polarizations ν and adding together the cross sections for all possible ν'. This gives

$$d\sigma^{ss'}=\frac{\pi}{(2j_s+1)k_s^2}\sum_{rr'}\Big|\sum_{ll'm'}(2l+1)^{\frac{1}{2}}\times\{(-)^lU_{srl0;\,s'r'l'm'}-\delta_{srl0;\,s'r'l'm'}\}\times P_{l'm'}(\Omega_{s'})\Big|^2d\Omega_{s'}, \quad (42)$$

for the differential cross section for the production of s' systems in a collision between unpolarized s systems. Integration of (42) over $d\Omega_{s'}$ leads to the total cross section.

$$\sigma^{ss'}=\frac{\pi}{(2j_s+1)k_s^2}\sum_{rr'l'm'}\Big|\sum_l(2l+1)^{\frac{1}{2}}\times\{(-)^lU_{srl0;\,s'r'l'm'}-\delta_{srl0;\,s'r'l'm'}\}\Big|^2. \quad (43a)$$

If the $\mathfrak{U}$ is replaced by the $\mathfrak{u}^J$ by means of (35) this expression reduces, upon making use of the unitary character of the matrices formed by the s coefficients, to

$$\sigma^{ss'}=\frac{\pi}{(2j_s+1)k_s^2}\sum_{ll'J}\times(2J+1)|(-)^l\mathfrak{u}_{sl;\,s'l'}{}^J-\delta_{sl;\,s'l'}|^2. \quad (43b)$$

One should remember when using the formulae (42), (43) that s (and s') specify not only the nature of the subsystems which react (and are formed by the reaction) but also their state of excitation and the resultant of their spin angular momentum j_s (and $j_{s'}$). The cross section for the formation of a pair of nuclei without regard to the resultant $j_{s'}$ of their spins is given by summing (42) and (43) over all s' which refer to the same pair of nuclei. Similarly, if one is interested in the cross section of a pair designated by s' without regard to j_s, one must average (42) and (43) over all s (which now refer to a definite pair of nuclei). This may be done by adding together the $d\sigma^{ss'}$ or $\sigma^{ss'}$ for the possible values of s with the statistical weights $(2j_s+1)/\sum_s(2j_s+1)$.

V. DISCUSSION: THE GENERALIZED ONE-LEVEL FORMULA

The results of the preceding sections have very great generality inasmuch as they permit one to express all scattering and reaction cross sections in terms of the energy-independent parameters E_λ, $\gamma_{\lambda sl}$, etc. Their most unsatisfactory feature is that all these parameters depend on the arbitrary location of the boundary S of the internal region, i.e., on the constants a_s. Naturally the expressions (42) and (43) for the cross sections are independent of these quantities. It would be desirable to abstract from our representation of the

cross sections new concepts which have physical significance. Unfortunately, E_λ and $\gamma_{\lambda sl}$, since they depend on the a_s, cannot be given direct physical interpretation. Clearly, a close investigation of the dependence of the quantities E_λ, $\gamma_{\lambda sl}$ on the a_s is well warranted; such an investigation, however, has not yet been made.

Let us first choose the a_s as small as possible, i.e., choose an internal region which just barely satisfies the conditions enumerated in Section II. If we assume that $|X_{\lambda\mu}|^2$ is just about as great on S as inside S, the integral of $|X_{\lambda\mu}|^2$ over S will be of the order of magnitude of the reciprocal of the a_s. The integral of the $|\mathfrak{v}_{sl\mu}|^2$ over S is $M_s/\hbar$. As a result, $\gamma_{\lambda sl}$, the integral of the product of $X_{\lambda\mu}{}^*\mathfrak{v}_{sl\mu}$ over S, is by Schwartz's inequality limited by

$$\gamma_{\lambda sl} < \frac{\hbar}{(2M_s)^{\frac{1}{2}}}\left[\int |X_{\lambda\mu}|^2 dS\right]^{\frac{1}{2}} \approx \frac{\hbar}{(M_s a_{\min})^{\frac{1}{2}}}, \quad (44)$$

where $a_{\min}$ is a quantity of the order of the diameter of the compound nucleus. Actually the inequality sign in (44) is a very strong one and the comparison with observed neutron widths indicates[12] that the left side of (44) is usually a few thousand times smaller than the right side. (The relation between the $\gamma_{\lambda sl}$ and the level width will be given later in this section.) This is not surprising considering that any similarity between the $X_{\lambda\mu}$ and the $\mathfrak{v}_{sl\mu}$ would seem to be rather accidental. On the other hand, Eq. (44) suggests that the $\gamma_{\lambda sl}$ should be of the same order of magnitude for different s and l.

We shall now assume that the interaction of the particles of the pair s has, in the external region, no term which goes to infinity for $r_s \to 0$ except perhaps as Ze^2/r_s. If this is true, and if $k_s r_s \ll 1$, the $\mathfrak{v}_{sl\mu}$ defined in (9) will be proportional to r_s^{-l-1}, and the $X_{\lambda\mu}$ will have the same behavior near the surface given by $r_s = a_s$. Hence, $X_{\lambda\mu}$ which satisfies a boundary condition similar to (8) for a given a_s, will satisfy it also for another a_s as long as $k_{\lambda s} a_s \ll 1$. (k_s is the wave number of the separated pair s for the energy $E = E_\lambda$.) This shows that, as long as $k_{\lambda s} a_s \ll 1$, the E_λ are independent of the a_s. On the other hand, the $\gamma_{\lambda sl}$ will depend on a_s like a_s^{-l}, because the $X_{\lambda\mu}$ depends on r_s like r_s^{-l} in the neighborhood of $r_s = a_s$. As a result of this and (44), we can write

$$\gamma_{\lambda sl} = \theta_{\lambda sl}\hbar/(M_s a_{\min})^{\frac{1}{2}}(a_{\min}/a_s)^l, \quad (45)$$

where $\theta_{\lambda sl}$ is in many cases a number of the order of 10^{-3}.

This last estimate of the γ will permit us to discuss the results of the preceding section under some simplifying assumptions. Since a complete discussion of those results would be tantamount to a discussion of scattering and reaction cross sections in general, this is all we can hope for at present.

For sake of simplicity, we shall consider only the $\mathfrak{U}^J$ of (38). In principle, it should always be easy to obtain $\mathfrak{U}$, and hence also the cross sections, from $\mathfrak{U}^J$ by means of (35). Thus, $U_{srlm;s'r'l'm'}$ is actually equal to $u_{sl;s'l'}{}^J\delta_{ll'}\delta_{mm'}$, if $j_s = 0$, i.e., if the spins of the colliding particles and of the reaction products both vanish (the ν and ν' as components of j_s and $j_{s'}$ are also zero in this case).

The difficulty in obtaining $\mathfrak{U}^J$ from $\mathfrak{R}^J$ is one of matrix multiplication or division. As was pointed out in the last section of reference 1b, the matrix algebra can be carried out simply only if $\mathfrak{R}$ is one or two dimensional, or if it is sufficient to restrict oneself to one or two terms in (24). These cases have been dealt with in reference 1b and will not be taken up again. We assume, instead, that one can replace all the terms of $\mathfrak{R}$, excepting one, by an energy-independent term:

$$\mathfrak{R}(E) = \frac{\boldsymbol{\gamma}_\lambda \times \boldsymbol{\gamma}_\lambda}{E_\lambda - E} + \mathfrak{R}_\infty. \quad (46)$$

This $\mathfrak{R}(E)$ has the same form which was obtained in reference 1a and consequently the following discussion shows a certain similarity with the one carried out there. In particular, it will lead to the generalized one-level formula obtained there, with the difference, however, that the orbital angular momenta of the particles will not be restricted to zero.

For convenience we introduce the abbreviations, $\mathfrak{B}\mathfrak{R}_\infty\mathfrak{B} + \mathfrak{C} = \mathfrak{C}'$, and $\mathfrak{B}\boldsymbol{\gamma}_\lambda = \boldsymbol{\beta}_\lambda$. Making use of the theorem $\mathfrak{M}(\mathbf{y}\times\mathbf{y})\mathfrak{N} = (\mathfrak{M}\mathbf{y}\times\mathfrak{N}\mathbf{y})$, if $\mathbf{y}$ is an arbitrary vector and $\mathfrak{N}$ a symmetric matrix we may write for (38)

$$\omega^{-1}\mathfrak{U}^J\omega^{-1} = \frac{1 + i[(\boldsymbol{\beta}_\lambda \times \boldsymbol{\beta}_\lambda)/(E_\lambda - E)] + i\mathfrak{C}'}{1 - i[(\boldsymbol{\beta}_\lambda \times \boldsymbol{\beta}_\lambda)/(E_\lambda - E)] - i\mathfrak{C}'}. \quad (47)$$

[12] L. J. Rainwater, W. W. Havens, C. S. Wu, and J. R. Dunning, Phys. Rev. **71**, 65 (1947); R. B. Sawyer, E. O. Wollan, K. C. Peterson, and S. Bernstein, Phys. Rev. **70** 791 (1946).

TABLE I. Coefficients in the cross-section formula (no interaction in the external region); $x_s = k_s a_s$.

l	B_{sl}	ω_{sl}	C_{sl}	$\Gamma_{\lambda sl}(\Re_{ss'}=0)$	$\Delta_{\lambda sl}(\Re_{ss'}=0)$
0	$k_s^{\frac{1}{2}}$	$\exp(-ix_s)$	0	$k_s\gamma_{\lambda s0}^2$	0
1	$k_s^{\frac{1}{2}}$	$\exp(-ix_s)$	$-\frac{1}{x_s}$	$\frac{k_s x_s^2\gamma_{\lambda s1}^2}{1+x_s^2}$	$-\frac{k_s x_s\gamma_{\lambda s1}^2}{1+x_s^2}$
2	$\frac{k_s^{\frac{1}{2}}}{x_s}(1+x_s^2)^{\frac{1}{2}}$	$-i\exp\{-i(x_s-\varphi_s)\}$ $(\varphi_s=\tan^{-1}x_s)$	$-\frac{1}{x_s^3}(3+2x_s^2)$	$\frac{k_s x_s^4\gamma_{\lambda s2}^2(1+x_s^2)}{(3+2x_s^2)^2+x_s^6}$	$\frac{-k_s x_s\gamma_{\lambda s2}^2}{\times\frac{(1+x_s^2)(3+2x_s^2)}{(3+2x_s^2)^2+x_s^6}}$

We shall try to choose a parameter η so that the numerator of (47) may be written

$$1+i[(\beta_\lambda\times\beta_\lambda)/(E_\lambda-E)]+i\mathfrak{C}'$$
$$=[1+i\mathfrak{C}'+i\eta(1-i\mathfrak{C}')^{-1}(\beta_\lambda\times\beta_\lambda)]$$
$$\times[1-i(1-i\mathfrak{C}')^{-1}(\beta_\lambda\times\beta_\lambda)/(E_\lambda-E)]. \quad (48)$$

Upon performing the multiplication and collecting terms, (48) reduces to

$$2(\beta_\lambda\times\beta_\lambda)=\eta[(E_\lambda-E)(\beta_\lambda\times\beta_\lambda)$$
$$-i(\beta_\lambda\times\beta_\lambda)(1-i\mathfrak{C}')^{-1}(\beta_\lambda\times\beta_\lambda)]. \quad (49)$$

If the elements of $(\beta_\lambda\times\beta_\lambda)(1-i\mathfrak{C}')^{-1}(\beta_\lambda\times\beta_\lambda)$ are written in terms of the individual matrices involved it is seen that

$$(\beta_\lambda\times\beta_\lambda)(1-i\mathfrak{C}')^{-1}(\beta_\lambda\times\beta_\lambda)=\xi(\beta_\lambda\times\beta_\lambda), \quad (50)$$

where ξ is given by the scalar product

$$\xi=(\beta_\lambda,\ (1-i\mathfrak{C}')^{-1}\beta_\lambda). \quad (51)$$

Introducing (50) into (49) we get

$$\eta=2/(E_\lambda-E-i\xi). \quad (52)$$

If now we factor $1-i\mathfrak{C}'$ out of the denominator of (47) so that both numerator and denominator have the common factor $[1-i(1-i\mathfrak{C}')^{-1}(\beta_\lambda\times\beta_\lambda)/(E_\lambda-E)]$, we may replace (47) by

$$\omega^{-1}\mathfrak{U}^J\omega^{-1}=\frac{1+i\mathfrak{C}'}{1-i\mathfrak{C}'}+\frac{2i}{E_\lambda-E-i\xi}$$
$$\times\{[(1-i\mathfrak{C}')^{-1}\beta_\lambda]\times[(1-i\mathfrak{C}')^{-1}\beta_\lambda]\}. \quad (53)$$

(In writing the last matrix of (53) we have made use of the symmetry of $(1-i\mathfrak{C}')^{-1}$ which follows from the symmetry of $\mathfrak{C}'$.)

It is convenient to introduce a vector α_λ defined by

$$\alpha_\lambda=(1-i\mathfrak{C}')^{-1}\beta_\lambda=(1-i\mathfrak{C}')^{-1}\mathfrak{B}\gamma_\lambda, \quad (54)$$

so that

$$\beta_\lambda=(1-i\mathfrak{C}')\alpha_\lambda=(1+i\mathfrak{C}')\alpha_\lambda^*; \quad (54a)$$

the last result follows from the reality of β_λ. By making use of (54) and (54a) we may divide ξ into its real and imaginary parts:

$$Re\,\xi=\tfrac{1}{2}\Gamma_\lambda=(\alpha_\lambda^*,\ \alpha_\lambda)=\sum_{sl}|\alpha_{\lambda sl}|^2=\tfrac{1}{2}\sum_{sl}\Gamma_{\lambda sl};$$
$$Im\,\xi=\Delta_\lambda=(\alpha_\lambda^*,\ \mathfrak{C}'\alpha_\lambda) \quad (55)$$

Γ_λ will play the role of a level width: the $2|\alpha_{\lambda sl}|^2=\Gamma_{\lambda sl}$ may be interpreted as the partial widths. As will be seen immediately, the Δ_λ represents a shift in the position of the resonance from E_λ. With the help of (54) and (55) we may rewrite (53) as

$$\mathfrak{U}^J=\omega\left(\frac{1+i\mathfrak{C}'}{1-i\mathfrak{C}'}\right)\omega+\frac{2i\omega(\alpha_\lambda\times\alpha_\lambda)\omega}{E_\lambda+\Delta_\lambda-E-\frac{1}{2}i\Gamma_\lambda}. \quad (56)$$

The total cross section (43b) may be obtained from the absolute squares of the elements of the matrix $(-)^l\mathfrak{U}^J-1$. The squares of the elements of the second matrix on the right of (56) represent the resonance part of the scattering or reaction. The elements of $(-)^l\omega(1+i\mathfrak{C}')(1-i\mathfrak{C}')^{-1}\omega-1$, which are slowly varying functions of the energy, give rise to what one may call "potential" scattering or reaction. The cross products represent the effects of interference between the resonance and potential terms. The potential term includes two contributions corresponding to the two terms of $\mathfrak{C}'$: the part which arises from $\mathfrak{C}$ alone repre-

sents the scattering (since $\mathfrak{C}$ is diagonal) of the incident particles which would be caused by the presence of an infinite positive potential within the internal region. The contribution of the $\mathfrak{B}\mathfrak{R}_\infty\mathfrak{B}$ represents the effect of all levels other than the level E_λ. It will in general produce both scattering and reaction terms.

If $\mathfrak{C}'$ is diagonal, the contribution to the total *reaction* cross section by the level E_λ is by (55), (56), and (43b)

$$\sigma^{ss'}=\frac{\pi}{(2j_s+1)k_s^2}\sum_{ll'}\frac{(2J+1)\Gamma_{\lambda sl}\Gamma_{\lambda s'l'}}{(E_\lambda+\Delta_\lambda-E)^2+\frac{1}{4}\Gamma_\lambda^2}. \tag{57}$$

Let us investigate now the dependence on a_s and energy of the different quantities which enter (56) and hence (57), at least in the case where the $\mathfrak{R}_\infty$ of (46) can be neglected. We consider for simplicity the case of no interaction in the external region. The $\mathfrak{C}_{sl}$ and $\mathfrak{s}_{sl}$ which satisfy (8) are easily computed; comparison of the results with Eqs. (26) and (29) leads to the results of Table I. In computing this table we made use of the relations

$$\tfrac{1}{2}\Gamma_{\lambda sl}=(B_{sl}\gamma_{\lambda sl})^2/(1+C_{sl}^2), \tag{58a}$$

$$\Delta_\lambda=\sum_{sl}\Delta_{\lambda sl};\quad \Delta_{\lambda sl}=\tfrac{1}{2}C_{sl}\Gamma_{\lambda sl}, \tag{58b}$$

$$\alpha_{\lambda sl}=(B_{sl}\gamma_{\lambda sl})^{-1}(\tfrac{1}{2}\Gamma_{\lambda sl}+i\Delta_{\lambda sl}), \tag{58c}$$

which follow from (55) and (54) when $\mathfrak{C}'$ is diagonal. The x_s in the table is an abbreviation for k_sa_s.

If the energy of the s systems is small and the a_s are taken small so that $k_sa_s\ll 1$, it is seen that the $\Gamma_{\lambda sl}$ depend on energy as $E^{(l+\frac{1}{2})}$. Moreover, since $\gamma_{\lambda sl}$ varies with a_s as a_s^{-1} (Eq. 45) it is seen that the $\Gamma_{\lambda sl}$, and hence the Γ_λ are approximately independent of a_s as long as a_s is small enough so that $k_sa_s\ll 1$. Under the conditions given, therefore, the $\Gamma_{\lambda sl}$ have physical significance. It is to be noted also that because of (45), the partial widths for the higher orbital angular momenta are related to the partial widths for $l=0$, as far as order of magnitude is concerned, by

$$\Gamma_{\lambda sl}\approx x_s^{2l}\Gamma_{\lambda s0}. \tag{59}$$

The Δ_λ is roughly proportional to E if x_s is small. From (59) and (58b) it follows that the order of magnitude of the $\Delta_{\lambda sl}$ is given by

$$\Delta_{\lambda sl}\sim -x_s\Gamma_{\lambda s0}(a_{\min}/a_s)^{2l}. \tag{60}$$

Thus the partial shifts are all very small and E_λ is practically independent of the a_s. As has already been mentioned, the fact that E_λ is essentially independent of a_s is a consequence of the boundary conditions which have been imposed on the $X_{\lambda\mu}$ and $\mathfrak{C}_{sl}$.

For small k_sa_s the elements of the first matrix on the right of (56) are approximately

$$(-)^l+\text{terms of order } x^{2l+1}, \tag{61}$$

from which it is seen that the contributions to the potential scattering, for small x, are small and that they decrease rapidly with increasing l.

The one-level formula which is essentially contained in Eq. (57), or in (56) and (43b), is only a rather special case of the general formula (38). If the approximation (46) is not permissible, (38) still contains a representation of the cross section even though it may not be possible to put it into so pragmatic a form as (57). Nevertheless, an evaluation of the cross section may still be possible in closed form, as evidenced e.g., in the two-level formulae and the formulae for two alternative reactions, given in reference 1b. However, in such cases it may not always be possible to associate large values of the cross sections with energies in the neighborhood of E_λ or to predict even the qualitative behavior of the cross section as a function of energy from a knowledge of the γ_λ and E_λ alone.

As an example, we consider the collision of systems with zero spins between which there is no interaction whatever, so that the scattering cross section vanishes for all E. The wave function for the free particles with $l=0$ may be put in the form of (13) if we take

$$R=k^{-1}\tan ka. \tag{62}$$

This may be written as a series of partial fractions in conformity with (23):

$$R=\sum_\lambda\frac{\gamma_\lambda^2}{E_\lambda-E}, \tag{63}$$

with

$$E_\lambda=\frac{\hbar^2}{2M}(2\lambda-1)^2\left(\frac{\pi}{2a}\right)^2;\qquad \gamma_\lambda=(-)^\lambda\left(\frac{\hbar^2}{Ma}\right)^{\frac{1}{2}}. \tag{64}$$

Of course these equations follow also from the formalism of Section III. Substitution of $\omega=\exp(-ika)$, $B=k^1$, $C=0$, as given for the case of no interaction in the external region (Table I), and R from (62) into (38) leads to $u^J=1$, i.e., to zero scattering cross section, as it must. However, this result appears as a cancellation of the effect of the resonance levels given in (64) with the effect of the deviation of ω from 1. Obviously the knowledge of the E_λ and γ_λ alone is insufficient to provide us with a picture of the variation of the cross section with energy. In fact, if one tries, e.g., to estimate the scattering cross section at low energies by using for R the first term in its expansion (63) one obtains about $0.1a^2$. This result is not so bad if one has chosen a small value of a. However, if one chooses a large a, as one is entirely at liberty to do formally, this gives a grossly inaccurate picture of the cross section. Only by considering the effect of all levels on R does one obtain the correct zero cross section.

This article is based on work performed under Contract No. w-35-058-eng-71 for the Manhattan Project at Clinton Laboratories.

PHYSICAL REVIEW VOLUME 72, NUMBER 1 JULY 1, 1947

Stress Relaxation across Grain Boundaries in Metals*

T'ING-SUI KÊ
Institute for the Study of Metals, The University of Chicago, Chicago, Illinois
(Received March 28, 1947)

In order to elucidate further the concept of relaxation of shear stress across grain boundaries in metals, the temperature dependence of internal friction and rigidity modulus of 99.991 percent aluminum have been measured as a function of frequency of torsional vibration and as a function of grain size of the specimen. It has been found that for the same specimen, an increase of frequency of vibration shifts the internal friction curve and the rigidity relaxation curve (Q^{-1} and G/G_U *versus* temperature) to higher temperatures; and when the frequency of vibration is kept constant, a change in grain size of the specimen has the same effect as a change of the frequency of vibration The observed internal friction and rigidity relaxation can be expressed as functions of the parameter $(\text{G.S.})\times f \times\exp(H/RT)$, where (G.S.) is the grain size or average grain diameter of the specimen, f is the frequency of vibration, and H is the heat of activation. It is shown that all these observed phenomena are necessary manifestations of the stress relaxation across grain boundaries arising from the viscous behavior of the grain boundaries in metals, which behavior has been demonstrated by previous anelastic-effect measurements.

1. INTRODUCTION

IT has been demonstrated[1] that the grain boundaries in metals behave in a viscous manner in the sense that they cannot sustain a shear stress. Thus, when an over-all stress, however small, is applied to a specimen, the shear stress across all grain boundaries will gradually relax. Because of this relaxation of shear stress, the stress no longer remains a unique function of the strain, and vice versa, in the conventionally elastic region, and this causes all kinds of anelastic effects. The locking effect of the grain edges and corners will insure that the over-all stress relaxation will be of limited extent for a fixed over-all strain. The maximum amount of macroscopic shear stress relaxation in 99.991 percent polycrystalline aluminum (average grain diameter = 0.03 cm) determined by four independent types of anelastic-effect measurements (namely, internal friction, temperature variation of rigidity modulus, creep under constant stress and stress relaxation at constant strain) is 33 percent, which agrees fairly well with the theoretical value of 36 percent[2] calculated by assuming the grain boundaries to be viscous.

It has also been shown that the rate of the stress relaxation across grain boundaries is a function of the temperature of measurement and

* This research was supported by ORI (Contract No. N6ori-20-IV).

[1] T. S. Kê, Phys. Rev. **70**, 105(A) (1946); *ibid.*, **71**, 142(A) and 533 (1947).

[2] C. Zener, Phys. Rev. **60**, 906 (1941).

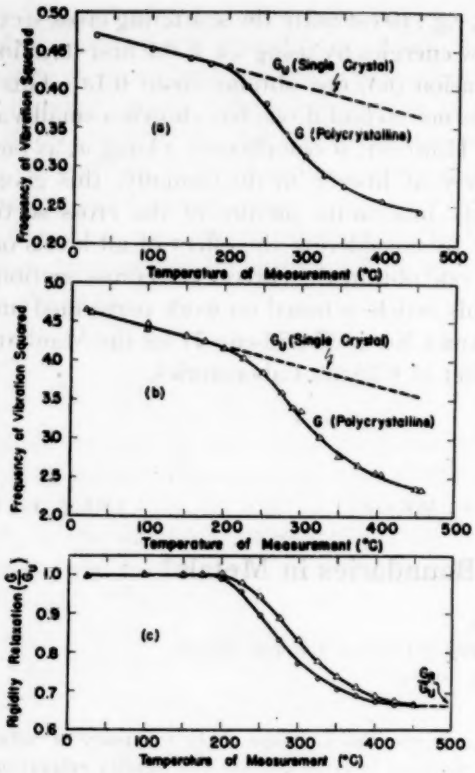

FIG. 1. Effect of frequency of vibration on rigidity and rigidity relaxation in aluminum (average grain diameter = 0.02 cm).
(a) frequency of vibration = 0.69 c.p.s. at room temperature;
(b) frequency of vibration = 2.16 c.p.s. at room temperature;
(c) rigidity relaxations for two frequencies of vibration: ⊙, 0.69 c.p.s.; △, 2.16 c.p.s.

has a heat of activation. This led to an estimation of the coefficient of viscosity at the grain boundary. The estimated value of the coefficient of viscosity for the grain boundary in 99.991 percent aluminum was found to be consistent with the experimentally determined value of molten aluminum at the same temperature.

The concept of stress relaxation across grain boundaries leads to predications as to the effect of grain size and frequency of vibration on this stress relaxation. In order to elucidate further the concept of stress relaxation across grain boundaries, the temperature dependence of internal friction and rigidity modulus of 99.991 percent aluminum were measured as a function of grain size of the specimen and as a function of frequency of vibration. The apparatus used is practically identical with that described before.[3] The experimental results are reported below.

2. EFFECT OF FREQUENCY OF VIBRATION

Accepting the concept of viscous grain boundary, an increase of the frequency of vibration will shift the internal friction curve (Q^{-1} *versus* temperature) to higher temperatures. This can be shown as follows. Similar to other types of relaxation phenomena, such as relaxation by diffussion (thermal, atomic, magnetic), relaxation of ordered distributions and relaxation of preferential distributions,[4] the internal friction due to stress relaxation across grain boundaries is appreciable only when the period of the applied cyclic stress is comparable to the time of relaxation associated with the stress relaxation across grain boundaries. As has been found in previous experiments,[5] the rate of the stress relaxation across grain boundaries is increased by a rise of temperature. The time of relaxation is thus reduced with an increase of temperature. Therefore when the frequency of vibration is raised, a higher temperature is required to reduce the relaxation time so that it remains comparable to the period of vibration. Exactly similar considerations apply to the case of rigidity relaxation. That is, an increase of the frequency of vibration will shift the rigidity relaxation curve (G/G_U *versus* temperature) to higher temperatures, where G_U is the unrelaxed rigidity, corresponding to the rigidity in the case of single crystal aluminum.

The effect of frequency of torsional vibration on rigidity modulus and internal friction was studied with 99.991 percent aluminum wires having an average grain diameter of 0.02 cm (the

TABLE I. Heat of activation associated with the stress relaxation across grain boundaries in aluminum as determined by four types of anelastic-effect measurements.

Type of measurement	H (calories/mole)
Creep	34,000
Stress relaxation	34,500
Internal friction	32,000
Rigidity	32,000

[3] T. S. Kê, Phys. Rev. **71**, 533 (1947).
[4] A comprehensive account on relaxation phenomena is given in C. Zener, *Elasticity and Anelasticity of Metals*, Institute for the Study of Metals Monograph Series (The University of Chicago Press, to be published).
[5] T. S. Kê, Phys. Rev. **71**, 533 (1947).

specimen was subjected to a cold-working of 70 percent reduction in area and was then annealed at 450°C for two hours). Two frequencies having a ratio of 3.14 were used in the measurement. The higher frequency was obtained by attaching a smaller auxiliary inertia member to the specimen. As visual observation of successive amplitudes of vibration is impossible at the higher frequency, the internal friction was determined by applying the formula

$$Q^{-1}=(\ln n)/\pi\tau_n f, \qquad (1)$$

when τ_n is the time required for the amplitude of vibration to be reduced to a factor $1/n$ of its initial value, and f is the frequency of vibration.

It is seen from Figs. 1 and 2 that the rigidity curve and internal friction curve do shift to higher temperatures when the frequency of vibration is raised.[6] As expected, the maximum internal friction and the ratio G_R/G_U do not change with frequency of vibration, where G_R is the relaxed rigidity.

In order to obtain a quantitative correlation between the effects of frequency of vibration and the temperature of measurement, let us proceed to determine if there is a heat of activation associated with the stress relaxation across grain boundaries from the above measurements. It has been described previously that there is a time-temperature relationship for the observed creep under constant stress, and stress relaxation at constant strain caused by the stress relaxation across grain boundaries. Thus it has been found that the observed creep and stress relaxation can be expressed as functions of the parameter

$$t\times\exp(-H/RT), \qquad (2)$$

where t is the time of observation and H is the heat of activation associated with the stress relaxation across grain boundaries. In the present case, which is dynamic, we can consider the observed internal friction and rigidity relaxation as functions of the parameter

$$f\times\exp(H/RT), \qquad (3)$$

[6] The cold-working applied to the specimen preceding annealing was 70 percent reduction in area in this experiment instead of 95 percent reduction in area as in previous experiments. As the high temperature branch of the internal friction curve is quite sensitive to the amount of cold-working applied to the specimen prior to annealing, this branch of the internal friction curve is somewhat different from the corresponding curve previously reported.

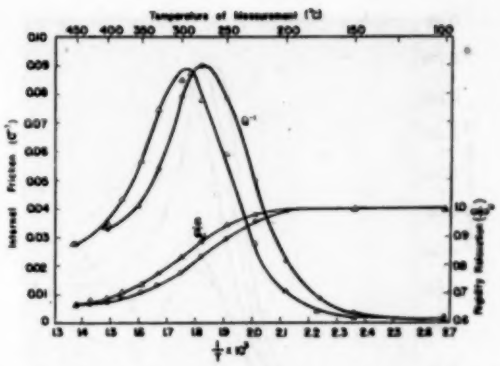

FIG. 2. Effect of frequency of vibration on internal friction and rigidity relaxation in aluminum plotted against $1/T$ (average grain diameter = 0.02 cm). Frequency of vibration at room temperature: ⊙, 0.69 c.p.s.; △, 2.16 c.p.s.

where f is the frequency of vibration. It can be shown that in order to obtain identical values of Q^{-1} or G/G_U in different measurements with different frequencies of vibration, the frequency of vibration and the temperature of measurement must be related so that

$$d(\ln f)/d(1/T)=-H/R, \qquad (4)$$

or

$$H=R[\ln(f_2/f_1)]/[1/T_1-1/T_2], \qquad (5)$$

when two frequencies f_1 and f_2 are used.

In Fig. 2, the internal friction and rigidity relaxation measured with two frequencies of vibration are plotted as a function of $1/T$. In order to bring the two curves shown to coincidence with each other, the horizontal shift in $1/T$ required in each case is 0.075×10^{-3}. As the two frequencies of vibration used have a constant ratio of 3.14 over the whole temperature range, we have

$$H=32{,}000 \text{ calories per mole}$$

from both internal friction and rigidity measurements.

The values of the heat of activation determined by the four independent types of anelastic-effect measurements are summarized in Table I. It is seen that they agree within the experimental error.

3. EFFECT OF GRAIN SIZE

The concept of viscous grain boundary predicts that a change in grain size of the specimen will have the same effect as a change in the fre-

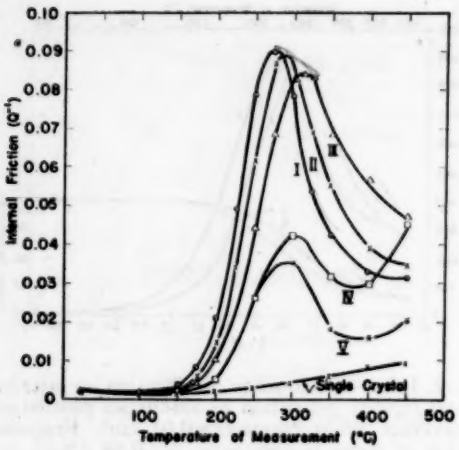

FIG. 3. Effect of grain size on internal friction in aluminum (pre-annealing cold-working = 70 percent reduction in area).

I. ⊙, 450°C annealing for 2 hours, average grain diameter = 0.02 cm;
II. ×, 500°C annealing for 4 hours, average grain diameter = 0.04 cm;
III. △, 550°C annealing for 2½ hours, average grain diameter = 0.07 cm;
IV. □, 600°C annealing for 4 hours, average grain diameter larger than 0.084 cm;
V. ✳, 600°C annealing for 12 hours, average grain diameter larger than 0.084 cm;
(diameter of wire = 0.084 cm).

quency of vibration. This is due to the fact that the relaxation time associated with the stress relaxation across grain boundaries increases with an increase of grain size. This is obvious when we consider the viscous slip along grain boundaries associated with a given over-all stress. With the larger grain size, a larger relative displacement can take place at the grain boundary before it is blocked at the grain edges and corners. A longer time will thus be required to reach the equilibrium state at which further slip is completely blocked. Since the viscous slip along grain boundaries and the stress relaxation across grain boundaries take place simultaneously, it is evident that the times of relaxation associated with both processes increase with an increase of grain size. Thus when the frequency of vibration is kept constant, an increased grain size will shift the internal friction curve and the rigidity relaxation curve to higher temperatures.

It can also be shown that as long as the grain size is smaller than the linear dimensions of the specimen, the maximum internal friction will be independent of grain size. This can be illustrated by the following considerations. Consider the internal friction caused by the stress relaxation across grain boundaries in a unit volume of the specimen. The total surface of a grain is proportional to the square of the grain size, and the volume of a grain is proportional to the cube of the grain size. The total grain boundary surface area per unit volume is thus proportional to the reciprocal of grain size. The internal friction per unit volume is proportional to the energy dissipated per half-cycle. The energy dissipated per half-cycle at a given grain boundary is proportional to the shear displacement, which takes place along the grain boundary during a half-cycle, times the total grain boundary surface area per unit volume. The maximum shear displacement along the grain boundary is proportional to grain size and thus the internal friction maximum is independent of grain size.

By similar considerations, it can be shown that the rigidity relaxation curve (G/G_U *versus* temperature) also shifts toward higher temperatures with an increase of grain size, and the value of the ratio G_R/G_U is independent of grain size.

The considerations described above hold only when the grain size is smaller than the linear dimensions of the specimen. For wire specimens, this means that the grain size should be smaller than the diameter of the wire. When a grain is extended completely across the specimen, we can no longer consider its grain boundaries as isolated viscous regions surrounded by an elastic matrix. The locking effect of the grain edges and corners may not exist and the stress relaxation may be unlimited, as in the case when shear stress is applied to a piece of amorphous substance such as pitch.

In the study of the effect of grain size, the specimen used was 99.991 percent aluminum wire having a diameter of 0.033 inch, and one foot in length. This wire was subjected to a cold-working

TABLE II. Annealing conditions and the corresponding grain size of 99.991 percent aluminum (diameter of wire specimen = 0.084 cm).

Anneal	Average grain diameter (cm)	Curve in Figs. 2 and 3
450°C, 2 hours	0.021_7	I
500°C, 4 hours	0.04_7	II
550°C, 2½ hours	0.07_2	III
600°C, 4 hours	>0.084	IV
600°C, 12 hours	>0.084	V

giving a 70 percent reduction in area prior to annealing. It has been found that in order to remove or to minimize the interfering effect due to the cold-working, the annealing temperature should be 450°C or higher and the annealing time should be 2 hours or longer.** The wire was thus annealed at 450°C for 2 hours, cooled down slowly in air to room temperature and measurements of internal friction and rigidity were made from room temperature up to 450°C, and then down again to room temperature. After the measurement, the test piece placed in the furnace was examined microscopically for grain size. Similar measurements were made after the wire was annealed at 500°C for 4 hours, 550°C for 2½ hours, 600°C for 4 hours and 600°C for 12 hours.

The heat treatment and the corresponding grain size obtained are shown in Table II. The grain size is defined in the conventional way; namely,

$$(\text{G.S.}) = 1/n^{\frac{1}{2}},$$

where n is the mean number of grains per cm². The internal friction and rigidity relaxation

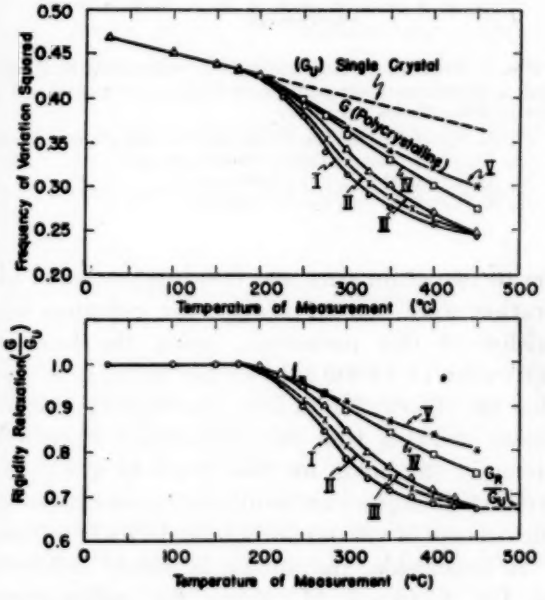

FIG. 4. Effect of grain size on rigidity and rigidity relaxation in aluminum (pre-annealing cold-working = 70 percent reduction in area). Descriptions on curves I–V are the same as shown in Fig. 3.

** The effect of prior-annealing cold-working upon the viscous behavior of the grain boundaries in a recrystallized material will be reported later.

FIG. 5. Micrographs of 99.991 percent aluminum specimen with different grain size. Pre-annealing cold-working = 70 percent reduction in area.

(a) (G.S.) =0.02 cm; (450°C annealing for 2 hours).
(b) (G.S.) =0.04 cm; (500°C annealing for 4 hours).
(c) (G.S.) =0.07 cm; (550°C annealing for 2½ hours).
Diameter of wire =0.084 cm.
Magnification: 5×.

curves corresponding to these grain sizes are shown, respectively, in Figs. 3 and 4. It is seen that curves I, II, and III are just what was expected, a shift toward higher temperatures with an increase of grain size. The internal friction maxima (see Fig. 3) and the ratio G_R/G_U (see Fig. 4) from curves I and II are approximately the same. In curve III, a few grains of the specimen have already extended completely across the wire, and the internal friction maximum is somewhat smaller than those in curves I and II. The micrographs of the three grain sizes corresponding to curves I, II, and III are shown in Fig. 5. Corresponding to curves IV and V, most of the grains are extended completely across the specimen, the internal friction maximum becomes much smaller, and the rigidity curves decrease continuously without a sign of flattening out (Fig. 4). Under such conditions, the internal friction and rigidity modulus are independent of stress only at extremely small stress levels corresponding to a maximum shearing strain of about

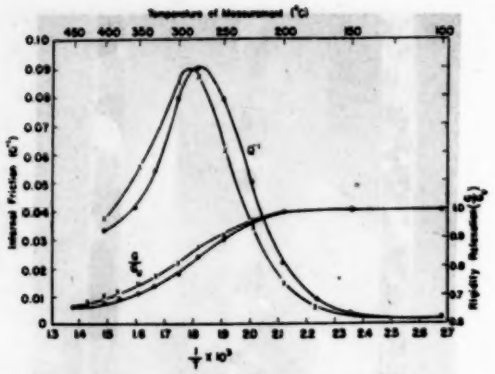

FIG. 6. Effect of grain size on internal friction and rigidity relaxation in aluminum plotted against $1/T$ (frequency of vibration = 0.69 c.p.s. at room temperature). Average grain diameter: ⊙, 0.02 cm; ×, 0.04 cm.

5×10^{-7}. The internal friction (*versus* temperature) in "single-crystal" aluminum, as has been previously reported, is included in Fig. 3 for reference.

As has been mentioned above, the concept of viscous grain boundary predicts that a change in grain size of the specimen has the same effect as a change in the frequency of vibration. We should therefore be able to consider the observed internal friction and rigidity relaxation as functions of the parameter

$$(\text{G.S.})\times\exp(H/RT), \tag{6}$$

where (G.S.) is the grain size or average grain diameter of the specimen and H is the heat of activation. In order to test whether this is true, the observed internal friction and rigidity relaxation for two different grain sizes (from curves I and II in Figs. 3 and 4) are plotted in Fig. 6 against $1/T$. If there is a heat of activation over the temperature range studied, these two sets of curves should be superposed on each other by a horizontal shift of $1/T$. This has been found to be the case, and the horizontal shift $(1/T_1-1/T_2)$ required in each set of curves is 0.050×10^{-3}. Following similar procedures as used in treating the effect of the frequency of vibration, the heat of activation should be given by

$$H=R\ln[(\text{G.S.})_2/(\text{G.S.})_1]/(1/T_1-1/T_2). \tag{7}$$

Taking H as 32,000 calories per mole, as determined according to Eq. (5), we get from Eq. (7) that $[(\text{G.S.})_2/(\text{G.S.})_1]=2.2$, which is consistent with the value obtained by grain size measurements given in Table II.

We can now test our statement that the observed internal friction and rigidity relaxation are functions of (G.S.), f and T only through the parameter

$$(\text{G.S.})\times f\times\exp(H/RT). \tag{8}$$

This should be true if the concept of viscous grain boundary is correct. In Fig. 7, the observed internal friction and rigidity relaxation correspond-

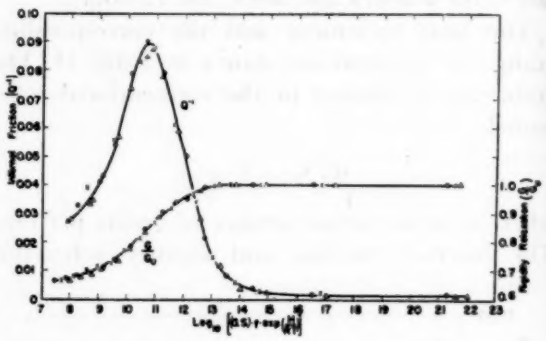

FIG. 7. Internal friction and rigidity relaxation in aluminum as functions of the parameter $(\text{G.S.})\times f\times\exp(H/RT)$, $H=32{,}000$ calories per mole.
⊙, (G.S.) = 0.02 cm, f_{RT} (frequency of vibration at room temperature) = 0.69 c.p.s.;
×, (G.S.) = 0.04 cm, f_{RT} = 0.69 c.p.s.;
△, (G.S.) = 0.02 cm, f_{RT} = 2.16 c.p.s.

ing to two grain sizes and two frequencies of vibration were plotted against the common logarithm of this parameter, using the heat of activation of 32,000 calories per mole. It is seen that the observed data form essentially a smooth curve, showing that the generalized statement given in (8) holds for the range of grain size studied. This gives an additional corroboration of the concept of viscous grain boundaries in metals.

In conclusion, the author is deeply indebted to Dr. Clarence M. Zener for enlightening discussions.

The Milne Problem for a Large Plane Slab with Constant Source and Anisotropic Scattering*

R. E. MARSHAK**
University of California, Los Alamos Scientific Laboratory, Santa Fe, New Mexico

(Received January 13, 1947)

Formulas are derived for the asymptotic neutron density and the neutron current emerging from an infinite plane slab whose thickness is large compared to the scattering mean free path. It is supposed that the slab sustains a uniform source of neutrons. The neutrons suffer capture in addition to scattering. The scattering is assumed to take place in accordance with the law: $(1/4\pi)(1+3f_1\mu)$ where f_1 is a constant, and μ is the cosine of the angle of scattering. Expressions for the asymptotic neutron density in the slab and the emerging current, in the limiting case of isotropic scattering, are also given.

1. INTRODUCTION

WE consider the following problem: an infinite plane slab of material of half-thickness d, bounded by vacuum on both sides, contains a source of neutrons uniformly distributed throughout the slab. The neutrons are scattered anisotropically[1] without change of energy and also suffer capture. The half-thickness, d, is assumed large compared to the scattering mean free path. We wish to obtain expressions for (a) the asymptotic neutron density inside the slab (i.e., the neutron density at distances large compared to a scattering mean free path from either face), and (b) the neutron current leaving either face.

The transport equation governing the distribution of neutrons in the slab in the case of linear scattering and with constant neutron production is:

$$\mu\frac{\partial\psi(z,\mu)}{\partial z}+\psi(z,\mu)=\frac{1}{2\sigma}[\psi_0(z)+3f_1\mu\psi_1(z)]+\frac{q_0}{2}. \quad (1)$$

In Eq. (1), the origin of the z-axis is taken on one face of the slab, μ is the cosine of the angle between the direction of the neutron velocity and the positive z-axis, $\psi(z,\mu)d\mu$ is the number of neutrons per unit volume at the point z with direction cosine between μ and $\mu+d\mu$, σ is the ratio of the scattering mean free path to the total mean free path, q_0 is the number of neutrons produced per unit volume (assumed constant), f_1 is a measure of the deviation of the scattering function from isotropy, and, finally, $\psi_0(z)$ and $\psi_1(z)$ are the zero and first moments of the neutron distribution function, namely:

$$\psi_0(z)=\int_{-1}^{1}d\mu\psi(z,\mu), \quad (1a)$$

$$\psi_1(z)=\int_{-1}^{1}d\mu\mu\psi(z,\mu). \quad (1b)$$

The quantity $\psi_0(z)$ is the neutron density and the negative of $\psi_1(z)$ is the neutron current. The total mean free path has been taken as the unit of length and the neutron velocity set equal to unity. Equation (1) is to be solved subject to the boundary conditions:

$$\psi(0,\mu)=0 \quad \text{for} \quad \mu>0, \quad (A)$$

$$\partial\psi_0(z)/\partial z=0 \quad \text{at} \quad z=d. \quad (B)$$

Condition (A) follows because the vacuum does not return any neutrons, condition (B) because of the symmetry of the problem. We shall use the asymptotic part of the solution for $\psi_0(z)$ in (B) since the half-thickness d has been assumed large compared to the scattering mean path.

2. GENERAL SOLUTION

We solve Eq. (1) by the standard Wiener-Hopf[2] procedure. Taking the Laplace transform

* This paper will appear in Division V of the Manhattan Project Technical Series as part of the contribution of the Los Alamos Laboratory of the University of California.

** Now at the University of Rochester.

[1] We work with linear scattering, i.e., the scattering function is assumed to be expressible in terms of the zero and first harmonics; the generalization to a higher number of harmonics is also possible.

[2] Cf. N. Wiener and E. Hopf, Berliner Ber. Math. Phys. Klasse 696 (1931); see also E. Hopf, "Mathematical Problems of Radiative Equilibrium," Cambridge Tract No. 31 (1934); O. Halpern, R. Lueneburg, and O. Clark, Phys. Rev. **53**, 173 (1938); E. A. Schuchard and E. A. Uehling, Phys. Rev. **58**, 611 (1940).

of both sides of Eq. (1), we get:

$$(1+s\mu)\phi(s,\mu) = \frac{1}{2\sigma}[\phi_0(s)+3f_1\mu\phi_1(s)]+\frac{q_0}{2s}+\mu\psi(0,\mu), \quad (2)$$

where

$$\phi(s,\mu)=\int_0^\infty dz e^{-sz}\psi(z,\mu),$$

$$\phi_0(s)=\int_{-1}^1 d\mu\phi(s,\mu),$$

$$\phi_1(s)=\int_{-1}^1 d\mu\mu\phi(s,\mu).$$

Integrating both sides of (2) over $d\mu$ from -1 to 1, we find:

$$s\phi_1(s)=\frac{1-\sigma}{\sigma}\phi_0(s)+\frac{q_0}{s}+\int_{-1}^0 d\mu\mu\psi(0,\mu) \quad (3)$$

where we have made use of boundary condition (A). On substitution for $\phi_1(s)$ into (2), division by $(1+s\mu)$ and integration over $d\mu$ from -1 to 1, Eq. (2) is transformed into:

$$\phi_0(s)\left[1-\frac{\tanh^{-1}s}{\sigma s}+\frac{3f_1(\sigma-1)}{\sigma^2s^2}\left(1-\frac{\tanh^{-1}s}{s}\right)\right] = \frac{\sigma q_0}{s}\left[\frac{3f_1}{\sigma^2s^2}\left(1-\frac{\tanh^{-1}s}{s}\right)+\frac{\tanh^{-1}s}{\sigma s}\right] + g_+(s)+\frac{3f_1g_+(0)}{\sigma s^2}\left(1-\frac{\tanh^{-1}s}{s}\right). \quad (4)$$

In Eq. (4), we have written:

$$g_+(s)=\int_{-1}^0 d\mu\frac{\mu\psi(0,\mu)}{(1+s\mu)} \quad (5)$$

so that

$$g_+(0)=\int_{-1}^0 d\mu\mu\psi(0,\mu);$$

$g_+(0)$ represents the negative of the neutron current flowing into vacuum.

Equation (4) can be rewritten in the form:

$$[s\phi_0(s)+\sigma q_0]K(s)=3f_1/\sigma s^2H(s)\times[sg_+(0)+\sigma q_0]+[sg_+(s)+\sigma q_0], \quad (6)$$

where

$$K(s)=1-\frac{\tanh^{-1}s}{\sigma s}+\frac{3f_1(\sigma-1)}{\sigma^2s^2}\left(1-\frac{\tanh^{-1}s}{s}\right),$$

$$H(s)=(s-\tanh^{-1}s)/s.$$

Expressing $H(s)$ in terms of $K(s)$:

$$H(s)=\frac{\sigma^2s^2K(s)-\sigma(\sigma-1)s^2}{\sigma s^2+3(\sigma-1)f_1},$$

we may transform Eq. (6) into:

$$\Phi(s)K(s)=G(s), \quad (7)$$

where

$$\Phi(s)=[s\phi_0(s)+\sigma q_0][\sigma s^2+3(\sigma-1)f_1]-3f_1\sigma[\sigma g_+(0)+\sigma q_0], \quad (7a)$$

$$G(s)=[sg_+(s)+\sigma q_0][\sigma s^2+3(\sigma-1)f_1]-3f_1(\sigma-1)[sg_+(0)+\sigma q_0]. \quad (7b)$$

In Eq. (7), $\Phi(s)$ is analytic in the plane $Re(s)>\nu$ (where ν is the positive root of $K(s)$), $G(s)$ is analytic in the half-plane $Re(s)<1$, and $K(s)$ is analytic in the strip $|Re(s)|<1$.

Just as in the case of no capture,[2] it can be shown that in the strip $|Re(s)|<1$, $K(s)$ has two zeros, namely, $\pm\nu$, and approaches unity as $|s|\to\infty$. We may, therefore, adopt the usual device of defining a function:

$$\tau(s)=\left(\frac{s^2-1}{s^2-\nu^2}\right)K(s). \quad (8)$$

The function $\log\tau(s)$ is analytic and single-valued in the strip $|Re(s)|<1$, provided a particular determination of the logarithm is chosen,[3] and approaches zero as $|s|\to\infty$ in the strip. The usual decomposition then follows:

$$\tau(s)=\tau_+(s)/\tau_-(s), \quad (8a)$$

where

$$\tau_+(s)=\exp\left[\frac{1}{2\pi i}\int_{\beta-i\infty}^{\beta+i\infty}du\frac{\log\tau(u)}{(u-s)}\right],$$

$$\tau_-(s)=\exp\left[\frac{1}{2\pi i}\int_{-\beta-i\infty}^{-\beta+i\infty}du\frac{\log\tau(u)}{(u-s)}\right],$$

and $|Re(s)|<\beta$ with $\nu<\beta<1$. Introducing (8) and (8a) into (7) yields:

$$\Phi(s)\frac{(s^2-\nu^2)}{(s+1)}\cdot\frac{1}{\tau_-(s)}=\frac{(s-1)}{\tau_+(s)}G(s). \quad (9)$$

The left-hand side of Eq. (9) is analytic in the half-plane $Re(s)>\nu$ and the right-hand side is analytic in the half-plane $Re(s)<\beta$. Since there is

[3] The determination $\log 1=0$ is chosen.

a region of overlap, each side is the analytic continuation of the other. Examination of the behavior of the two sides of (9) as $|s|\to\infty$ in the plane shows that they approach infinity as $|s|^3$. By an extension of Liouville's theorem, it follows that each side may be equated to a polynomial of order three. We therefore write:

$$\Phi(s)\frac{(s^2-\nu^2)}{(s+1)\tau_-(s)}=C_0+C_1s+C_2s^2+C_3s^3 =(s-1)G(s)/\tau_+(s) \qquad (10)$$

where C_0, C_1, C_2, and C_3 are constants.

The problem is now to evaluate the C's. From (10) it is evident that $C_0=-G(0)/\tau_+(0)$, which is zero, since $G(0)=0$ (cf. (7b)) and $\tau_+(0)$ is finite. C_1 is also zero as can be seen by writing

$$C_1s+C_2s^2+C_3s^3=(s-1)G(s)/\tau_+(s),$$

differentiating both sides with respect to s and setting $s=0$. Hence:

$$G(s)=s^2(C_2+C_3s)\tau_+(s)/(s-1). \qquad (11)$$

Inserting (7b) for $G(s)$ and rearranging terms, we find:

$$[sq_+(s)+\sigma q_0]=\frac{s^2(C_2+C_3s)\tau_+(s)+3f_1(\sigma-1)[sg_+(0)+\sigma q_0](s-1)}{(s-1)[\sigma s^2+3(\sigma-1)f_1]}. \qquad (12)$$

From (12) it would follow that $[sg_+(s)+\sigma q_0]$ has poles at $s=\pm\zeta$ where[4] $\zeta=i[3f_1(1-1/\sigma)]^{\frac{1}{2}}$; since this is impossible, it follows that the numerator of the right-hand side of (12) must vanish for $s=\zeta$ and $s=-\zeta$, i.e.,

$$(C_2+C_3\zeta)\tau_+(\zeta) -\sigma[\zeta g_+(0)+\sigma q_0](\zeta-1)=0, \qquad (13a)$$

$$(C_2-C_3\zeta)\tau_+(-\zeta) -\sigma[-\zeta g_+(0)+\sigma q_0](-\zeta-1)=0. \qquad (13b)$$

Equations (13a) and (13b) yield values for C_2 and C_3, namely:

$$C_2=\frac{\zeta^2g_+(0)(\alpha+\beta/\zeta)-\sigma q_0(\alpha+\beta\zeta)}{(\alpha^2-\beta^2)}, \qquad (14a)$$

$$C_3=\frac{-g_+(0)(\alpha+\beta\zeta)+\sigma q_0(\alpha+\beta/\zeta)}{(\alpha^2-\beta^2)}, \qquad (14b)$$

with

$$\alpha=(2\sigma)^{-1}[\tau_+(\zeta)+\tau_+(-\zeta)],$$
$$\beta=(2\sigma)^{-1}[\tau_+(\zeta)-\tau_+(-\zeta)]. \qquad (14c)$$

Equations (14a) and (14b) express C_2 and C_3 in terms of the unknown constant $g_+(0)$; that is as it should be since we still must take into account boundary condition (B). To determine $g_+(0)$, we find the asymptotic solution for $\psi_0(z)$ and then impose the boundary condition (B).

To find the asymptotic solution for $\psi_0(z)$, we write down the expression for $\phi_0(s)$ given by (10) and (7a) and find the contribution to the Laplace inverse from the poles.[5] For $\phi_0(s)$, we have:

$$\phi_0(s)=-\frac{\sigma q_0}{s}+\frac{3f_1[sg_+(0)+\sigma q_0]}{s(s^2-\zeta^2)} +\frac{\tau_-(s)s(s+1)(C_2+C_3s)}{\sigma(s^2-\zeta^2)(s^2-\nu^2)}. \qquad (15)$$

The contribution to $\psi_0(z)$ (the Laplace inverse of $\phi_0(s)$) from the poles is:

$$\psi_0(z)_{\text{asymp}}=\frac{\sigma q_0}{(\sigma-1)} +\frac{C_2}{2\sigma(\nu^2-\zeta^2)}[\tau_-(\nu)(1+\nu)e^{\nu z} +(1-\nu)e^{-\nu z}\tau_-(-\nu)] +\frac{C_3\nu}{2\sigma(\nu^2-\zeta^2)}[(1+\nu)e^{\nu z}\tau_-(\nu) -(1-\nu)e^{-\nu z}\tau_-(-\nu)]. \qquad (16)$$

We may rewrite (16) in the form:

$$\psi_0(z)_{\text{asymp}}=\frac{\sigma q_0}{\sigma-1}+C_2A(\nu,\zeta)\cosh[\nu(z+z_0)] +C_3\nu A(\nu,\zeta)\sinh[\nu(z+z_0)], \qquad (17)$$

[4] If $f_1<0$, ζ is real; however, $|\zeta|<1$ so that the pole still cannot exist.

[5] The branch-point contribution yields the non-asymptotic part of the solution.

where

$$A(\nu,\zeta)=[(1-\nu^2)\tau_-(\nu)\tau_-(-\nu)]^{\frac{1}{2}}/\sigma(\nu^2-\zeta^2), \quad (17a)$$

$$z_0=\frac{1}{2\nu}\log\left\{\frac{(1+\nu)\tau_-(\nu)}{(1-\nu)\tau_-(-\nu)}\right\}. \quad (17b)$$

The boundary condition (B) applied to (17) now yields:

$$C_2+C_3\nu\coth[\nu(d+z_0)]=0. \quad (18)$$

Using the definitions (14a) and (14b) for C_2 and C_3, Eq. (18) permits us to solve for $g_+(0)$ with the result:

$$g_+(0)=\sigma q_0\frac{\{(\alpha+\beta/\zeta)-\nu^{-1}(\alpha+\beta\zeta)\tanh[\nu(d+z_0)]\}}{\{(\alpha+\beta\zeta)-\nu^{-1}\zeta^2(\alpha+\beta/\zeta)\tanh[\nu(d+z_0)]\}}. \quad (19)$$

Equations (17), (17a), (17b), and (19) constitute the asymptotic solution for the neutron density in the slab; the negative of (19) is the current leaving the $z=0$ face of the slab. The quantities $\tau_-(\nu)$ and $\tau_-(-\nu)$ can be evaluated by converting their contour integral representations into real integrals.

3. LIMITING CASE OF ISOTROPIC SCATTERING

It is interesting to mention the limiting case of isotropic scattering; allowing f_1 and therefore ζ to approach zero, the asymptotic solution for $\psi_0^{(i)}(z)$ becomes:

$$\psi_0^{(i)}(z)_{\text{asymp}}=(\sigma/(\sigma-1))q_0 +A(\nu_0)\cosh[\nu_0(d-z)], \quad (20)$$

where

$$A(\nu_0)=\frac{-\sigma^2 q_0}{\cosh[\nu_0(d+z_0^{(i)})]}\cdot\left\{\frac{2(1-\nu_0^2)}{[1-\sigma(1-\nu_0^2)](\sigma-1)}\right\}^{\frac{1}{2}}. \quad (20a)$$

The emerging current $g_+^{(i)}(0)$ becomes:

$$g_+^{(i)}(0)=-\sigma q_0\{\nu_0^{-1}\tanh[\nu_0(d+z_0^{(i)})] -1-[\tau_+'^{(i)}(0)/\tau_+^{(i)}(0)]\}. \quad (21)$$

In Eqs. (20) and (21) the quantities ν_0 and $z_0^{(i)}$ are defined by:

$$\nu_0^{-1}\tanh^{-1}\nu_0=\sigma, \quad (22a)$$

$$z_0^{(i)}=(2\nu_0)^{-1}\log\left\{\frac{(1+\nu_0)\tau_-^{(i)}(\nu_0)}{(1-\nu_0)\tau_-^{(i)}(-\nu_0)}\right\}. \quad (22b)$$

The term $[\tau_+'^{(i)}(0)/\tau_+^{(i)}(0)]$ in Eq. (21)is the logarithmic derivative of $\tau_+^{(i)}(s)$ evaluated at $s=0$. The definitions of $\tau_+^{(i)}(s)$ and $\tau_-^{(i)}(s)$ are:

$$\tau_+^{(i)}(s)=\exp\left\{\frac{1}{2\pi i}\int_{\beta-i\infty}^{\beta+i\infty}du\frac{\log\tau^{(i)}(u)}{(u-s)}\right\}, \quad (23a)$$

$$\tau_-^{(i)}(s)=\exp\left\{\frac{1}{2\pi i}\int_{-\beta-i\infty}^{-\beta+i\infty}du\frac{\log\tau^{(i)}(u)}{(u-s)}\right\}, \quad (23b)$$

where

$$\tau^{(i)}(s)=[(s^2-1)/(s^2-\nu_0^2)] \times(1-(\sigma s)^{-1}\tanh^{-1}s). \quad (23c)$$

From (23b) it is possible to show that

$$[\tau_+'^{(i)}(0)/\tau_+^{(i)}(0)]=\bar{z}_0-1$$

where:[6]

$$\bar{z}_0=\frac{1}{\pi}\int_0^{\pi/2}\left\{\frac{3}{\sin^2 x}-\frac{1}{1-x\cot x}\right\}dx =0.7104\cdots. \quad (24)$$

The simplest case of all is the case of isotropic scattering and no capture. In this case, the current becomes $(q_0 d)$ while the asymptotic neutron density $\bar{\psi}_0^{(i)}$ is:

$$\bar{\psi}_0^{(i)}(z)_{\text{asymp}}=-\tfrac{3}{2}q_0 z^2+A[z_0+\bar{z}_0^{(i)}], \quad (25)$$

where $A=3q_0 d$,

$$\bar{z}_0^{(i)}=\bar{z}_0+(15\bar{z}_0^2-1)/30d,$$

with $\bar{z}_0$ defined by (24).

It is a pleasure to thank Dr. Carson Mark for helpful discussion.

This paper is based on work performed under Contract No. W-7405-Eng-36 with the Manhattan Project at the Los Alamos Scientific Laboratory of the University of California.

[6] E. Hopf, "Mathematical Problems of Radiative Equilibrium," Cambridge Tract No. 31 (1934).

Refraction of Plane Shock Waves*

A. H. TAUB
Mathematics Department, University of Washington, Seattle, Washington

(Received March 6, 1947)

It is assumed that when a plane shock wave is incident on an interface between two gases of different densities ρ and ρ_1, and different ratios of specific heats γ and γ_1, respectively, a three shock configuration results, involving an incident shock, a reflected shock, and a transmitted shock. It is further assumed that in the various angular domains the pressure is constant. The Rankine-Hugoniot equations are used to formulate the following conditions: (a) the pressure across the interface is continuous and (b) the deflection of the flow caused by the incident and reflected waves is equal to that caused by the transmitted wave. Rational polynomial equations of the twelfth degree are obtained, the roots of which determine the position and strength of the reflected and transmitted waves as functions of the strength, angle of incidence of the incident wave, and three parameters characterizing the pair of gases involved. The solutions of these equations are studied as multiple branched functions of the five parameters. It is shown that one branch behaves similarly to the acoustic case, and it is suggested that this branch is the only physically realizable one. Relations are obtained between the strength of the incident shock, its angle of incidence, and the three parameters characterizing the pair of gases which determine the ranges of these parameters where real physically realizable solutions may exist. One of these relations shows that the configuration is impossible for angles of incidence corresponding to the angle of total reflection. The cases for which numerical computations were made are listed, and the method of computation is briefly described. These computations were planned and supervised by Mrs. Adele Goldstein and were carried out on the Eniac which was made available through the cooperation of the Army Ordnance department.

1. INTRODUCTION

THE purpose of this paper is to give a discussion of some results on the phenomena associated with the reflection and refraction of a plane shock wave incident upon an interface between two gaseous media. We shall assume that the neighborhood of the line of intersection of the incident wave, I, and the surface separating the two media is divided into angular regions by a reflected shock wave, R, and a transmitted shock wave, M, as illustrated in Fig. 1. We shall also assume that all quantities of interest are constant in each of these angular regions. Thus we implicitly assume that the phenomenon of reflection is stationary as seen by one traveling with the line of intersection of the incident wave and the interface.

The computation of all relevant quantities may be reduced to that of determining the angles DOR and DOM of Fig. 1, that is, the angle between the reflected wave and the interface, the angle of reflection, and the angle between the transmitted wave and interface, the angle of refraction, respectively. These angles in turn may be determined by use of the fact that the Rankine-Hugoniot equations must hold across any shock and that the appropriate boundary conditions must be satisfied. These are:

(A) In the domain ROM there is no discontinuity in pressure. Using the notation of Fig. 1 we have $p''=p_1'$.

(B) The total deflection of the flow through the incident and reflected wave, $\delta+\delta'$, must equal the deflection through the transmitted wave, δ_1. Thus $\delta+\delta'=\delta_1$. (See Section 2 for the notation.)

When these conditions are imposed, as is done

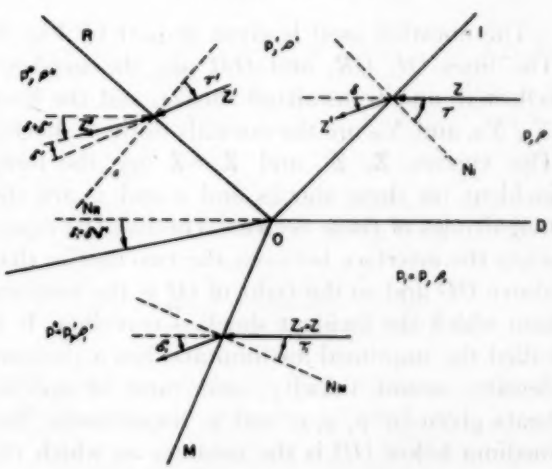

FIG. 1. The assumed shock configuration. For notation see Section 2.

* This work was started while the author was employed at Princeton University on work sponsored by the Office of Naval Research, contract N6ori-105 Task II.

below, we are led to an algebraic equation for the tangent of the angle τ', and the angle between the normal to the reflected wave and the flow incident upon that wave. Solving this equation is equivalent to solving a polynomial of twelfth degree, the coefficients of which are functions of the parameters characterizing the incident wave, essentially the angle of incidence and some measure of the strength of the incident wave. They are also functions of the characteristics of the two gases. These will be taken as the ratio of the velocities of sound in the two media, and the ratios of the specific heats for each medium. Thus each equation which has to be solved has coefficients which are functions of five parameters.

In general there will be many real solutions of these equations. Some of these may be dismissed on the ground that they violate some physical requirement such as the requirement that the flow incident upon the reflected shock wave be supersonic. However, after this is done we are still left with multiple solutions. We shall consider the solutions as a multiple branched function of the parameters involved and select those solutions which lie on branches which behave as $\eta \to 1$ as do sound waves.

In particular we shall not consider in detail solutions with positive values of τ', that is, configurations in which the reflected wave lies ahead of the normal to the flow behind the incident wave, for in the sonic case such solutions do not seem to occur.

2. NOTATION

The notation used is given in part by Fig. 1. The lines OI, OR, and OM are the incident, reflected, and transmitted shocks, and the lines N_I, N_R, and N_M are the normals to these shocks. The vectors $\mathbf{Z}$, $\mathbf{Z}'$, and $\mathbf{Z}_1=\mathbf{Z}$ are the flows incident on these shocks and z and z' are the magnitudes of these vectors. The line OD represents the interface between the two media; that above OD and to the right of OI is the medium into which the incident shock is traveling. It is called the unprimed medium and has a pressure density, sound velocity, and ratio of specific heats given by p, ρ, c, and γ, respectively. The medium below OD is the medium on which the incident shock impinges, and its characteristics are labeled by the same letters as those in the upper medium but are distinguished by a subscript 1. The pressure between the incident shock and the reflected shock is denoted by p', and other quantities are similarly labeled. The pressure behind the reflected shock is denoted by p'' and that behind the transmitted shock by p_1', with a similar convention for other quantities.

The angle between the normal to a shock and the flow incident upon it is denoted by τ with an appropriate superscript or subscript. It is positive when the direction from the normal to the flow is counter-clockwise.

The angle between the emergent flow and the prolongation of the incident flow is denoted by δ with appropriate sub- or superscripts. These angles are taken to be positive if the direction from the latter to the former is counter-clockwise.

In addition we shall use the following symbols defined in terms of the symbols used in Fig. 1.

$$\eta=\rho'/\rho, \quad \eta'=\rho''/\rho', \quad \eta_1=\rho_1'/\rho_1,$$

$$x=\tan\tau, \quad x'=\tan\tau', \quad x_1=\tan\tau_1,$$

$$\Delta=\tan\delta, \quad \Delta'=\tan\delta', \quad \Delta_1=\tan\delta_1,$$

$$D=\tan(\delta+\delta')=(\Delta+\Delta')/(1-\Delta\Delta'),$$

$$B^2=(1+\eta^2x^2)(1+x'^2)^{-1}, \quad \Gamma=(c/c_1)^2,$$

$$x_m'=\left[\frac{A(1+\eta^2x^2)}{(1+x^2)\Gamma\eta+A-1+\frac{1}{2}(\gamma-1)(\eta-1)}-1\right]^{\frac{1}{2}},$$

$$x_M'=\left[\frac{1+\eta^2x^2}{1+\frac{1}{2}(\gamma+1)(\eta-1)}-1\right]^{\frac{1}{2}},$$

$$z_M=1+x_M'^2,$$

$$A=\gamma(\gamma_1+1)/\gamma_1(\gamma+1), \quad a=\gamma_1/\gamma,$$

$$P=a\Gamma=(\gamma_1/\gamma)(c/c_1)^2=\rho_1/\rho,$$

$$1+x_T^2=(2\eta P)^{-1}[2\eta a+(1-a)(\eta-1)].$$

3. THE RANKINE-HUGONIOT EQUATIONS

We shall use the Rankine-Hugoniot equations in the form

$$\frac{p'-p}{p}=\frac{2\gamma}{\gamma+1}[(z/c)^2\cos^2\tau-1]$$

$$=\frac{2\gamma}{\gamma+1}\left(\frac{(z/c)^2}{1+x^2}-1\right), \tag{3.1}$$

$$\eta=\frac{\rho'}{\rho}=\frac{(\gamma+1)(p'/p)+\gamma-1}{(\gamma-1)(p'/p)+\gamma+1};$$

$$\frac{p'}{p}=\frac{(\gamma+1)\eta-(\gamma-1)}{(\gamma+1)-(\gamma-1)\eta}, \tag{3.2}$$

$$(z'/c')^2\cos^2(\tau+\delta)=(2\gamma)^{-1}[\gamma-1+(\gamma+1)(p/p')], \tag{3.3}$$

$$\tan(\tau+\delta)=\eta\tan\tau. \tag{3.4}$$

In these equations, γ is the ratio of specific heats for the gas under consideration, p'/p is the ratio of the pressure behind the shock to that ahead of it, η is the ratio of the density behind the shock to that ahead of it, z and z' are the magnitudes of the flow vectors ahead and behind the shock, respectively, c and c' are the sound velocities in these media, the angle τ is the angle between the normal to the shock and the incident flow vector, and δ is the angle of deflection of the flow. Both of these angles are illustrated in Fig. 1 and the sign convention used there is held throughout.

Equations analogous to Eqs. (3.1) to (3.4) hold across any of the shocks, I, R, and M when appropriate changes in the symbols are introduced.

Equation (3.3) may also be written as

$$(z'/c')^2(1+\eta^2x^2)^{-1}=(2\gamma)^{-1}[\gamma-1+(\gamma+1)(p/p')], \tag{3.3'}$$

and (3.4) as

$$\Delta=\tan\delta=(\eta-1)(1+\eta x^2)^{-1}x. \tag{3.4'}$$

4. THE PRESSURE CONDITION

The requirement (A), namely, $p''=p_1'$, when formulated in terms of the Rankine-Hugoniot equations leads to an expression for $x_1=\tan\tau_1$, as a function of η, x, $x'=\tan\tau'$, $(c/c_1)^2$, γ and γ_1. This expression is obtained as follows:

Applying (3.1) to the flow incident on the reflected wave we have

$$(p''-p')/p'=2\gamma(\gamma+1)^{-1}[(z'/c')^2(1+x'^2)^{-1}-1].$$

Substituting for $(z'/c')^2$ from (3.3') we obtain

$$\frac{p''}{p'}=B^2\left[\frac{(\gamma-1)p'+(\gamma+1)p}{(\gamma+1)p'}\right]-\frac{\gamma-1}{\gamma+1}. \tag{4.1}$$

Where

$$B^2=(1+\eta^2x^2)(1+x'^2)^{-1}. \tag{4.2}$$

Hence

$$p''/p=1+(B^2-1)[1+(\gamma-1)p'/(\gamma+1)p]. \tag{4.3}$$

Similarly,

$$(p_1'-p)/p=2\gamma_1(\gamma_1+1)^{-1}[(z/c)^2(1+x_1^2)^{-1}-1].$$

Substituting in this equation for z/c we obtain

$$\frac{p_1'}{p}=\frac{2\gamma_1}{\gamma_1+1}\times\left\{\Gamma\frac{1+x^2}{1+x_1^2}\left[\frac{(\gamma+1)(p'-p)}{2\gamma p}+1\right]-1\right\}. \tag{4.4}$$

Equating (4.4) and (4.3) gives the equation for x_1, namely,

$$1+x_1^2=\frac{(1+x^2)\Gamma\eta(1+x'^2)}{A(\eta^2x^2-x'^2)+\frac{1}{2}[(\gamma+1)-(\gamma-1)\eta](1+x'^2)}=\frac{(1+x^2)\Gamma\eta}{A(B^2-1)+\frac{1}{2}[(\gamma+1)-(\gamma-1)\eta]}. \tag{4.5}$$

Consideration of Eq. (4.5) leads to relations between the variables x, η, A, and Γ which must hold in order for a real solution to exist. It follows from (4.5) that $1+x_1^2$ is a monotonic increasing function of x'^2. If

$$1-A\geqslant\tfrac{1}{2}(\gamma-1)(\eta-1),$$

the largest value of $1+x_1^2$ is finite and occurs when x' is infinite. If

$$1-A<\tfrac{1}{2}(\gamma-1)(\eta-1)$$

$1+x_1^2$ becomes infinite at x' given by

$$1+x'^2=\frac{A(1+\eta^2x^2)}{A-1+\frac{1}{2}(\gamma-1)(\eta-1)}.$$

We shall see later that for physical reasons x' must be restricted to the range given by

$$1+x'^2\leqslant 1+x'_M{}^2=\frac{1+\eta^2x^2}{1+\frac{1}{2}(\gamma+1)(\eta-1)}.$$

The value of $1+x_1^2$ corresponding to this value of $1+x'^2$ is finite and positive in both cases and given by

$$1+x_1^2=\frac{(1+x^2)\Gamma\eta}{\eta+\frac{1}{2}(A-1)(\gamma+1)(\eta-1)}.$$

Hence x_1 is not real in the range we are interested in unless

$$(1+x^2)\Gamma\geqslant 1+\tfrac{1}{2}(1-a)(\eta-1)/a\eta. \quad (4.6)$$

The inequality (4.6) reduces to the well-known condition for the existence of a transmitted wave in the acoustic approximation obtained by setting $\eta=1$, namely, $(1+x^2)\Gamma\geqslant 1$. The value of x for which the equality holds defines the angle of total reflection. However, if the equality holds in (4.6), the only possible allowable value of x'^2 is $x'_M{}^2$ and for this value of x'^2, $x_1=0$. This means that the deflection by the transmitted wave is zero but the deflection by the incident and (sonic) reflected wave is different from zero. Hence we cannot have an allowable solution if the equality in (4.6) holds. That is, there can be no analog of total reflection in the case of shocks.

Of course, if $\Gamma>1$ and $a>1$, (4.6) is satisfied for any real values of x and η. In case $\Gamma>1$ and $a<1$ the equality in (4.6) will lead to a real curve in the x, η plane for some values of x and η if

$$2/(\gamma+1)>(\Gamma-1)a/(1-a).$$

In case $\Gamma<1$ and $a<1$ the equality in (4.6) leads to a real curve in the x, η plane for all values of x and η. In case $\Gamma<1$ and $a>1$ this curve becomes partly imaginary if the inequality given above holds.

Since x_1^2 must be real and positive, it follows from (4.5) that

$$1+x'^2\geqslant 1+x'_m{}^2=\frac{A(1+\eta^2x^2)}{(1+x^2)\Gamma\eta+A-1+\frac{1}{2}(\gamma-1)(\eta-1)}. \quad (4.7)$$

That is, if x, η, Γ, and A are such that the right-hand side of (4.7) is greater than one, then allowable values of x'^2 are bounded from below. If this right-hand side is less than one, this lower bound is zero.

It may readily be verified that (4.6) is equivalent to the condition

$$1+x'_M{}^2\geqslant 1+x'_m{}^2.$$

There are choices of the parameters x,η, Γ, and A such that $1+x'_m{}^2\geqslant 1$ and $1+x'_m{}^2\leqslant 1$. In such a case (4.6) is satisfied, and x and η satisfy the condition:

$$x^2>\tfrac{1}{2}(\gamma+1)(\eta-1)/\eta^2.$$

5. DEFLECTION BY THE UPPER PATH

In order to calculate the deflection of the flow through the shocks I and R, the upper path, we calculate $\tan\delta$ and $\tan\delta'$. These are given by (3.4′), namely,

$$\Delta=\tan\delta=(\eta-1)(1+\eta x^2)^{-1}x, \quad (5.1)$$

$$\Delta'=\tan\delta'=(\eta'-1)(1+\eta'x'^2)^{-1}x', \quad (5.2)$$

and hence

$$D=\tan(\delta+\delta')=(\Delta+\Delta')/(1-\Delta\Delta')^{-1}. \quad (5.3)$$

Our next concern is to calculate η' as a function of η, x, x', A, and Γ. From Eq. (3.2) we have

$$\eta'=\frac{(\gamma+1)(p''/p')+\gamma-1}{(\gamma-1)(p''/p')+\gamma+1}.$$

Substituting in this equation from (4.1) we obtain after some algebraic manipulation

$$\eta'=\frac{(\gamma+1)B^2}{(\gamma-1)(B^2-1)+(\gamma+1)\eta}=\frac{(\gamma+1)(1+\eta^2x^2)}{(\gamma-1)(\eta^2x^2-x'^2)+(\gamma+1)\eta(1+x'^2)}. \quad (5.4)$$

On substituting (5.4) in (5.2) and (5.3) we obtain

$$\Delta'=\frac{[2(B^2-1)-(\eta-1)(\gamma+1)]x'}{(\gamma+1)(1+\eta x^2)\eta-2(B^2-1)}=\frac{(x'_M{}^2-x'^2)x'}{(1+x'^2)[1+\frac{1}{2}(\gamma+1)(1+x'_M{}^2)]-(1+x'_M{}^2)} \quad (5.5)$$

where $1+x'_M{}^2$ is defined by (5.7) below.

$$\Delta'=\frac{[2(\eta^2x^2-x'^2)-(\eta-1)(\gamma+1)(1+x'^2)]x'}{(\gamma+1)\eta(1+\eta x^2)(1+x'^2)-2(\eta^2x^2-x'^2)}, \quad (5.5')$$

and

$$D=\frac{(\eta x-x')(\gamma+1)(1+x'^2)(\eta-1)(1+x^2)+2(\eta^2x^2-x'^2)(x'(1+\eta x^2)-(\eta-1)x)}{(\gamma+1)(1+x'^2)[\eta(1+\eta x^2)^2+(\eta-1)^2xx']-2(\eta^2x^2-x'^2)(1+\eta x^2+(\eta-1)xx')}. \tag{5.6}$$

Since, by assumption, the reflected wave must be a shock wave, we must have $\eta' \geqslant 1$. Hence we must have

$$1+x'^2 \leqslant 1+x'_M{}^2=\frac{1+\eta^2x^2}{1+\tfrac{1}{2}(\gamma+1)(\eta-1)}. \tag{5.7}$$

Thus $|x_M'|$ is an upper limit for $|x'|$. In case the right-hand side of Eq. (5.7) is less than one, no reflected shock is possible. The equation $x_M'=0$ is equivalent to

$$1+\eta^2x^2=1+\tfrac{1}{2}(\gamma+1)(\eta-1).$$

This equation determines an angle of incidence for each shock strength η, such that the reflected wave is sonic, and for x, less than that given by this equation; the reflected wave does not exist because the flow behind the incident wave is subsonic.

6. THE FUNCTION $D(x')$

For the purpose of the discussion to follow it is convenient to summarize some of the properties of the function $D(x')$ for fixed values of γ, η, and x, that is, for an incident shock of given strength passing through a fixed medium at a fixed angle of incidence. We shall assume that

$$z_M=1+x'_M{}^2=\frac{1+\eta^2x^2}{1+\tfrac{1}{2}(\gamma+1)(\eta-1)} \geqslant 1.$$

$D(x')$ is positive if x' is negative and $x'^2>x'_M{}^2$. As x' increases $D(x')$ decreases monotonically and at $x'=-|x_M'|$ it is equal to Δ. As x' increases further $D(x')$ passes through a minimum for a negative x' such that

$$1+x'^2=1+(x'^2)_{\min}=\frac{z_M}{1+\tfrac{1}{2}(\gamma+1)z_M}\times\{1-\tfrac{1}{4}(\gamma+1)z_M+[(\tfrac{1}{4}(\gamma+1))^2z_M{}^2+\tfrac{1}{2}(\gamma^2-1)z_M+\gamma+1]^{\frac{1}{2}}\} \geqslant z_M. \tag{6.1}$$

This is the only minimum $D(x')$ possesses. There is also a maximum at the positive value of x' satisfying (6.1). This maximum is greater than Δ since $\Delta=D(x')$ at $x'=0$, as well as x', such that $x'^2=x'_M{}^2$.

After passing through the maximum $D(x')$ decreases monotonically with increasing x' and crosses the x' axis at $x'=\eta x$.

The minimum of $D(x')$ will be negative if and only if x, η, and γ are such that

$$x^2>\frac{2(\eta-1)[(\gamma-1)(1+\eta x^2)+2](1+\eta x^2)}{z_M(1+\eta^2x^2)}. \tag{6.2}$$

If this inequality holds there are two negative roots of the equation $D(x')=0$, given by

$$x'=z_M\left\{\frac{-x}{1+\eta x^2}\pm\left[\frac{x^2}{(1+\eta x^2)^2}-\frac{2(\eta-1)[(\gamma-1)(1+\eta x^2)+2]}{(1+\eta^2x^2)(1+\eta x^2)z_M}\right]^{\frac{1}{2}}\right\}.$$

If the inequality in (6.2) becomes an equality, the minimum of $D(x')$ is zero. The angle of incidence defined by the resulting equation is the so-called extreme angle beyond which regular reflection of shocks from a rigid wall is impossible.[1]

7. DEFLECTION BY THE LOWER PATH

We next calculate η_1 in order to compute

$$\Delta_1=(\eta_1-1)(1+\eta_1x_1^2)^{-1}x. \tag{7.1}$$

We have

$$\eta_1=\frac{(\gamma_1+1)(p_1'/p)+\gamma_1-1}{(\gamma_1+1)+(\gamma_1-1)(p_1'/p)}=\frac{(\gamma_1+1)(p''/p)+\gamma_1-1}{\gamma_1+1+(\gamma_1-1)(p''/p)}.$$

Substituting from (4.3) we obtain

$$\eta_1=\gamma_1(\gamma+1)\frac{2A(B^2-1)+[\gamma+1-(\gamma-1)\eta]}{2\gamma(\gamma_1-1)(B^2-1)+\gamma_1(\gamma+1)[\gamma+1-(\gamma-1)\eta]}, \tag{7.2}$$

[1] cf. J. Von Neumann, *Oblique Reflection of Shocks* (Explosives Research Report No. 12, U. S. Navy Department, Bureau of Ordnance, October 1943).

and

$$\Delta_1=\frac{2\gamma(B^2-1)x_1}{(\gamma+1)(1+x^2)\gamma_1\Gamma\eta-2(B^2-1)\gamma} \tag{7.3}$$

$$\Delta_1=\frac{2\gamma(\eta^2x^2-x'^2)x_1}{(\gamma+1)(1+x^2)(1+x'^2)\gamma_1\Gamma\eta-2(\eta^2x^2-x'^2)\gamma}. \tag{7.4}$$

We note that the condition that the transmitted wave be a shock wave is $\eta_1\geqslant 1$ which is automatically satisfied since $\gamma_1\geqslant 1$.

The deflection condition (B) is then satisfied by finding an x' such that

$$D=\Delta_1 \tag{7.5}$$

where D is given by (5.6) and Δ_1 by (7.4). The x' must be such that

$$1+x'_m{}^2\leqslant 1+x'^2\leqslant 1+x'_M{}^2. \tag{7.6}$$

In case $x'_m{}^2$ is negative the left-hand inequality is replaced by $1+x'^2\geqslant 1$. One solution of (7.5) is given by $x'=\eta x$ for then $D=\Delta_1=0$. However, this value of x' violates (7.6) and does not correspond to a physically possible position of the reflected shock.

8. THE FUNCTION $\Delta_1(x')$

The problem has been reduced to solving (7.5) where the quantities involved are defined by (7.4), (5.6), and (4.5); in addition we are interested only in those solutions satisfying (7.6). We have already seen that no physically real solutions can exist unless

$$(1+x^2)\Gamma>1+(1-a)(\eta-1)/2a\eta$$

and

$$1+\eta^2x^2\geqslant 1+\tfrac{1}{2}(\gamma+1)(\eta-1). \tag{8.1}$$

We now discuss some properties of the function $\Delta_1(x')$. Since the behavior of x_1, as a function of x' has already been discussed, it is convenient to write Δ_1 as a function of x_1 and the parameters x, η, γ, γ_1, and Γ. It follows from (4.5) and (7.3) that

$$\Delta_1=\frac{[z_{1M}-(1+x_1^2)]x_1}{(1+x_1^2)[1+\frac{1}{2}(\gamma_1+1)z_{1M}]-z_{1M}}, \tag{8.2}$$

where

$$z_{1M}=\frac{2\eta(1+x^2)\Gamma}{2\eta-(\gamma+1)(\eta-1)}>1, \tag{8.3}$$

as a consequence of the first of (8.1).

Equation (8.2) may be obtained from the relation between Δ' and x' by replacing x' by x_1, z_M by z_{1M}, and γ by γ_1. The character of Δ_1 as a function of x_1 may be readily obtained, therefore, from that of Δ' as a function of x'. In any case it may be seen readily that it is an odd function of x_1 and as x' increases from minus infinity Δ_1 decreases, becoming zero at the value of x_1 given by $1+x_1^2=z_{1M}$. As x_1 increases further, Δ_1, passes through a negative minimum and then increases to zero at $x_1=0$. The value of x_1 for which the minimum occurs may be obtained by making the replacements mentioned above in Eq. (6.1).

In discussing Δ_1 as a function of x' we distinguish between four cases:

$$1+x'_m{}^2\geqslant 1,\quad 1-A<\tfrac{1}{2}(\gamma-1)(\eta-1), \tag{8.4}$$

for which

$$\infty\geqslant 1+x_1^2\geqslant 1$$

as

$$\frac{2A(1+\eta^2x^2)}{2(A-1)+(\gamma-1)(\eta-1)}\geqslant 1+x'^2\geqslant 1+x'_m{}^2,$$

$$1+x'_m{}^2\geqslant 1,\quad 1-A\geqslant\tfrac{1}{2}(\gamma-1)(\eta-1), \tag{8.5}$$

for which

$$N\geqslant 1+x_1^2\geqslant 1 \quad\text{as}\quad \infty\geqslant 1+x'^2>1+x'_m{}^2,$$

$$1+x'_m{}^2<1,\quad 1-A\geqslant\tfrac{1}{2}(\gamma-1)(\eta-1), \tag{8.6}$$

for which

$$N\geqslant 1+x_1^2\geqslant M \quad\text{as}\quad \infty\geqslant 1+x'^2\geqslant 1,$$

and

$$1+x'_m{}^2<1,\quad 1-A<\tfrac{1}{2}(\gamma-1)(\eta-1), \tag{8.7}$$

for which

$$\infty\geqslant 1+x_1^2\geqslant M$$

as

$$\frac{2A(1+\eta^2x^2)}{2(A-1)+(\gamma-1)(\eta-1)}\geqslant 1+x'^2\geqslant 1.$$

The quantities N and M are functions of the parameters x, η, Γ, γ, and γ_1, which are determined by setting $1+x'^2$ equal to infinity and

unity, respectively, in Eq. (4.5). They are positive and greater than unity for all allowed values of the parameters.

The graph of Δ_1 as a function of x' is symmetrical with respect to both axes when positive and negative values of x_1 are taken, since Δ_1 is an even function of x'. We shall describe it in the first quadrant for the various cases. When (8.4) holds, Δ_1 is imaginary for $x' < |x_m'|$. It is zero at $x' = |x_m'|$ and has an infinite slope at this point. As x' increases, Δ_1 increases, passes through a maximum, and then vanishes at $x' = \eta x$.

The function in the first quadrant has two branches at $x' = \eta x$. The branch which emerges from this point for increasing x' is increasing and has a vertical asymptote at the value of x' given in Eq. (8.4). The function of Δ_1 is imaginary beyond this vertical asymptote.

When (8.5) holds, the character of this second branch of Δ_1 at the point $x' = \eta x$ changes. It is still increasing, but instead of having a vertical asymptote it remains finite as x' goes to infinity.

When (8.6) holds, the function Δ_1 is real for all values of x' less than ηx and does not vanish anywhere except at $x' = \eta x$. It has a second branch which behaves as in the case described by (8.4). When (8.7) holds, the function Δ_1 behaves as in (8.6) for $x' \leqslant \eta x$ and as in (8.5) for $x' > \eta x$.

9. EXISTENCE OF SOLUTIONS FOR $x' > -\eta x$

From the facts already cited about the functions $D(x')$ and $\Delta_1(x')$, it is possible to discuss various solutions of the equation $\Delta_1 = D$ as a function of the parameter x for a given combination of gases (Γ, γ, and γ_1 fixed) and for a strength given of incident shock (η fixed). The different solutions of $\Delta_1 = D$ will correspond to different branches of the function $x'(x)$. Two branches may or may not intersect. We shall now show that for suitable choices of parameters Γ, γ_1, γ, and η, branches which pass through the point $x' = -|x_M'|$, exist. At this point, the reflected wave disappears. This phenomenon occurs in acoustics, and this suggests that only those solutions which lie on this branch correspond to physically possible ones.

We begin the discussion by assuming x large, so that the incident wave strikes the density discontinuity almost head on. At the point $x' = -\eta x$, Δ_1 is zero and D is positive so that $\Delta_1 - D$ is positive. Moreover, it is decreasing as x' increases in the neighborhood of $x' = -\eta x$. This point is, of course, outside the range of a physically possible solution, since that range is given by

$$1 + x'^2 \leqslant 1 + x'_M{}^2 \leqslant \eta^2 x^2.$$

We now compare the value of Δ_1 and D at $x' = -|x_M'|$. The latter is given by Δ since $\Delta' = 0$ here. It follows from (7.3) that for $1 + x'^2 = 1 + x'_M{}^2$

$$\Delta_1 = \frac{(\eta - 1)x_1}{(1 + x^2)P\eta - (\eta - 1)}, \tag{9.1}$$

where

$$P = a\Gamma = \gamma_1 c^2 / \gamma c_1^2 = \rho_1 / \rho, \tag{9.2}$$

and

$$1 + x_1^2 = \frac{(1 + x^2)\Gamma\eta a}{a\eta + \frac{1}{2}(1 - a)(\eta - 1)} = \frac{1 + x^2}{1 + x_T^2} \geqslant 1, \tag{9.3}$$

as follows from the first condition expressed in (8.1), where

$$1 + x_T^2 = \frac{2\eta a + (1 - a)(\eta - 1)}{2\eta P} > 0. \tag{9.4}$$

Writing

$$\Delta_1^2(x'_M{}^2) - \Delta^2 = \frac{(\eta - 1)^2 d}{[(1 + x^2)P\eta - (\eta - 1)]^2 (1 + \eta x^2)^2},$$

it may readily be verified that

$$d = \frac{1 + x^2}{1 + x_T^2}[x^4\eta^2(1 - P^2(1 + x_T^2)) + 2\eta x^2 \times (1 - [\tfrac{1}{2}\eta(P - 1)^2 + P](1 + x_T^2)) - x_T^2]. \tag{9.5}$$

Hence $d = 0$ if and only if

$$x^2 = \frac{(P + \frac{1}{2}\eta(P - 1)^2)(1 + x_T^2) - 1 \pm \{(1 + x_T^2)[\eta(1 + x_T^2)(P + \frac{1}{4}\eta(P - 1)^2) - (\eta - 1)]\}^{\frac{1}{2}}(P - 1)}{\eta(1 - P^2(1 + x_T^2))}. \tag{9.6}$$

When $a=1$ there is only one positive root to $d=0$, and (9.6) reduces to

$$x^2=\frac{1-P}{2P}+\left[\left(\frac{1-P}{2P}\right)^2+\frac{1}{P\eta^2}\right]^{\frac{1}{2}}. \tag{9.7}$$

When $\eta=1$ there is only one possible choice of the sign in (9.6), and it reduces to

$$x^2=\frac{\Gamma-1}{P^2-\Gamma}=\frac{(c/c_1)^2-1}{(\rho_1/\rho)^2-(c/c_1)^2}. \tag{9.8}$$

In the usual linear theories of reflection and refraction of sound waves the condition for the absence of a reflected wave is shown[2] to be given by (9.8).

The sign of d in (9.5) depends on the size of $P^2(1+x_T^2)$ relative to unity. This quantity is the analog of the square of the acoustic impedance of the two media involved for

$$P^2(1+x_T^2)=P\left(a+\tfrac{1}{2}(1-a)\left(1-\frac{1}{\eta}\right)\right),$$

and when $\eta=1$ we have

$$P^2(1+x_T^2)=Pa=\gamma_1\rho_1/\gamma\rho=(\rho_1c_1/\rho c)^2.$$

Our subsequent discussion then falls into two cases:

$$P^2(1+x_T^2)\gtrless 1, \quad \text{and} \quad P^2(1+x_T^2)<1.$$

In the first case the incident wave impinges on a "denser" medium in an almost head-on direction, and d is negative as is the difference between Δ_1, and D at $x'=\eta x$. As x' increases, one branch of Δ_1 increases to a positive maximum and D decreases to a minimum value which we can make negative by choosing x large enough. We shall assume that for this choice of parameters η, x, γ, γ_1, and Γ the point $x'=-|x_m'|$ is greater than at least one of the two real negative roots of $D=0$. This condition can be satisfied by choosing x sufficiently large. For such a combination of parameters there must be two negative values of x' such that $\Delta_1=D$, as is obvious from a consideration of the graphs of the functions involved.

As x decreases d decreases, and one negative solution x' moves toward the point $x'=-|x_M'|$. As x decreases it may happen that both negative solutions disappear while d is still negative. This would be similar to the situations encountered in the study of three shock configurations where it is found that a limiting angle of incidence exists beyond which no three shock solutions exist. If such a thing happens, the curves $D(x')$ and $\Delta_1(x')$ are tangent for some value of x and for smaller values of x never intersect. It is evident from a consideration of the graphs of the function involved that this may occur even when $D(x')=0$ has real solutions, that is, in the region of regular reflection.

It may also happen for some choices of the parameters γ, γ_1, Γ, and η that both negative solutions still exist for the values of x greater than or equal to the greatest value for which $d=0$. In case x satisfies (9.6), $x'=-|x_M'|$ is one solution, and the reflected wave disappears. For values of x slightly less than this value, one solution lies between $x'=-\eta x$ and $x'=-|x_M'|$, and this corresponds to acoustic theory, for in that theory a compression is reflected from a "denser" medium as a compression for head-on incidence. As the angle of incidence is made more glancing, a critical angle given by (9.8) is reached at which the reflected wave disappears, and beyond this angle the reflected wave is a rarefaction.

Thus one branch of the function $x'(x)$ describing the solutions of $D=\Delta_1$ for fixed η, γ, γ_1, and Γ, and varying x passes through the point $x'=-|x_M'|$ and then lies between $x'=-\eta x$ and $x'=-|x_M'|$. Since a similar phenomenon takes place in acoustic theory and since the other branch behaves in a physically implausible manner, as we shall see below, we propose to identify this branch as the physically realizable one.

Presumably the reflected shock wave should be replaced by a Prandtl-Meyer rarefaction for values of x less than the critical value for which $d=0$. We shall not discuss this point further here.

When the value of x is decreased from that taken initially, the absolute value of the minimum of $D(x')$ decreases. This means that the second negative solution mentioned above is somewhere given by a value of x' for which $D(x')$ and $\Delta_1(x')$ are small; hence x_1 is small and x' is close to $-|x_m'|$. Since the slope of the

[2] cf. Rayleigh, *Theory of Sound* (Dover Publications, New York, 1945), Vol. II, p. 81.

$\Delta_1(x')$ curve is infinite at $x'=-|x_m'|$, x' can be close to $-|x_m'|$ and $\Delta_1(x')$ can be sizable. When this solution is in the neighborhood of $x'=-|x_m'|$ the pressure behind the transmitted wave must be very large, since x_1 is close to zero. This means that this wave is almost normal to the interface and yet it must have a large velocity parallel to the interface since it must keep up with the incident wave. Such a solution does not seem physically plausible.

The foregoing discussion may be summarized as follows: If $P(1+x_T^2)\gtrless 1$, the lower medium is acoustically the more dense. Then for x larger than the largest value for which $d=0$, that is, for x larger than the largest value given by (9.6), a physically realizable three-shock configuration may exist. It cannot exist for values smaller than this critical value, and presumably the reflected shock is replaced by a Prandtl-Meyer rarefaction. For x larger than the critical value, the existence or non-existence of a solution is determined as in the problem of three-shock configurations in a single gas. This is done at present by numerical means.

10. THE CASE $P^2(1+x_1^2)<1$

In this case, it follows from arguments similar to those used above that at $x'=-\eta x$, Δ_1-D is negative, and at $x'=-|x_M'|\Delta_1-D$ is positive for large x. Hence there is a solution of $\Delta_1=D$ between these two values of x'. There must be another solution between $x'=|x_M'|$ and $x'=-|x_m'|$ as follows from a consideration of the graphs involved. However, there is no solution on the physically realizable branch. This is to be expected, since in the case $P^2(1+x_T^2)<1$ the lower medium is the "rarer," and for head-on incidence in such a case the reflected wave is a rarefaction. Presumably the assumption of a reflected shock wave is incorrect, and this wave should be replaced by a Prandtl-Meyer rarefaction.

If x is now decreased to the greatest value given by (9.6), the solution between $x'=-\eta x$ and $x'=-|x_M'|$ moves toward $x'=-|x_M'|$. When x satisfies (9.6), there is a solution at $x'=-|x_M'|$ for which no reflected wave exists. For values of x less than this critical value, solutions of the type assumed may exist.

However, they cannot exist for all values of x less than the greatest value satisfying (9.6). It is evident that if there are two real values of x satisfying (9.6) this type of solution again disappears at the smaller value. Even if there is only one real value of x satisfying (9.6), this type of solution cannot exist for we have seen that there is a lower bound for x given by the requirement that x_1 must be real, namely, (8.1), which is

$$1+x^2>1+x_T^2=\frac{2\eta a+(1-a)(\eta-1)}{2\eta P}. \quad (10.1)$$

There is another lower bound given by the requirement that the flow behind the incident shock be supersonic, namely,

$$1+x_M'^2=\frac{1+\eta^2x^2}{1+\tfrac{1}{2}(\gamma+1)(\eta-1)}\gtrsim 1. \quad (10.2)$$

We have already pointed out that the solutions cease to exist before the first of these lower bounds is reached and, there is therefore, no analogue of total reflection.

The greatest lower bound for x for the existence of solutions of the type we are considering is a function of η and the parameters characterizing the two gases. Geometrically it is determined by the condition that the curve $D(x')$ have one point of contact with the curve $\Delta_1(x')$ between the limits $x'=-\eta x$ and $x'=0$ at which the two curves are tangent.

Mathematically, this is the same type of condition which determines the greatest lower bound for the existence of solutions in case $P^2(1+x_T^2)\gtrsim 1$, in the three-shock configuration problem and in the regular reflection problem. In the last problem, for values of x less than this greatest lower bound a Mach reflection takes place. This suggests that the analog of a Mach reflection may take place for values of x between the greatest solution of (9.6) and (10.1), provided (10.2) is satisfied in case $P^2(1+x_T^2)<1$.

We may summarize the case $P^2(1+x_T^2)<1$ as follows: For each η, a physically realizable three-shock configuration such as assumed can exist only if x is within a certain range. The upper limit for this range is the greatest value of x satisfying (9.6). A lower limit for this range is the largest of the following three numbers, (1) the smallest solution of (9.6) if it is distinct from

TABLE I. Key to computations.

Case	γ	γ_1	γ_1/γ	$\Gamma=(c/c_1)^2$	$P=\rho_1/\rho$	$\rho c/\rho_1 c_1$	Gases
I	1.66	1.4	0.84	0.825	0.693	1.31	
II	1.4	1.66	1.19	0.12	0.143	7.63	Air-He
III	1.4	1.4	1	0.875	0.875	1.07	O_2-N_2
IV	1.4	4/3	0.95	0.60	0.57	1.36	Air-CH_4
V	4/3	1.4	1.05	0.60	0.63	1.23	CO_2-Air
VI	1.139	1.4	1.23	0.19	0.23	1.86	Freon-Air
VII	1.139	5/3	1.46	0.02	0.03	4.71	Freon-He

the largest, (2) $|x_T|$, or (3) $(\gamma+1)(\eta-1)/2\eta^2$. Neither (2) nor (3) can be the greatest lower bound for defining this range but there must exist a value of x depending on η greater than (2) or (3) for which solutions of this type cease existing. Presumably for such η and x (and also smaller x's), an analog of Mach reflection takes place.

11. NUMERICAL COMPUTATIONS[3]

Equation (7.5) was solved numerically on the Eniac, which was made available through the cooperation of the Army Ordnance Department, for seven combinations of the parameters γ, γ_1, and Γ. These are listed in Table I. Mrs. Adele Goldstine planned and supervised the computations.

The method of computation was the following: For each combination of gases, (γ, γ_1, and Γ), an integral value of η satisfying $1\leqslant\eta\leqslant 2/(\gamma-1)$ was chosen. For each value of these parameters τ was allowed to take on values varying from zero to 89 degrees. For each choice of these five parameters $|x_M'|$ was computed. D, Δ_1, and $D-\Delta_1$ were then computed for $x'=-|x_M'|$ and all other

$$x'=-|x_M'|+ndx'\leqslant|x_M'|,$$

where $n=0, 1, 2, \cdots$ and dx' was taken to be 0.05 for some computations and 0.01 for others. The values of x' and $x'+dx'$, between which $D-\Delta_1$ changed sign, were noted and the value of $x'+dx'$ was called a solution. This method did not locate double roots. However these may be inferred in many cases from graphs of x' against x for fixed η for a given pair of gases.

The detailed results of these computations will not be given here but will be summarized briefly.

For all cases for which computations were made, the lower medium was the "rarer," and hence from the preceding discussion it was to be expected that for values of x greater than that given by (9.6) no solutions on the branch we have called physically realizable were to be found. However, for these values of x a positive and negative solution was found, and the values of x' were approximately equal to $\pm|x_m'|$. This result is caused in part by the fact that the curve $\Delta_1(x')$ has an infinite slope at $x'^2=x'_m{}^2$ and in part to the nature of the function $D(x')$.

In many of the cases computed, the interval of x within which the physically relizable branch can exist is less than a degree, and hence it was not explored in the numerical computations. In other cases some points on these branches were determined.

12. ACKNOWLEDGMENTS

This work was greatly aided by the cooperation received from the Office of Naval Research, The Army Ordnance Department, Mrs. Adele Goldstine, and Professor Walker Bleakney of Princeton University. In addition, I am indebted to Professor J. Von Neumann for calling this problem to my attention and for many stimulating discussions regarding it.

[3] A detailed report on the numerical computations is in preparation.

Absolute Sensitivity of a Graphite Ionization Chamber

MELVIN LAX
*Massachusetts Institute of Technology, Cambridge, Massachusetts**
(Received February 10, 1947)

A thick-walled graphite ionization chamber is suggested as a simple instrument for measuring the total intensity in the x-ray beam emitted by the betraton. The chamber would consist of two layers of carbon, each about 1/5 of a radiation length, or 4.5 cm thick, separated by a thin gas layer whose width is not critical. The transverse dimensions of the carbon layers should be sufficiently large to cover completely the x-ray beam as well as to catch the electrons produced at an angle in the carbon. The absolute sensitivity of the ionization chamber is computed to an accuracy of about 5 percent by comparison with the ionization which would be produced in an infinitely thick carbon block.

1. INTRODUCTION

THE determination of cross sections for nuclear reactions induced by a high energy x-ray beam requires a knowledge of the total power in the beam and of the spectral distribution of this power.

Ionization chambers designed for measurements at several Mev have their sensitivities computed according to the assumption that the electrons produced by the x-ray beam have a maximum range less than the thickness of the ionization chamber walls.[1] If the walls are kept less than one radiation length[1a] in thickness, this assumption certainly fails for the x-ray beam emitted by the 100-Mev betatron.

A chamber consisting of two thick graphite layers separated by a thin gas layer was suggested by Bethe and Feynman, and preliminary calculations were made by Feynman for a chamber whose walls are $\frac{1}{8}$ of a radiation length, or 4.5 cm thick. Such walls will stop 25-Mev electrons. Below 25 Mev, the chamber will therefore behave as an ordinary ionization chamber. Above 25 Mev, there will be a reduction in sensitivity because the wall thickness will be less than the range of some of the electrons produced.

The purpose of this paper is to compute the sensitivity of such an ionization chamber taking into account: (1) Finite thickness of the graphite walls; (2) attenuation of the x-ray beam in the walls; (3) non-linearity in the range-energy relationship; (4) multiple scattering; (5) radiation.

The sensitivity of the chamber is determined predominantly by factors (1) and (2). Fortunately, the effects of these factors can be taken into account precisely. The range-energy non-linearity is never more than 20 percent for electrons from 0 to 100 Mev, and the effect of this non-linearity on the final sensitivity is less than 10 percent. The non-linearity effect is corrected by using the range-energy relationship for electrons given by Rossi and Greisen.[2] Multiple scattering and radiation are hard to compute precisely, but their effects are kept to less than 5 percent by use of a light element, such as carbon, for the walls, and by an appropriate choice of wall thickness.

2. GENERAL DESIGN CONSIDERATIONS

The basic principle of the design is to reproduce as nearly as possible the ideal situation of an infinite carbon block in which electrons are produced uniformly throughout. In this case, the ionization energy produced per unit volume is equal to the energy given to electrons per unit volume by the x-ray beam. This will be true even if electron scattering takes place.

Unfortunately, uniform electron production is limited by two factors: (1) attenuation of the x-ray beam in the carbon, and (2), production of showers for thicknesses of a radiation length or

* This work was done while the author was employed at the Research Laboratory, General Electric Company, during the summer of 1946.

[1] G. C. Laurence, Can. J. Research **A15**, 16 (1937).

[1a] The term *radiation length* may be defined roughly as the distance in which the energy of a fast particle is reduced to $1/e$ of its original value by radiative processes. A more precise definition is given in B. Rossi and K. Greisen, Rev. Mod. Phys. **13**, 240 (1941).

[2] B. Rossi and K. Greisen, Rev. Mod. Phys. **13**, 240 (1941); see p. 247, Eq. (1.12).

more. Each of these factors requires that the thickness of the carbon block be small compared with a radiation length. It is this requirement which prevents the use of carbon blocks thick enough to stop the highest energy electrons produced by the x-ray beam.

The effect of using a carbon block of finite thickness T will now be considered. Electrons whose range R is less than T must come from a layer of thickness R adjacent to the gas in order to produce ionization in the gas. This is the same number of electrons as would be counted if the block were infinite in thickness.

On the other hand, if R is greater than T, the electrons come from a layer of thickness T instead of R, and the number of electrons crossing the gas layer is reduced in the ratio T/R. Assuming a linear range-energy relationship, $E=\epsilon R$, this ratio also represents the decrease in ionization in the gas compared with the case of the infinite block. Thus the efficiency for electrons, compared with an infinite medium can be represented by

$$\begin{aligned} \eta &= 1 && E<E_0, \\ \eta &= E_0/E = T/R && E>E_0, \end{aligned} \tag{1}$$

where $E_0=\epsilon T$ is the energy lost by an electron on traversing thickness T.

The electron efficiency η can be thought of as the fraction of the electron energy created per unit volume which is converted to ionization per unit volume. For energies less than E_0, this efficiency is unity because no electrons escape; those electrons which leave a given unit volume are replaced by others which enter it, so that all energy eventually goes into ionization. This result is true even if scattering takes place.

For energies greater than E_0, however, the amount of ionization produced in the gas layer depends on the angle at which the electrons cross it, and this is not quite compensated for by the change in thickness from which the electrons come. For these energies ($E>E_0$), therefore, it is necessary to keep the scattering small.

To keep the error less than 5 percent we should set[3]

$$\langle\theta^2\rangle_{Av}=(21/E_0)^2(T/2)<0.1, \tag{2}$$

where T is the thickness in radiation lengths, and $E_0=\epsilon T$ is the energy in Mev required to cross the block. The value $T/2$ is used, since electrons are produced, on the average, in the middle of the block. Using $E_0=\epsilon T$ we obtain

$$\epsilon^2 T>2000. \tag{3}$$

The largest collision losses per radiation length, ϵ, occur for the lightest elements (ϵ varies as $1/Z$). If carbon is used, $\epsilon=120$ Mev/(radiation length), and (3) gives $T>0.14$ radiation length.

We have already shown, however, that to keep attenuation and shower effects small, T must be small compared with a radiation length. This pretty well fixes the choice of T to be about $\frac{1}{8}$ of a radiation length, or about 4.5 cm of carbon.

The second carbon block serves the purpose of compensating for back scattering in the first block. It should be the same thickness as the first block, although this dimension is not critical.

3. SENSITIVITY CALCULATION

If one x-ray of energy W is absorbed, producing an electron of energy E, the fraction of the absorbed energy ending up as ionization is given by $(E/W)\eta(E)$, since E/W is the fraction of x-ray energy given to the electron and $\eta(E)$ is the fraction of electron energy ending up as ionization. In general, the x-ray of energy W will produce a distribution of electron energies $\sigma(W, E)dE$, so that the average fraction of absorbed x-ray energy which ends up as ionization is given by

$$S(W)=\frac{\int (E/W)\eta(E)\sigma(W, E)dE}{\int \sigma(W, E)dE}. \tag{4}$$

If $Wf(W)dW$ is the incident x-ray energy, and $1/G(W)$ is the absorption coefficient per radiation length in carbon, the absorbed energy in a thickness Δt radiation lengths is given by

$$(\Delta t/G(W))Wf(W)dW,$$

and the ionization energy produced in this layer is given by

$$I=\Delta t\int Wf(W)S(W)/G(W)dW, \tag{5}$$

$$I=\Delta t\langle S/G\rangle_{Av}\int Wf(W)dW, \tag{6}$$

[3] Reference 2, p. 263.

where a comparison of (6) and (5) defines the average sensitivity $\langle S/G\rangle_{Av}$ for a given incident spectrum.

Formulas (5) and (6) require a slight correction for the fact that the gas layer is not also made of carbon. This correction has been shown by L. H. Gray[4] to be simply the ratio of stopping powers in the gas to that in the carbon, this ratio being roughly independent of electron energy if the gas is also a light element. In our units, this correction factor is given by R_c/R_g, where R_c and R_g are the electron ranges in carbon, and in the gas, both measured in radiation lengths.

According to Eq. (4), $S(W)$ can also be written in the form

$$S(W)=P_cS_c(W)+P_pS_p(W), \qquad (7)$$

where P_p is the relative probability for pair production in carbon (see Figs. 1a, and 1b), $P_c=1-P_p$, and S_c and S_p are the sensitivities which would prevail if only the Compton effect, or only pair production took place. Thus S_c is computed using Eq. (4) with σ replaced by the cross section for the Compton effect, and S_p is computed in a similar manner, except for a factor 2 because two electrons are produced in each pair.

The decomposition of $S(W)$ by means of Eq. (7) is useful because S_c and S_p are independent of the material chosen for the chamber walls, whereas P_c and P_p are not.

The sensitivities S_p and S_c were computed using $\eta(E)=1$ for $E<25$, $\eta(E)=25/E$ for $E>25$. Furthermore, the cross section for pair production was assumed to be independent of electron energy since it is very close to constant for electron energies from $E=0$ to $E=W-2mc^2=(W-1)$ Mev. Using Eq. (4) this gives

$$S_p(W)=(W-1)/W, \qquad W<26 \text{ Mev}, \quad (8a)$$

$$S_p(W)=50(W-13.5)/W(W-1), \qquad W>26 \text{ Mev}. \quad (8b)$$

It should be noted that Eq. (8a) is independent of the assumption of a constant cross section, and merely represents the fact that a gamma-ray of energy W gives energy $(W-1)$ to the electron and positron pair. All of this energy is converted to ionization if $W<26$ Mev, and only part of it if $W>26$ Mev.

[4] L. H. Gray, Proc. Roy. Soc. **A156**, 578 (1936).

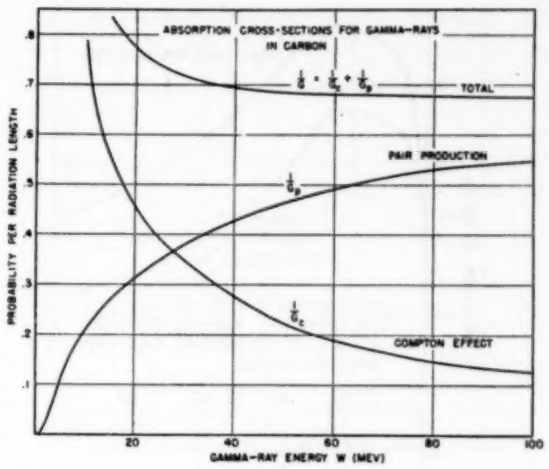

FIG. 1a. Absorption cross sections for gamma-rays in carbon.

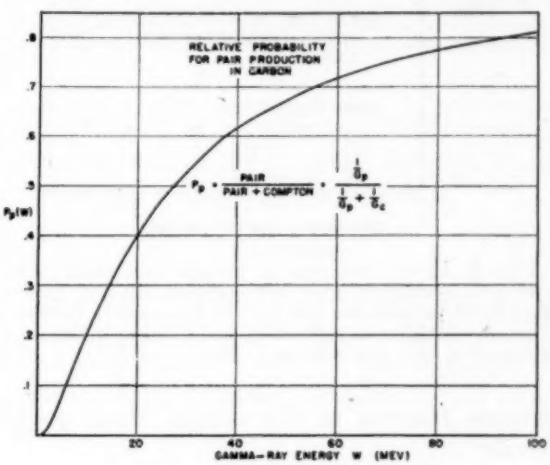

FIG. 1b. Relative probability for pair production in carbon.

For the Compton effect the cross section used was the usual one[5]

$$\sigma_c(W,E)dE=k(x)dx =(c/\gamma)[1+x^2-x\sin^2\theta]dx/x, \qquad (9)$$

where $x=W'/W$, $W'=W-E$ is the energy carried off by the recoil x-ray, and $\gamma=W/mc^2\simeq 2W$. The Compton recoil angle and energy are related by

$$\sin^2\theta=\frac{2(1-x)}{\gamma x}-\frac{(1-x)^2}{\gamma^2x^2}, \qquad (10)$$

and x takes all values from $1/(2\gamma+1)$ to 1. The

[5] Reference 2, p. 251.

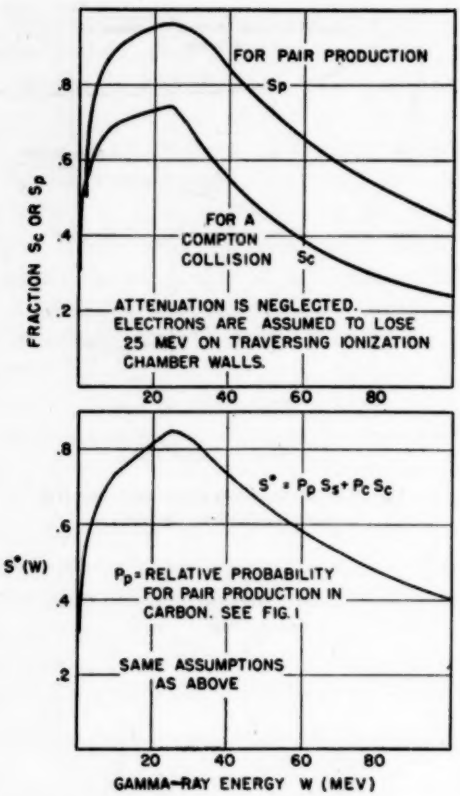
FOR PAIR PRODUCTION
Sp
FOR A COMPTON COLLISION
Sc
ATTENUATION IS NEGLECTED. ELECTRONS ARE ASSUMED TO LOSE 25 MEV ON TRAVERSING IONIZATION CHAMBER WALLS.
FRACTION Sc OR Sp
S°(W)
S° = Pp Ss + Pc Sc
Pp = RELATIVE PROBABILITY FOR PAIR PRODUCTION IN CARBON. SEE FIG. 1
SAME ASSUMPTIONS AS ABOVE
GAMMA-RAY ENERGY W (MEV)

FIG. 2. Above: Fraction of gamma-ray energy which goes into ionization after one collision. Below: Average fraction of gamma-ray energy which goes into ionization after one collision in carbon. (The equation between the abscissae .6 and .8 should read: $S^0=P_pS_p+P_cS_c$.)

average fraction of the energy given to the recoils

$$\bar{x}(W)=\int xk(x)dx \Big/ \int k(x)dx \qquad (11)$$

varies from 0.20 at 100 Mev, to 0.30 at 10 Mev, to 0.55 at 1 Mev.

Using the Compton cross section (9) in (4) gives

$$S_c(W)=1-\bar{x}(W), \qquad W<25, \quad (12a)$$

$$S_c(W)=\frac{25}{W}-\frac{8-9x_0+x_0^3+6x_0\ln x_0}{3+2\ln(4W+1)}, \qquad W>25, \quad (12b)$$

where $x_0=1-25/W$.

$S_c(W)$ and $S_p(W)$ are shown in Fig. 2, together with the values of $S^0=P_cS_c+P_pS_p$ for carbon. The superscript ^{0} is used, because the sensitivity just obtained is uncorrected for attenuation, scattering, and radiation. In the next section, we shall find, that to a good approximation, including all corrections,

$$S(W)=e^{-T/G}S^0(W). \qquad (13)$$

Referring to Eq. (5), we see that the proper measure of the relative sensitivity of the chamber as a function of x-ray energy is $S(W)/G(W)$. This is plotted in Fig. 3. An examination of the curve shows that it can be fitted closely by

$$\begin{aligned} S/G&=0.84e^{-0.017W}, \quad W<25, \\ &=0.71e^{-0.011W}, \quad W>25. \end{aligned} \qquad (14)$$

Although this sensitivity varies by a factor of about 3 from the low energies to 100 Mev, the average sensitivity $\langle S/G\rangle_{Av}$ is not influenced much by the exact shape of the assumed spectrum $Wf(W)dW$. This is true for any smooth spectrum such as the betatron spectrum. For example, if we assume $Wf(W)=1$ from 0 Mev to 100 Mev, the resulting sensitivity $\langle S/G\rangle_{Av}$ is 0.45. On the other hand, the markedly different assumption $Wf(W)=1-0.01W$ gives $\langle S/G\rangle_{Av}=0.54$.

For simplicity, the sensitivity $\langle S/G\rangle_{Av}$ is computed for a flat spectrum up to any betatron energy U. The sensitivity thus obtained varies smoothly from 0.45 at 100 Mev, to 0.61 for betatron operation at 20 Mev (see Fig. 4). It should be noted that for betatron operation at energies less than 100 Mev, $\langle S/G\rangle_{Av}$ is even less sensitive to assumptions about the betatron spectrum since $S(W)/G(W)$ varies over a smaller range.

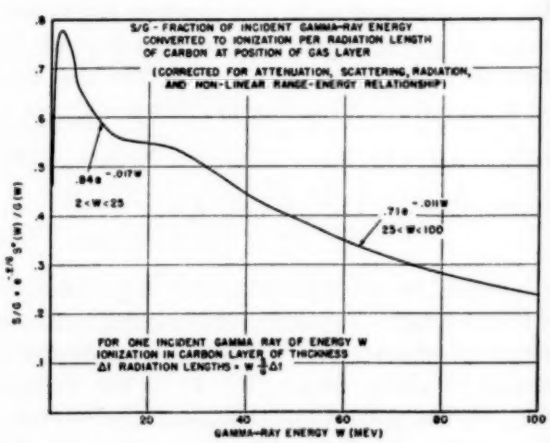
S/G - FRACTION OF INCIDENT GAMMA-RAY ENERGY CONVERTED TO IONIZATION PER RADIATION LENGTH OF CARBON AT POSITION OF GAS LAYER
(CORRECTED FOR ATTENUATION, SCATTERING, RADIATION, AND NON-LINEAR RANGE-ENERGY RELATIONSHIP)
.84e^-.017W
2<W<25
.71e^-.011W
25<W<100
FOR ONE INCIDENT GAMMA RAY OF ENERGY W IONIZATION IN CARBON LAYER OF THICKNESS Δt RADIATION LENGTHS = W ± Δt
GAMMA-RAY ENERGY W (MEV)

FIG. 3. S/G is fraction of incident gamma-ray energy converted to ionization per radiation length of carbon at position of gas layer (corrected for attenuation, scattering, radiation, and non-linear range-energy relationships).

4. FACTORS WHICH AFFECT THE ELECTRON EFFICIENCY

A. Attenuation

In place of the gamma-ray intensity at the surface of the ionization chamber, one should use an intensity averaged over the region in which those electrons are produced which cause the ionization in the gas layer. (If $R<T$ this layer is of thickness R, running from $T-R$ to T. If $R>T$, the layer is of thickness T.) The average decrease in sensitivity resulting from attenuation is thus given by

$$R<T,\quad \frac{1}{R}\int_{T-R}^{T} e^{-z/G}dz=\frac{G}{R}e^{-T/G}[e^{R/G}-1]$$

$$\simeq e^{-T/G}[1+R/2G], \quad (15a)$$

$$R>T,\quad \frac{1}{T}\int_{0}^{T} e^{-z/G}dz=\frac{G}{T}[1-e^{-T/G}]$$

$$\simeq e^{-T/G}[1+T/2G]. \quad (15b)$$

For purposes of computation, it is sufficiently accurate to replace $1/G$ by 0.7 in the brackets (see Figs. 1a and 1b) while retaining it in the exponential.

B. Non-Linearity in the Range-Energy Relationship

The efficiency for an electron of energy $E>25$ is not $25/E$, but is given by the actual fraction of energy lost by such an electron on traversing the block of thickness T.

$$\eta=[E(R)-E(R-T)]/E(R),\quad R>T, \quad (16a)$$

$$=(25/E)\{[E(R)-E(R-T)]/25\}. \quad (16b)$$

For a linear range-energy relationship, the number in braces { } in Eq. (16b) can be made exactly unity for all energies, simply by choosing T to be the thickness which will just stop a 25-Mev electron. In the non-linear case, it is better to choose T such that the bracketed member has an average value close to unity over the range from 25 Mev to 100 Mev. This can be done sufficiently accurately by choosing $T=0.2$ radiation lengths.

Below 25 Mev, the efficiency is $\eta=1$ regardless of a non-linear loss of energy to ionization along the path, since all of the energy is converted to ionization (except for a small amount of radiation).

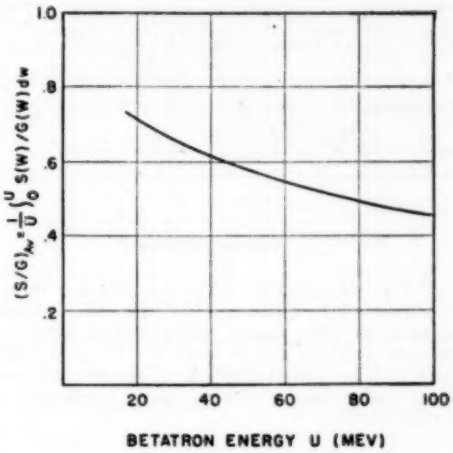

FIG. 4. Fraction of incident gamma-ray energy converted to ionization per radiation length if incident intensity is flat from 0 to U Mev. Ionization energy in gas layer = (incident energy) $\langle S/G\rangle_{Av}\Delta t(R_c/R_g)$, where Δt is the thickness of gas layer in radiation lengths, and R_c/R_g is the ratio of electron ranges in carbon and in the gas, both measured in radiation lengths.

C. Scattering

For electrons which have enough energy to traverse the block, scattering was kept small in the original design (cf. Eq. 2). The effect of this scattering is to increase the path in the block from T to T_s, where

$$T_s\simeq\int_0^T[1+\tfrac{1}{2}\langle\theta^2(t)\rangle_{Av}]dt, \quad (17)$$

and $\langle\theta^2(t)\rangle_{Av}$, the mean-square deflection angle on traversing a finite thickness t, is given by[6]

$$\langle\theta^2(t)\rangle_{Av}=\int_0^t(21/E')^2dt. \quad (18)$$

For a linear range-energy relationship, $E'=E-\epsilon t$,

$$\langle\theta^2(t)\rangle_{Av}=[(21)^2/E(E-\epsilon t)]t, \quad (19)$$

and

$$T_s/T\cong 1-0.066[y+\ln(1-y)] \quad (20)$$

where $y=25/E$, and $\epsilon=120$ Mev/(radiation length) in carbon.

The increase in collision loss due to this length-

[6] Reference 2, p. 264.

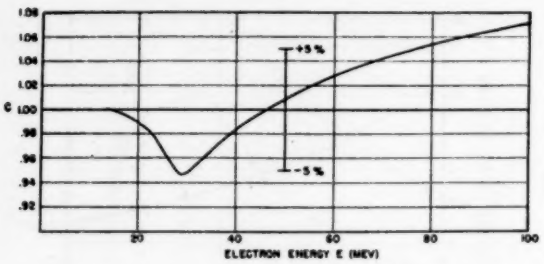

FIG. 5. C is the ratio of the actual fraction of electron energy converted to ionization, to the fraction used for computation in this paper. $C=\eta(\text{actual})/\eta(\text{used})$. The fraction used was: for $E<25$ Mev, $e^{-T/G}$; for $E>25$ Mev, $(25/E)e^{-T/G}$. The actual fraction takes into account attenuation, radiation, scattering and non-linear range-energy relationship.

ening of path is obtained by replacing T in (16) by T_s.

For electrons of energy less than 25 Mev, the scattering does not change the total path length, or the total ionization of an electron. However, it does reduce the thickness of the layer from which electrons can reach the gas from R to R', but this affects only the attenuation correction (15a) which is already a small correction.

An estimate of the straight line path R' is given by

$$R'\simeq\int_0^{t_0}[1-\tfrac{1}{2}\langle\theta^2(t)\rangle_{Av}]dt \tag{21}$$

$$\simeq R[0.6E-\ln(1+0.6E)]/0.6E, \tag{22}$$

when the upper limit t_0 is chosen so that

$$\langle\theta^2(t_0)\rangle_{Av}=2,$$

i.e., so that the integrand remains positive.

D. Radiation

For electrons of energy less than 25 Mev, the effect of radiation is to shorten the range from R to R_r, thus decreasing the ionization loss in the ratio $\mu=R_r/R$. If we represent the energy loss roughly by

$$dE/dt=\epsilon+fE, \tag{23}$$

where the second term is the contribution attributable to radiation, and $f\simeq 1-(1/E^{\frac{1}{2}})$, we find an efficiency

$$\mu=R_r/R=1-(f^2/2\epsilon), \tag{24}$$

where $\epsilon\simeq 100$ Mev/(radiation length) for electrons of less than 25 Mev. The largest correction, at $E=25$ Mev is $\mu=0.92$.

For energies greater than 25 Mev, only high energy radiation produces a decrease in efficiency. For example, a 75-Mev electron will still lose about 25 Mev by collision, on traversing the block, unless it radiates more than 50 Mev, which is very unlikely. Thus above 25 Mev, the efficiency will be given by $\eta=(25/E)\mu$, where the factor μ as the result of radiation will increase rapidly from 0.92 to 1.

To estimate the effect of this radiation straggling, we use Bethe's formula[7] for the distribution of electron energies $w(U)dU$ for an electron of incident energy U_0, after traversing a plate of thickness t, radiation lengths

$$w(U)dU=\frac{dU}{U_0}\frac{[\ln(U_0/U)]^{(t-\ln 2)/\ln 2}}{\Gamma(t/\ln 2)}. \tag{25}$$

The effect of collision losses, which is neglected in (25), can be taken roughly into account by using for U_0 not the incident energy, but an average energy, say $(E-12.5)$ Mev, i.e., by regarding the radiation as taking place in the middle of the plate. This gives

$$\eta(E)=\int_0^{12.5}W(U)(12.5+U)/EdU+(25/E)\int_{12.5}^{E-12.5}W(U)dU, \tag{26}$$

$$\eta(E)=(25/E)\mu,$$

where μ increases from 0.92 at 25 Mev, to 0.985 at 40 Mev, to 0.997 at 100 Mev.

E. Summary

The efficiency, $S(W)$, with which x-ray energy is converted to ionization, was computed using an electron efficiency

$$\begin{aligned}\eta&=Ce^{-T/G} && E<25,\\ \eta&=C(25/E)e^{-T/G} && E>25,\end{aligned} \tag{27}$$

with $C=1$; whereas according to the preceding sections C is given by

$$\begin{aligned}C&=(1+0.35R')\mu && E<25,\\ C&=(1+0.35T)\mu[E(R)-E(T_s)]/25 && E>25.\end{aligned} \tag{28}$$

The correction factor C is plotted in Fig. 5.

[7] Reference 2, p. 256.

By a fortunate coincidence, the increase in efficiency for $E<25$ due to the term $(1+0.35R')$ is cancelled within 1 percent by the decrease caused by radiation μ. Also the thickness of the plate T and hence T_s, was adjusted to reduce the correction factor for $E>25$. Thus, on the average, C is close to unity. Since η is integrated once over electron energies, and then over x-ray energies, the effect of the fluctuations in C about the value unity can be neglected.

5. COMPTON RECOILS

In the preceding calculations, no account was taken of the possibility that some of the Compton recoil x-rays could have a second collision, thus producing additional ionization. For high energy x-rays pair production is the primary effect. The probability of a Compton collision is small, so that the number of recoil x-rays available for a second collision is small. Furthermore, the recoil x-rays, having lower energies, are more likely to produce a Compton collision, in which they transfer only a fraction of their energy to an electron.

This can be illustrated by a rough calculation for x-rays as low as 25 Mev in energy. If 100 x-rays of 25 Mev are incident, the total number of primary collisions is $100(0.2/G)\exp(-0.2/G)=100(0.147)(0.863)=12.7$. Since the relative probability of pair production is $P_p=0.47$, this corresponds to about 6 pairs and 6.7 Compton recoil electrons. The energy converted to ionization is $25[6S_p+6.7S_c]=25[6(0.96)+6.7(0.74)]=268$ Mev. The average energy carried off by each of the Compton recoils is $25(1-0.74)=6.5$ Mev, or a total of 43.5 Mev.

The probability that these 6.5-Mev recoils will have a second collision is $0.1/G(6.5)\simeq 0.13$, since on the average the recoil traverses only 0.1 radiation lengths. The fraction of absorbed energy converted to ionization is $S^0(6.5)\simeq 0.67$. Thus the Compton recoil energy which eventually gets into ionization is $(43.5)(0.13)(0.67)=3.8$ Mev, or 1.3 percent of the 268-Mev ionization obtained from the primary collisions. Note that by using $S^0(6.5)$, which neglects the attenuation factor $\exp[-0.1/G(6.5)]\simeq 0.9$, we have overestimated the secondary collisions in such a manner as to take into account roughly that there are tertiary and higher collisions.

A similar calculation at 10 Mev, shows that about 5 percent of the energy is recaptured by second collisions. Below 10 Mev, the error would be worse. However, this region is not too important since we are interested chiefly in the average sensitivity from 0 to 100 Mev.

ACKNOWLEDGMENT

The author wishes to express his appreciation to Dr. K. H. Kingdon and the other members of the staff of the Research Laboratory of the General Electric Company. The attitude of freedom and stimulation of research in the Laboratory was very gratifying and greatly facilitated this research.

The Electromagnetic Field in Quantized Space-Time

HARTLAND S. SNYDER
Northwestern University, Evanston, Illinois

(Received February 26, 1947)

Relativistically invariant equations of motion for the electromagnetic field are set up in quantized space-time. These equations are solved by a process similar to a Fourier analysis.

IN a previous paper[1] it was shown that a Lorentz invariant space-time is not necessarily a continuum, and an example was given of a discrete Lorentz invariant space-time. This paper is a report on work done to determine whether relativistically invariant field equations could be introduced into quantized space-time, and whether such field equations are solvable. In continuous space-time the field quantities are taken to be functions of the space and time coordinates, and the field equations are partial differential equations. In quantized space-time, coordinates do not commute, thus one has difficulty in giving a general definition of functions of non-commuting variables. Also, since the space-time is discrete, partial derivatives are not definable in the ordinary sense. Now, in the transition from continuous space-time to quantized space-time, the space-time coordinates which were real variables become Hermitian operators; therefore, it is reasonable to suppose that field quantities which were functions of the space-time coordinates will become operators on the Hilbert space on which the coordinate operators operate. I assume that this is the case.

The next thing which must be done is to find replacements for partial derivatives. We note that the displacement operators[2] p_x, p_y, p_z, p_t defined in [*I*] have the same transformation properties as do ∂/∂_x, ∂/∂_y, ∂/∂_z, and ∂/∂_t, and that their commutators with x, y, z, and t approximate, with the exception of numerical factors, those of the partial differential operators with the x, y, z, and t of ordinary space. Consequently, I assume that if $A(x, y, z, t)$ is a field quantity of continuous space-time and if a term of the form $\partial A/\partial x$ appears in the field equations, this term will be replaced by $i[p_x, A]$ in the transition to quantized space-time. It is evident that if A is a Hermitian operator, then $i[p_x, A]$ will also be Hermitian, so that this replacement of partial derivatives preserves reality conditions. If we make the replacements suggested above into the usual form of the vacuum Maxwell's equations, we obtain[3] a relativistically invariant set of equations,

$$i[\mathbf{p}\cdot, \cdot\mathbf{E}]=4\pi\rho, \tag{1}$$

$$i[\mathbf{p}\times, \times\mathbf{H}]-i[p_t, \mathbf{E}]=4\pi\mathbf{S}, \tag{2}$$

$$i[\mathbf{p}\cdot, \cdot\mathbf{H}]=0, \tag{3}$$

$$i[\mathbf{p}\times, \times\mathbf{E}]+i[p_t, \mathbf{H}]=0, \tag{4}$$

in which the symbols $\mathbf{E}$, $\mathbf{H}$, ρ, and $\mathbf{S}$ have their usual meanings and transformation properties. We are using a system of units such that $\hbar=1$ unit of action, $c=1$ unit of velocity, and the vacuum has a unit dielectric constant.

Now, from the first two of Maxwell's equations, (1), (2), one can show that

$$i[p_t, \rho]+i[\mathbf{p}\cdot, \cdot\mathbf{S}]=0, \tag{5}$$

which is our analog of the differential equation for the conservation of charge.

By taking the scalar product of Eq. (2) by $\mathbf{E}$ on both right and left, the scalar product of Eq. (4) by $\mathbf{H}$ on both right and left, and performing other algebraic manipulations, one obtains

$$\tfrac{1}{2}i[p_t, \mathbf{E}^2+\mathbf{H}^2]+\tfrac{1}{2}i[\mathbf{p}\cdot, \cdot(\mathbf{E}\times\mathbf{H}-\mathbf{H}\times\mathbf{E})] +2\pi(\mathbf{S}\cdot\mathbf{E}+\mathbf{E}\cdot\mathbf{S})=0. \tag{6}$$

This result is our analog of the usual differential

[1] Hartland S. Snyder, Phys. Rev. 71, 38 (1947). This paper will be referred to as [*I*] throughout the remainder of this paper.

[2] We will use the general forms for p_x, p_y, p_z, p_t, which are

$$p_x=\frac{\hbar}{a}\frac{\eta_1}{\eta_4}f\left(\frac{\eta_4}{\eta}\right), \cdots, \quad p_t=\frac{\hbar c}{a}\frac{\eta_0}{\eta_4}f\left(\frac{\eta_4}{\eta}\right)$$

as given in [*I*], reference 3.

[3] In these equations $[\mathbf{p}\cdot, \cdot\mathbf{E}]=\mathbf{p}\cdot\mathbf{E}-\mathbf{E}\cdot\mathbf{p}$, $[\mathbf{p}\times, \times\mathbf{H}]=\mathbf{p}\times\mathbf{H}+\mathbf{H}\times\mathbf{p}$, and the dot and cross products have their usual meanings. The use of the double dot and double cross notation inside the commutators helps to avoid confusion.

power equation for the electromagnetic field. Equation (6) is independent of the commutation properties of $\mathbf{E}$, $\mathbf{H}$, ρ, and $\mathbf{S}$.

As in the case of the ordinary Maxwell equations, one can introduce scalar and vector potentials in such a manner that Eqs. (3) and (4) become identities. We introduce the operators V, and $\mathbf{A}$ and set

$$\mathbf{E}=-i[\mathbf{p}, V]-i[p_t, \mathbf{A}], \tag{7}$$

$$\mathbf{H}=i[\mathbf{p}\times, \times\mathbf{A}]. \tag{8}$$

It is readily seen that if the values of $\mathbf{E}$ and $\mathbf{H}$ given by (7) and (8) are substituted into (3) and (4), then (3) and (4) are satisfied identically. If we set $V=V'-i[p_t, \lambda]$, $\mathbf{A}=\mathbf{A}'+i[\mathbf{p}, \lambda]$, in which λ is a scalar operator, we find that $\mathbf{E}$ and $\mathbf{H}$ are expressible in terms of V' and $\mathbf{A}'$ in exactly the same form as Eq. (7) and (8), with V' and $\mathbf{A}'$ replacing V and $\mathbf{A}$. This result gives the gauge invariance of Eqs. (1), (2), (3), and (4). As we can now see, all the derived relationships between the field quantities (such as (5)–(8)) which do not depend upon the commutation properties of the fields, could have been obtained from the relations derived from Maxwell's equation by replacing the operators $\partial/\partial x$, $\partial/\partial y$, $\cdots$, ∂/∂_t by the commutators $i[p_x, \quad]$, $\cdots$, $i[p_t, \quad]$. Thus, we find that the replacement of partial differential operators by these commutator brackets is a consistent procedure, as well as a relativistically invariant one.

A major question is whether such commutator equations as the above can be given meaning, and whether operators satisfying them can be found. The quantities, $\mathbf{E}$, $\mathbf{H}$, $\mathbf{S}$, V, $\mathbf{A}$, and ρ, are supposed to be operators on the Hilbert space on which x, y, z, and t operate. If we denote a vector of the Hilbert space by the symbol, χ, then the scalar (inner) product of the two such vectors, χ and χ', is

$$(\chi', \chi)=\int \frac{d\mathbf{p}dp_t}{D(p_t, \mathbf{p})}\chi'^*(\mathbf{p}, p_t)\chi(\mathbf{p}, p_t), \tag{9}$$

if we use a wave number-frequency space $(\mathbf{p}, p_t)$ representation for the vectors of the Hilbert space. The function $D(p_t, \mathbf{p})$ is a calculable relativistically invariant function of its arguments which depends on $f(\eta_4/\eta)$ and which makes x, y, z, and t Hermitian operators. $D^{-1}(p_t, \mathbf{p})d\mathbf{p}dp_t$ is essentially the volume element of the hyper surface $\eta^2=$constant. The asterisk on a function means the complex conjugate. The meaning of all terms such as orthogonal, Hermitian, unitary, etc., is determined by the usual definitions, with (9) giving the meaning to the scalar product of the vectors of Hilbert space.

For the purpose of finding operators satisfying Eqs. (1), (2), (3), and (4), consider an operator, $A_\mathbf{k}$, with the property that

$$A_\mathbf{k}\chi(\mathbf{p}, p_t)=\int d\omega f(\mathbf{p}, p_t, \mathbf{k}, \omega)\chi(\mathbf{p}-\mathbf{k}, p_t-\omega) \tag{10}$$

for every vector $\chi(\mathbf{p}, p_t)$ of Hilbert space, with $f(\mathbf{p}, p_t, \mathbf{k}, \omega)$ an arbitrary given function of its arguments which is independent of the function $\chi(\mathbf{p}, p_t)$. It is not difficult to verify that the operator, $A_\mathbf{k}$, satisfies the commutation relation,

$$[\mathbf{p}, A_\mathbf{k}]=\mathbf{k}A_\mathbf{k}. \tag{11}$$

Conversely, one can show that the general solution of (11) is an operator whose properties are given by Eq. (10). We note here that if two operators have the property given by (11), $[\mathbf{p}, A_\mathbf{k}]=\mathbf{k}A_\mathbf{k}$, $[\mathbf{p}, B_{\mathbf{k}'}]=\mathbf{k}'B_{\mathbf{k}'}$ then the product $A_\mathbf{k}B_{\mathbf{k}'}$ has the same property, $[\mathbf{p}, A_\mathbf{k}B_{\mathbf{k}'}]=(\mathbf{k}+\mathbf{k}')A_\mathbf{k}B_{\mathbf{k}'}$. Also, operators satisfying (11) necessarily possess complex adjoint operators. If $A_\mathbf{k}$ is an operator with a complex adjoint operator $A_\mathbf{k}^+$, then

$$(A_\mathbf{k}^+\chi', \chi)=(\chi', A_\mathbf{k}\chi).$$

Now,

$$A_\mathbf{k}^+\chi'(\mathbf{p}, p_t)=\int d\omega f^+(\mathbf{p}, p_t, \mathbf{k}, \omega)\chi'(\mathbf{p}+\mathbf{k}, p_t+\omega),$$

and

$$A_\mathbf{k}\chi(\mathbf{p}, p_t)=\int d\omega f(\mathbf{p}, p_t, \mathbf{k}, \omega)\chi(\mathbf{p}-\mathbf{k}, p_t-\omega),$$

then Eq. (9) requires that

$$D(\mathbf{p}, p_t)f^+(\mathbf{p}-\mathbf{k}, p_t-\omega, \mathbf{k}, \omega)=D(\mathbf{p}-\mathbf{k}, p_t-\omega)f^*(\mathbf{p}, p_t, \mathbf{k}, \omega).$$

This last equation is solvable for $f^*(\mathbf{p}, p_t, \mathbf{k}, \omega)$ with the consequence that every operator satisfying (11) has an adjoint.

We will now suppose that all of the field operators entering the field equations can be written as linear combinations of operators which satisfy

Eq. (11). For example, we assume that

$$\rho=\int d\mathbf{k}\rho_{\mathbf{k}}, \tag{12}$$

where

$$[\mathbf{p}, \rho_{\mathbf{k}}]=\mathbf{k}\rho_{\mathbf{k}}.$$

This assumption is the equivalent of the assumption usually made for field theories in continuous space-time, that the field can be Fourier analyzed. We will call the process exemplified by Eq. (12) a wave number analysis.

If we choose the gauge of the electromagnetic potentials, V and $\mathbf{A}$, so that

$$[\mathbf{p}\cdot, \cdot\mathbf{A}]=0, \tag{13}$$

and if we make a wave number analysis of $\mathbf{A}$, then it can be written

$$\mathbf{A}=\int d\mathbf{k}\sum_{\lambda=1}^{3}\boldsymbol{\varepsilon}_{\lambda\mathbf{k}}A_{\lambda\mathbf{k}}, \tag{14}$$

in which we take the $\boldsymbol{\varepsilon}_{\lambda\mathbf{k}}$ to be three mutually perpendicular unit vectors with $\boldsymbol{\varepsilon}_{3\mathbf{k}}$ in the direction of the vector $\mathbf{k}$. When we apply condition (13) to $\mathbf{A}$, we obtain

$$[\mathbf{p}\cdot, \cdot\mathbf{A}]=\int dk k A_{3\mathbf{k}}=0. \tag{15}$$

This implies that $A_{3\mathbf{k}}=0$, whereas $A_{1\mathbf{k}}$ and $A_{2\mathbf{k}}$ are, insofar as this condition is concerned, arbitrary operators satisfying

$$[\mathbf{p}, A_{\lambda\mathbf{k}}]=\mathbf{k}A_{\lambda\mathbf{k}}, \quad \lambda=1, 2.$$

This result corresponds to the usual result that the Fourier coefficients of the vector potential are perpendicular to the wave number vector if the divergence of the vector potential vanishes.

If the vector potential $\mathbf{A}$ satisfies (13), then by eliminating the electric field from (1) by the use of (7), we obtain the analog of Poisson's equation

$$[\mathbf{p}\cdot, \cdot[\mathbf{p}, V]]=4\pi\rho. \tag{16}$$

If we make a wave number analysis of V and ρ, we find for the components, $V_{\mathbf{k}}$ and $\rho_{\mathbf{k}}$, the relation

$$k^2V_{\mathbf{k}}=4\pi\rho_{\mathbf{k}}. \tag{17}$$

Equation (17) is identical in form with that given for the connection between the Fourier components of the potential and the Fourier components of the charge density. The solution of (17) gives us the following solution of (16):

$$V=4\pi\int\frac{d\mathbf{k}}{k^2}\rho_{\mathbf{k}}+V_0, \tag{18}$$

in which V_0 is an operator which satisfies the condition $[\mathbf{p}, V_0]=0$. The general form of V_0 is

$$V_0=\int d\omega V_{0\omega}, \tag{19}$$

where

$$V_{0\omega}\chi(\mathbf{p}, p_t)=g(\mathbf{p}, p_t, \omega)\chi(\mathbf{p}, p_t-\omega).$$

The presence of the term V_0 in the solution of the "Poisson" equation corresponds to the fact that in continuous space-time an arbitrary function of the time can be added to the scalar potential. This term V_0 in V can be removed by a gauge transformation which does not affect the vector potential.

We now write

$$\mathbf{A}=\int d\mathbf{k}\sum_{\lambda=1,2}\boldsymbol{\varepsilon}_{\lambda\mathbf{k}}(\alpha_{\lambda\mathbf{k}}+\alpha_{\lambda\mathbf{k}}^{+}), \tag{20}$$

$$\mathbf{E}=i\int d\mathbf{k}\sum_{\lambda=1,2}\boldsymbol{\varepsilon}_{\lambda\mathbf{k}}(\alpha_{\lambda\mathbf{k}}-\alpha_{\lambda\mathbf{k}}^{+})-i[\mathbf{p}, V], \tag{21}$$

in which equations $\alpha_{\lambda\mathbf{k}}^{+}$ is the complex adjoint to $\alpha_{\lambda\mathbf{k}}$, and in which V is given by (18). The $\alpha_{\lambda\mathbf{k}}$ are taken to satisfy $[\mathbf{p}, \alpha_{\lambda\mathbf{k}}]=\mathbf{k}\alpha_{\lambda\mathbf{k}}$ with the consequence that $[\mathbf{p}, \alpha_{\lambda\mathbf{k}}^{+}]=-\mathbf{k}\alpha_{\lambda\mathbf{k}}^{+}$. These particular forms for $\mathbf{A}$ and $\mathbf{E}$ guarantee that $\mathbf{E}$, $\mathbf{A}$, and $\mathbf{H}$ are Hermitian operators if ρ is Hermitian. The value of the magnetic field may then be computed by (8) using the above properties of $\alpha_{\lambda\mathbf{k}}$, and $\alpha_{\lambda\mathbf{k}}^{+}$ and is

$$\mathbf{H}=i\int d\mathbf{k}\,\mathbf{k}\times\boldsymbol{\varepsilon}_{\lambda\mathbf{k}}(\alpha_{\lambda\mathbf{k}}-\alpha_{\lambda\mathbf{k}}^{+}). \tag{22}$$

If we make a wave number analysis of $\mathbf{S}$, and if we substitute the values of $\mathbf{E}$ and $\mathbf{H}$ given by (21) and (22) into Eq. (2), we find that

$$\int d\mathbf{k}\sum_{\lambda=1,2}\boldsymbol{\varepsilon}_{\lambda\mathbf{k}}\{k^2(\alpha_{\lambda\mathbf{k}}+\alpha_{\lambda\mathbf{k}}^{+}) + k[p_t, \alpha_{\lambda\mathbf{k}}-\alpha_{\lambda\mathbf{k}}^{+}]-4\pi S_{\lambda\mathbf{k}}\}=0. \tag{23}$$

That part, the longitudinal part, of the current arising from $S_{3\mathbf{k}}$ is canceled out of the right-hand

side of Eq. (2) by that part of $-i[p_t, \mathbf{E}]$, on the left-hand side of (2), which comes from the term $-i[\mathbf{p}, V]$ in $\mathbf{E}$ because of the charge conservation Eq. (5). If we choose $\varepsilon_{1\mathbf{k}} = -\varepsilon_{1-\mathbf{k}}$, $\varepsilon_{2\mathbf{k}} = \varepsilon_{2-\mathbf{k}}$, Eq. (23) is satisfied by

$$k^2\alpha_{\lambda\mathbf{k}} + k[p_t, \alpha_{\lambda\mathbf{k}}] = 2\pi S_{\lambda\mathbf{k}} \tag{24}$$

$$k^2\alpha_{\lambda\mathbf{k}}{}^+ - k[p_t, \alpha_{\lambda\mathbf{k}}{}^+] = 2\pi(-)^\lambda S_{\lambda-\mathbf{k}}. \tag{25}$$

Equations (24) and (25) are complex adjoint equations of each other and require that $S_{\lambda\mathbf{k}}{}^+ = (-)^\lambda S_{\lambda-\mathbf{k}}$, which is just the condition for the current operator $\mathbf{S}$ to be Hermitian.

When $\mathbf{S}=0$, then Eq. (24) states that the operators $\alpha_{\lambda\mathbf{k}}$ have the property

$$\alpha_{\lambda\mathbf{k}}\chi(\mathbf{p}, p_t) = h(\mathbf{p}, p_t, \mathbf{k})\chi(\mathbf{p}-\mathbf{k}, p_t+k), \tag{26}$$

with $h(\mathbf{p}, p_t, \mathbf{k})$ an arbitrary function of its arguments. This result is essentially the same as if an electromagnetic wave had a wave number vector $\mathbf{k}$; its frequency is k for empty space.

If we make a frequency analysis of $\alpha_{\lambda\mathbf{k}}$ and $S_{\lambda\mathbf{k}}$,

$$\alpha_{\lambda\mathbf{k}} = \int d\omega \alpha_{\lambda\mathbf{k}\omega}, \quad S_{\lambda\mathbf{k}} = \int d\omega S_{\lambda\mathbf{k}\omega}, \tag{27}$$

in which $[p_t, \alpha_{\lambda\mathbf{k}\omega}] = \omega\alpha_{\lambda\mathbf{k}\omega}$ and $[p_t, S_{\lambda\mathbf{k}\omega}] = \omega S_{\lambda\mathbf{k}\omega}$, we obtain from (24) and (27)

$$k(k+\omega)\alpha_{\lambda\mathbf{k}\omega} = 2\pi S_{\lambda\mathbf{k}\omega}. \tag{28}$$

When we use (27) and (20), the solution of (28) gives the following for the vector potential:

$$\mathbf{A} = 2\pi \int d\mathbf{k} \sum_{\lambda=1,2} \varepsilon_{\lambda\mathbf{k}} \int d\omega \frac{S_{\lambda\mathbf{k}\omega} + S_{\lambda\mathbf{k}\omega}{}^+}{k(k+\omega)} + \int d\mathbf{k} \sum_{\lambda=1,2} \varepsilon_{\lambda\mathbf{k}}(\alpha_{\lambda\mathbf{k}}{}^0 + \alpha_{\lambda\mathbf{k}}{}^{0+}). \tag{29}$$

In (29) the integral over ω is taken in the sense of its principal value for the neighborhood of $\omega = -k$. The operator $\alpha_{\lambda\mathbf{k}}{}^0$ is as follows:

$$\alpha_{\lambda\mathbf{k}}{}^0\chi(\mathbf{p}, p_t) = h(\mathbf{p}, p_t, \mathbf{k})\chi(\mathbf{p}-\mathbf{k}, p_t+k)$$

for arbitrary vectors $\chi(\mathbf{p}, p_t)$ of the Hilbert space, and $h(\mathbf{p}, p_t, \mathbf{k})$ is an arbitrary function of its arguments.

As a summary of what we have obtained, it may be said that in quantized space-time, relativistically invariant field equations may be written. In these equations the field quantities are treated as operators, and partial differential operators $\partial/\partial x$, $\partial/\partial y$, $\partial/\partial z$, and $\partial/\partial t$ of continuous space-time are replaced by the commutators $i[p_x, \ ], \cdots, i[p_t, \ ]$. It has been shown that this replacement process is a consistent one. Operators satisfying the commutator field equations have been found. These operators are expressed in terms of wave number-frequency components of the operators, a process which is quite analogous to the usual Fourier analysis of fields. When the solutions of the Maxwell equations are expressed in terms of the wave number-frequency analysis, the solutions are of exactly the same form as those obtained by the Fourier analysis in the case of continuous space-time. In fact, the general procedure which we have used here applies equally as well to continuous space-time as it does to quantized space-time. However, in the continuous space-time case additional limitations are placed on the field operators. The wave number-frequency components $A_{\mathbf{k}\omega}$ of an operator, A, are restricted for this case so that

$$A_{\mathbf{k}\omega}\chi(\mathbf{p}, p_t) = f(\mathbf{k}, \omega)\chi(\mathbf{p}-\mathbf{k}, p_t-\omega),$$

as compared with the more general form we have used,

$$A_{\mathbf{k}\omega}\chi(\mathbf{p}, p_t) = f(\mathbf{p}, p_t, \mathbf{k}, \omega)\chi(\mathbf{p}-\mathbf{k}, p_t-\omega).$$

The above restriction guarantees for the continuous space-time case that the operator A may be written as a function of x, y, z, and t. I am not certain what restriction should be used in the quantized space-time case, although it is probably connected with the normalizing function $D(p_t, \mathbf{p})$. The essential differences between continuous and quantized space-time lie in the change of definition of the scalar products of the vectors of the Hilbert space, and in the value regions of wave number-frequency four-vectors.

Although we have dealt in this paper only with the vacuum Maxwell equations with given charge and current distributions, the same procedure can be applied to the Klein-Gordon equation, the Dirac equation, the Proca equation, and others. At the present time work is being done to determine appropriate limitations on the field operators, and to determine whether field operators can be quantized.

Non-Linear Invariants and the Problem of Motion

CHRISTOPHER GREGORY
University of Hawaii, Honolulu, Hawaii
(Received March 20, 1947)

The effect of adding quadratic invariants to the integrand of the usual variation principle in general relativity is considered in the light of a new approximation method. The case in which the quadratic invariant is a constant multiple of the square of the scalar curvature is treated up to the Newtonian approximation, insofar as the problem of motion is concerned. The Newtonian equations result for sufficiently large "distances" between particles regardless of the order of magnitude of the multiplying constant. The requirement that the "force function" be finite everywhere places restrictions on the number of "particles" p, comprising the system. When $p=1, 2$, the requirement is fulfilled. The less stringent requirement that the "force function" be finite when all "particles" coincide restricts p less severely. If the absolute values of the "masses" are not all equal there is no restriction on p, but if they are all equal p is restricted to certain integral values.

1. INTRODUCTION

BY means of an ingenious approximation method initiated by Einstein, Infeld, and Hoffmann,[1] it has been shown that the motion of matter, represented as point singularities of the field, is sufficiently determined by the gravitational equations for empty space. The four differential identities make possible the equations of motion. The non-linear character of the field equations is directly responsible for the interaction terms present in the equations of motion. It is possible, however, to construct an infinite number of non-linear field equations involving the metric tensor, all of which satisfy four differential identities. The Hamiltonian derivative[2] of any invariant involving the $g^{\mu\nu}$ and their partial derivatives satisfies four differential tensor identities, and the equations are non-linear in character. It is a well-known fact that the field equations for empty space can be obtained by setting the Hamiltonian derivative of the scalar curvature, $R=g^{\mu\nu}R_{\mu\nu}$, equal to zero. The restriction to the invariant R seems to be dictated by the assumption that the field equations be second-order partial differential equations. This has engendered the use of phenomenological devices in subsequent generalizations of the field equations in the presence of matter.

It is of some interest to consider the effect of the addition of other invariant functions of the metric tensors and their partial derivatives to the scalar curvature on the equations of motion. The simplest generalization of the scalar R seems to be effected by the addition of terms which lead to partial derivatives of the fourth order of the metric tensor and quadratic terms involving the curvature tensor. Lanczos[3] has investigated quadratic invariants and has come to the conclusion that only two independent ones, namely, R^2 and $R_{\mu\nu}R^{\mu\nu}$, exist. In this paper, the effect of adding the additional term $\frac{1}{6}a^2R^2$, where a is a constant, will be studied up to, and including the Newtonian approximation.

The addition of a linear combination of the two quadratic invariants $\alpha R^2+\beta R_{\mu\nu}R^{\mu\nu}$ to R, may be thought of as representing the contribution of matter. Now the above may be written as $(\alpha-\frac{1}{3}\beta)R^2+\frac{1}{3}\beta(R^2-3R_{\mu\nu}R^{\mu\nu})$. It can be readily shown that the Hamiltonian derivative of the second part, when multiplied by $g_{\mu\nu}$ to form a scalar, is identically nil. This, however, is a property of the electromagnetic stress-energy-momentum tensor. It seems possible, then, that the equations of motion deduced from the scalar $R+\alpha R^2+\beta R_{\mu\nu}R^{\mu\nu}$ may include interaction terms of Lorentz' type. The details and the conclusions to be drawn from these considerations will be presented at a later date.

[1] A. Einstein, L. Infeld, and B. Hoffmann, Ann. of Math. **39**, 65 (1938); A. Einstein and L. Infeld, *ibid.*, **41**, 455 (1940). This method is referred to herein as the E.I.H. method.

[2] A. S. Eddington, *The Mathematical Theory of Relativity* (Cambridge University Press, England, 1940), p. 141.

[3] C. Lanczos, Ann. of Math. **39**, 842 (1938).

2. HAMILTONIAN DERIVATIVES OF R^2 AND $R_{\mu\nu}R^{\mu\nu}$

The process of Hamiltonian differentiation is equivalent to the determination of the coefficient of the variation, $\delta g_{\mu\nu}$, when the invariant under consideration is regarded as the integrand of a variation principle. A straightforward application of the calculus of variations leads to the result

$$I^{\mu\nu} = -2RR^{\mu\nu} + \tfrac{1}{2}g^{\mu\nu}R^2 + 2(g^{\alpha\beta}g^{\mu\nu} - g^{\mu\beta}g^{\nu\alpha})R_{;\alpha\beta} \quad (1)$$

for the Hamiltonian derivative of the invariant R^2. The symbol $(\ )_{;\alpha\beta}\ldots$ denotes co-variant differentiation. The Hamiltonian derivative of the invariant $R_{\mu\nu}R^{\mu\nu}$ turns out to be

$$J^{\mu\nu} = -R_{\alpha}{}^{\mu}R^{\alpha\nu} - g^{\nu\gamma}R^{\alpha\beta}R_{\alpha\beta\gamma}{}^{\mu} + \tfrac{1}{2}g^{\mu\nu}R_{\alpha\beta}R^{\alpha\beta} + (R^{\alpha\beta}g^{\mu\nu} + R^{\mu\nu}g^{\alpha\beta} - R^{\mu\beta}g^{\nu\alpha} - R^{\nu\alpha}g^{\mu\beta})_{;\alpha\beta}. \quad (2)$$

With the aid of the Bianchi identities, it can be shown that $I^{\mu\nu}{}_{;\nu}$ and $J^{\mu\nu}{}_{;\nu}$ are identically zero.

It will now be shown, as a check upon the derivation of Eq. (1), that $I^{\mu\nu}{}_{;\nu} \equiv 0$.

$$I^{\mu\nu}{}_{;\nu} = -2R^{\mu\nu}{}_{;\nu}R - 2R^{\mu\nu}R_{;\nu} + g^{\mu\nu}RR_{;\nu} + 2g^{\alpha\beta}(R_{;\alpha\beta\nu} - R_{;\alpha\nu\beta}).$$

But,

$$R^{\mu\nu}{}_{;\nu} \equiv \tfrac{1}{2}g^{\mu\nu}R_{;\nu},$$

and

$$g^{\alpha\beta}g^{\mu\nu}(R_{;\alpha\beta\nu} - R_{;\alpha\nu\beta}) \equiv g^{\alpha\beta}g^{\mu\nu}R_{;\gamma}R_{\alpha\beta\nu}{}^{\gamma} = R^{\mu\nu}R_{;\nu}.$$

Consequently,

$$I^{\mu\nu}{}_{;\nu} = -g^{\mu\nu}RR_{;\nu} - 2R^{\mu\nu}R_{;\nu} + g^{\mu\nu}RR_{;\nu} + 2R^{\mu\nu}R_{;\nu} \equiv 0.$$

In a similar fashion $J^{\mu\nu}{}_{;\nu} \equiv 0$.

Upon lowering the indices by tensor multiplication, (1) and (2) may be written as

$$I_{\mu\nu} = -2RR_{\mu\nu} + \tfrac{1}{2}g_{\mu\nu}R^2 + 2(g_{\mu\nu}g^{\alpha\beta} - \delta_{\mu}{}^{\alpha}\delta_{\nu}{}^{\beta})R_{;\alpha\beta}, \quad (3)$$

$$J_{\mu\nu} = -R^{\alpha\beta}R_{\alpha\beta\mu\nu} - g_{\nu\beta}R^{\alpha\beta}R_{\mu\alpha} + \tfrac{1}{2}g_{\mu\nu}R^{\alpha\beta}R_{\alpha\beta} + g_{\mu\nu}R^{\alpha\beta}{}_{;\alpha\beta} + g^{\alpha\beta}R_{\mu\nu;\alpha\beta} - g_{\nu\beta}R^{\alpha\beta}{}_{;\mu\alpha} - g_{\mu\alpha}R^{\alpha\beta}{}_{;\beta\nu} \quad (4)$$

$$= -R^{\alpha\beta}R_{\alpha\beta\mu\nu} - g_{\nu\beta}R^{\alpha\beta}R_{\mu\alpha} + \tfrac{1}{2}g_{\mu\nu}R^{\alpha\beta}R_{\alpha\beta} + g^{\alpha\beta}R_{\mu\nu;\alpha\beta} + \tfrac{1}{2}g^{\alpha\beta}g_{\mu\nu}R_{;\alpha\beta} - R_{;\mu\nu}.$$

3. THE FIELD EQUATIONS DERIVED FROM THE INVARIANT $-R+\frac{1}{6}a^2R^2$

If one now considers the quadratic invariant

$$S = -(R + \tfrac{1}{6}a^2R^2), \quad (5)$$

the field equations become, upon applying (1) and recalling that the Hamiltonian derivative of $-R$ is $R^{\mu\nu} - \frac{1}{2}g^{\mu\nu}R$,

$$S^{\mu\nu} = R^{\mu\nu} - \tfrac{1}{2}g^{\mu\nu}R + \tfrac{1}{6}a^2(2RR^{\mu\nu} - \tfrac{1}{2}g^{\mu\nu}R^2 - 2g^{\alpha\beta}g^{\mu\nu}R_{;\alpha\beta} + 2g^{\mu\beta}g^{\nu\alpha}R_{;\alpha\beta}) \quad (6)$$
$$= 0,$$

which will be assumed equal to zero. Upon lowering indices and noting that on the basis of the assumption $S^{\mu\nu} = 0$

$$g_{\mu\nu}S^{\mu\nu} = g^{\alpha\beta}R_{;\alpha\beta} + a^{-2}R = 0, \quad (7)$$

Eq. (6) is equivalent to

$$S_{\mu\nu} = R_{\mu\nu} - \tfrac{1}{6}g_{\mu\nu}R + \tfrac{1}{3}a^2R_{;\mu\nu} - a^2g_{\mu\nu}R^2/12 + \tfrac{1}{3}a^2RR_{\mu\nu} = 0. \quad (8)$$

(8) and (7) may be written as

$$S_{\mu\nu} = R_{\mu\nu} - \tfrac{1}{6}g_{\mu\nu}R + \tfrac{1}{3}a^2R_{1\mu\nu} - \tfrac{1}{3}a^2R_{1\alpha}\{^{\alpha}_{\mu\nu}\} - a^2g_{\mu\nu}R^2/12 + \tfrac{1}{3}a^2RR_{\mu\nu} = 0, \quad (9)$$

and

$$a^2R_{111} - R = a^2R_{100} + a^2R_{1\alpha}[\{^{\alpha}_{11}\} - \{^{\alpha}_{00}\}] + a^2h^{\alpha\beta}R_{1\alpha\beta} - a^2h^{\alpha\beta}R_{1\gamma}\{^{\gamma}_{\alpha\beta}\}, \quad (10)$$

where $(\ )_{1\mu\nu}\ldots$ denotes ordinary partial differentiation; the h's, the deviation of the metric tensors from their Gailean values, and the Latin indices take the spatial values 1, 2, 3, while Greek indices range from 0 to 3. Upon making transformations of the type h to γ as in E.I.H. (reference 1), the field equations are equivalent to

$$\Phi_{00} + 2\Lambda_{00} + \tfrac{1}{3}a^2R_{111} + \tfrac{1}{3}R + \tfrac{1}{3}a^2R_{100} - \tfrac{1}{3}a^2[\{^{\alpha}_{00}\} + \{^{\alpha}_{11}\}]R_{1\alpha} + \tfrac{1}{6}a^2R^2 + \tfrac{1}{3}a^2(\Phi_{00} + 2\Lambda_{00})R - \tfrac{1}{3}\gamma_{00}R - \tfrac{1}{6}a^2\gamma_{00}R^2 = \Phi_{00} + 2\Omega_{00} = 0, \quad (11)$$

$$\Phi_{0n}+2\Lambda_{0n}+\tfrac{1}{3}2a^2R_{10n}-\tfrac{1}{3}\gamma_{0n}R-\tfrac{1}{3}2a^2R_{1\alpha}\{{}^{\alpha}_{0n}\}$$
$$-\tfrac{1}{6}a^2\gamma_{0n}R^2+\tfrac{1}{3}a^2(\Phi_{0n}+2\Lambda_{0n})R$$
$$=\Phi_{0n}+2\Omega_{0n}=0, \quad (12)$$

$$\Phi_{mn}+2\Lambda_{mn}-\tfrac{1}{3}\delta_{mn}R-\tfrac{1}{3}a^2\delta_{mn}R_{11}+\tfrac{1}{3}2a^2R_{1mn}$$
$$+\tfrac{1}{3}a^2\delta_{mn}R_{100}-\tfrac{1}{3}\gamma_{mn}R-\tfrac{1}{3}2a^2[\{{}^{\alpha}_{mn}\}$$
$$-\tfrac{1}{2}\delta_{mn}\{{}^{\alpha}_{11}\}+\tfrac{1}{2}\delta_{mn}\{{}^{\alpha}_{00}\}]R_{1\alpha}-\tfrac{1}{6}a^2\delta_{mn}R^2$$
$$+\tfrac{1}{3}a^2(\Phi_{mn}+2\Lambda_{mn})-\tfrac{1}{6}a^2\gamma_{mn}R^2$$
$$=\Phi_{mn}+2\Omega_{mn}=0, \quad (13)$$

where $\Omega_{\mu\nu}$ is accordingly defined. The Φ's and Λ's are defined in precisely the same manner as in the E.I.H. paper. If one compares (11), (12), and (13) with the transformed field equations treated there, it is readily seen that the new approximation method is applicable to the present equations with little change. The equations involving the $\Lambda_{\mu\nu}$ in E.I.H. have simply to be replaced by the $\Omega_{\mu\nu}$ implicitly defined in (11), (12), and (13). The equations to be solved at each stage of the approximation are similar, with the exception of the additional inhomogeneous wave equation (10).

4. EQUATION OF MOTION IN NEWTONIAN APPROXIMATION

Upon introducing the E.I.H. expansions for the field quantities and proceeding in a somewhat similar manner, the equations of motion in the Newtonian approximation turn out to be

$$m_k\left(\frac{\partial^2\xi}{\partial t^2}\right)^{(n)}_k$$
$$+\sum_{j\neq k}^{p}(m_jm_kV_{jk}+a^2r_{0j}r_{0k}W_{jk}/12)_{,n} \quad (14)$$
$$j,\ k=1,\ 2,\ \cdots,\ p,$$

where p denotes the number of "particles"; the m_k their masses; $(\xi_k^{(1)}, \xi_k^{(2)}, \xi_k^{(3)})$ the cartesian coordinates of the kth particle; the r_{0k} arbitrary constants associated with the kth particle; and $(\ )_{,n}$ denotes partial differentiation with respect to $\xi_k^{(n)}$. The V_{jk} and W_{jk} are given by

$$V_{jk}\equiv 1/r_{jk}; \quad W_{jk}\equiv V_{jk}e^{-r_{jk}/a};$$
$$r_{jk}\equiv[(\xi_j^{(s)}-\xi_k^{(s)})(\xi_j^{(s)}-\xi_k^{(s)})]^{\frac{1}{2}}. \quad (15)$$

The equation differs from the ordinary Newtonian equation by the appearance of an additional term in the summand of (14). If $a>0$, it is seen that for large "distances" between "particles" ($r_{jk}\gg a$) (14) reduces to the ordinary equations of motion *irrespective of the order of magnitude of* a. It is believed that this result is of importance in that it does not require one to treat the additional term in the variation principle as a perturbation.

5. ON RENDERING "FORCES" FINITE

The appearance of the arbitrary constants r_{0k}, associated with the kth particle in the equations of motion, leads one to speculate as to the possibility of rendering the "forces" finite everywhere in this order of approximation. To carry out this investigation, it is only necessary to examine the "potential function" corresponding to the equation of motion, namely,

$$U\equiv\sum_{j\neq k}^{p}[m_jm_kV_{jk}+a^2r_{0j}r_{0k}W_{jk}/12]. \quad (16)$$

If one defines

$$m_k\equiv p_k\mu_k, \quad p_k=\pm 1, \quad \mu_k>0; \quad (17)$$

and assumes

$$(a^4r_{0k}^2/12)^{\frac{1}{2}}=q_k\mu_k, \quad q_k=\pm 1; \quad (18)$$

then (15) becomes

$$U=\sum_{j\neq k}^{p}\mu_j\mu_k(p_jp_kV_{jk}+q_jq_kW_{jk}). \quad (19)$$

Thus, in order that U be finite everywhere for arbitrary μ's

$$p_jp_k+q_jq_k=0, \quad j\neq k. \quad (20)$$

It is possible to satisfy these conditions only when $p=2$.

The imposition of the requirement that the U be finite when all "particles" coincide places no restriction on the number of particles p if the μ's are not all equal. In this case, it is only necessary that

$$\sum_{j\neq k}^{p}\mu_j\mu_k(p_jp_k+q_jq_k)=0. \quad (21)$$

However, if the μ's are all equal, (21) degenerates into

$$\sum_{j\neq k}(p_jp_k+q_jq_k)=0. \tag{22}$$

Since the p's and q's take on values of ± 1 only, it is clear that (22) will not hold for abitrary p. Simple calculations show that if α_+ and α_- denote the number of positive and negative p's, respectively, and β_+ and β_- the number of positive and negative q's, respectively, then in order that (22) hold,

$$\begin{aligned}&\alpha_+=m^2+n^2+m, \quad \beta_+=m^2+n^2+n,\\ &\alpha_-=m^2+n^2-m, \quad \beta_-=m^2+n^2-n,\\ &p=2(m^2+n^2), \quad m, n=0, 1, 2, \cdots,\end{aligned} \tag{23}$$

for p even. If p is odd

$$\begin{aligned}&\alpha_+=m^2+n^2-n, \qquad \beta_+=m^2+n^2-m,\\ &\alpha_-=m^2+n^2-2m-n+1,\\ &\qquad\qquad \beta_-=m^2+n^2-m-2n+1,\\ &p=2(m^2+n^2-m-n)+1, \quad m, n=0, 1, 2, \cdots.\end{aligned} \tag{24}$$

Other solutions may be generated by interchanging α_+, α_-, β_+, and β_- in a suitable fashion. For these cases $|\alpha_+-\alpha_-|$ and $|\beta_+-\beta_-|$ yield any positive integer.

6. CONCLUSION

The E.I.H. method seems to be applicable to the field equations derived by the procedure of adding the invariant $\frac{1}{8}a^2R^2$ to the integrand of the usual variation principle. It is found that insofar as the Newtonian approximation is concerned, for sufficiently large "distances" between "particles," a reduction to the ordinary Newtonian equations ensues regardless of the order of magnitude of $a(>0)$. The investigation regarding the condition for the existence of finite "forces" between particles *may* be of physical significance to the theory of nuclear structure assuming, of course, that the invariant studied possesses physical significance. It is hoped that this study at least increases the conceptual possibilities insofar as field theories are concerned.

Letters to the Editor

PUBLICATION of brief reports of important discoveries in physics may be secured by addressing them to this department. The closing date for this department is, for the issue of the 1st of the month, the 8th of the preceding month and for the issue of the 15th, the 23rd of the preceding month. No proof will be sent to the authors. The Board of Editors does not hold itself responsible for the opinions expressed by the correspondents. Communications should not exceed 600 words in length.

(*d–n*) Reactions at 15 Mev

R. B. ROBERTS AND P. H. ABELSON
Carnegie Institution of Washington, Department of Terrestrial Magnetism, Washington, D. C.
May 24, 1947

NEUTRON emission is usually considered as "evaporation" from an excited nucleus. According to this picture most of the neutrons should have relatively low energies, and there should be no large directional effects.

Neutron emission has also been observed from the disintegration of the deuteron on striking the target. In this process the neutrons are predominately in the forward direction and have roughly one-half the energy of the incident deuteron. Although this process was suggested in 1933,[1] it has only been observed with 200-Mev deuterons.[2] At lower energies the only evidence for this type of disintegration comes from the *d–p* reactions in which the neutron is captured.

We have investigated the neutrons produced by the 60-inch cyclotron by placing threshold detectors[3,4] at 0° and 90° with respect to the cyclotron beam.

Table I shows the effects produced in various detectors for different bombarding particles and targets. The observed activities are reduced to numbers proportional to the number of radioactive atoms formed in the detector per particle impinging on the target. Each column is then normalized. A probe target was used, and the energies listed are calculated from the radius at the probe. The relative values for any one bombardment are considerably more accurate (10 percent) than relative values from one target to another (30 percent). Any background would tend to reduce the following prominent features of the observed distribution.

TABLE I. Summary of data.

Detector Threshold	$Cu^{63}(n, 2n)Cu^{62}$ 12–13 Mev	$Ag^{107}(n, 2n)Ag^{106}$ 5–7 Mev	$Al^{27}(n, \alpha)Na^{24}$ 3.77 Mev	$Al^{27}(n, p)Mg^{27}$ 1.95 Mev	$Mn^{55}(n, \gamma)Mn^{56}$ 0
Bombarding particle and target					
H^2+Au 0°	9	18	14	20	210
15 Mev 90°	<1	3	2	5	140
H^2+Cu 0°	230	290	210	360	1300
15 Mev 90°	<2	43	42	130	940
H^2+Al 0°	1000	1000	1000	1000	1000
15 Mev 90°	<20	550	42	110	690
H^2+C 0°	<20	230	830	1600	920
16 Mev 90°	<10	4	14	55	600
H^1+Cu 0°		<0.1	<0.2	0.08	50
7.5 Mev 90°		<0.05	<0.1	0.06	30
He^4+Cu 0°				13	82
30 Mev 90°				7	48

1. With protons and alpha-particles the distribution is symmetrical and agrees with evaporation from a compound nucleus.

2. The yield of neutrons from deuteron bombardment is far greater than from alpha-bombardment, although the total energy available is about the same and both are above the barrier.

3. With deuteron bombardment there is a large excess of neutrons in the forward direction.

4. This excess is greater for the higher energy neutrons.

5. Neutrons are emitted in the forward direction with sufficient energy to produce the $Cu^{63}(n, 2n)Cu^{62}$ reaction, which has a threshold of 12–13 Mev.[3]

6. The yield of high energy neutrons is far greater for aluminum than for gold or copper.

These observations indicate that the usual concept of neutron evaporation is not adequate to explain these *d–n* reactions. There is a considerable similarity to the deuteron disintegration observed at 200 Mev (forward distribution of high energy neutrons). However, certain differences are also apparent. The theory of deuteron disintegration[2,5,6] predicts an increase in cross section with Z. Our observations show far greater yields with aluminum than with copper or gold. Also neutrons are present with nearly the full kinetic energy of the incident deuteron.

The observations of Pool[7] at 6.3 Mev show practically no change in neutron yield from aluminum to silver.

Further work is in progress to determine whether the reaction Q is an important factor in this process, as might be indicated by the anomalous results obtained with carbon.

[1] E. O. Lawrence, M. S. Livingston, and G. N. Lewis, Phys. Rev. **44**, 56 (1933).
[2] J. R. Oppenheimer, Richtmyer Lecture, January 30, 1947.
[3] R. Sagane, Phys. Rev. **53**, 492 (1938).
[4] B. T. Feld, R. Scalettar, and L. Szilard, Phys. Rev. **71**, 464 (1947).
[5] J. R. Oppenheimer, Phys. Rev. **47**, 845 (1935).
[6] S. M. Dancoff, Abstract G5, Washington Meeting Am. Phys. Soc., 1947.
[7] M. L. Pool, Phys. Rev. **53**, 707 (1938).

The Magnetic Susceptibility of Sodium in Liquid Ammonia Solutions at Low Temperatures

R. B. GIBNEY AND G. L. PEARSON
Bell Telephone Laboratories, Inc., Murray Hill, New Jersey
June 4, 1947

R. A. OGG[1] has recently reported the existence of superconductivity in quickly frozen solutions of sodium in liquid ammonia at temperatures as high as 180 degrees Kelvin. Experimental evidence presented to support the occurrence of superconductivity at this remarkably high temperature includes the detection of persistent currents[1] by means of an adaption of the classical Kammerlingh Onnes "ring experiment" and a qualitative demonstration which led to the conclusion that these solutions have an abnormally high diamagnetic susceptibility.[2]

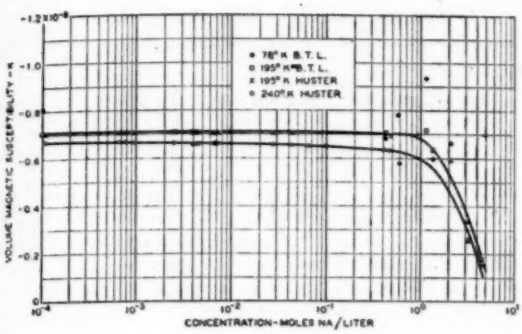

FIG. 1. Volume magnetic susceptibility in c.g.s. units of sodium in liquid ammonia *versus* concentration of solution.

The persistent current experiment is quite unsatisfactory, since cracking in the sample at the time of cooling may alter the result. A number of laboratories[3] have reported completely negative results, although Hodgins[4] found a perceptible indication in four experiments out of a total of one hundred and fifteen trials.

It appeared to us that a quantitative measurement of the magnetic susceptibility would be more significant in detecting superconductivity, since small cracks do not affect the results. A perfect superconductor has a volume diamagnetic susceptibility equal to $1/4\pi$ or 0.0795. Normal diamagnetic materials have values of 1×10^{-6} or less, whereas "alloy" superconductors have intermediate values.

The solutions were prepared by distilling ammonia from a sodium solution into the dried Pyrex tube. A calculated amount of sodium, contained in a 3-mm i.d. glass tube, was suspended in the ammonia. After solution was complete, the glass tube was removed and the container closed with a ground glass joint. After the magnetic measurement was made, the solution was poured into a beaker to evaporate, and the amount of sodium present was determined by titration with 0.429N sulfuric acid, using methyl orange as an indicator. The analysis usually checked very well with the calculated concentration.

The Gouy method, as modified by Freed and Sugarmann[5] for low temperature work, was used in making the susceptibility measurements. Weighings were made with and without the magnetic field (usually 4000 gausses, although weaker fields were tried) while the sample was suspended in dry nitrogen at the specified temperatures. The solutions were contained in closed Pyrex tubes 25 centimeters in length and 0.65 centimeters in internal diameter. In each case the solutions were quick-cooled from 240 degrees Kelvin (the boiling point of ammonia) by plunging into a flask of liquid nitrogen. For measurements at 195 degrees Kelvin they were subsequently warmed in a bath of dry ice and toluene. The results are presented in Fig. 1 where the volume magnetic susceptibility, K, in c.g.s. units is plotted *versus* the concentration of the solution. For comparison purposes, the measurements of Huster[6] on sodium in liquid ammonia solutions at 195 and 240 degrees Kelvin are given. Although we claim no greater accuracy than ±25 percent for our data, it is seen that the results at 195 check those of Huster and that quick cooling to 78 degrees Kelvin produces no appreciable increase in the diamagnetic susceptibility. The data indicate that if any of our sample is superconducting, the amount is not greater than 1 part in 10,000 by volume.

As a check on the persistent current effect, samples similar to those described by Ogg[1] were prepared between closely spaced microscope slides. These were plunged rapidly into a Dewar flask containing liquid nitrogen, situated in a magnetic field of 1500 gausses. The cells were then quickly transferred to a second liquid nitrogen bath near which a magnetometer capable of detecting a magnetic field of 10^{-5} gauss was situated. Four trials using approximately normal solutions all gave negative results.

[1] R. A. Ogg, Phys. Rev. **69**, 243 (1946); R. A. Ogg, *ibid.* **70**, 93 (1946).
[2] R. A. Ogg, Phys. Rev. **70**, 443 (1946).
[3] H. A. Boorse, D. B. Cook, R. B. Pontius, and M. W. Zemansky, Phys. Rev. **70**, 92 (1946); J. G. Daunt, M. Desirant, K. Mendelssohn, and A. J. Birch, *ibid.* 219. Luigi Guilotto and Alberto Gigli, *ibid.* **71**, 211 (1947).
[4] J. W. Hodgins, Phys. Rev. **70**, 568 (1946).
[5] S. Freed and N. Sugarmann, J. Chem. Phys. **11**, 354 (1943).
[6] E. Huster, Ann. d. Physik **33**, 477 (1938).

The Determination of the Self-Diffusion Coefficient of Methane

E. B. WINN AND E. P. NEY
Rouss Physical Laboratory, University of Virginia, Charlottesville, Virginia
May 27, 1947

THE self-diffusion coefficient of methane, not heretofore measured by direct experimental means, has been determined by a method similar to that developed by Ney and Armistead[1] and applied to uranium hexafluoride.

From kinetic theory one has the relation $\rho D = \epsilon\eta$, where ρ is the density of the gas, D its coefficient of self-diffusion, η its coefficient of viscosity, and ϵ a quantity which, according to molecular force law theory, varies from 1.200 to 1.543 depending upon the value of the force law exponent. Since the value of ϵ is uncertain, D can only be computed approximately. An experimental evaluation of ρD, however, enables one to arrive at a precise value for ϵ.

Seven diffusions of heavy methane, i.e., methane enriched in $C^{13}H_4$, into normal methane were performed, the rates of change of the concentrations of the two isotopes in the apparatus being determined by continuous analysis with a mass spectrometer. From these diffusions were obtained the values of ρD at 20°C shown in Table I.

Taking into consideration the precision with which the various factors entering into the computations could be ascertained, the final result is:

$$\rho D = 146 \pm 4 \text{ micropoise at } 20°\text{C}.$$

TABLE I.

Pressure (cm Hg)	Temp. (°C)	ρD at 20°C (micropoise)
6.16	19.2	145
6.02	20.7	138
5.15	21.4	145
6.18	23.5	147
6.24	23.8	156
6.18	24.0	147
6.30	24.7	145
		Average 146 micropoise

Taking the coefficient of viscosity of methane at 20°C to be 109.7 micropoise, it is seen that $\epsilon=1.33$.

It is known that the variation of η with temperature for molecules repelling each other as the inverse nth power of their separation is

$$\eta \propto T^s$$

where, as shown by Rayleigh,[2]

$$s=(n+3)/(2(n-1)).$$

If η is plotted as a function of T for the various values listed in the International Critical Tables for methane, it is found that s is very nearly unity. This then gives $n=5$, which results in a value of 1.543 for ϵ, according to an expression derived by Chapman and Cowling.[3] This is a wider divergence from our value than can be explained by experimental error. It should also be pointed out that because of the large thermal diffusion effect one would expect $n>5$ and an ϵ in better agreement with the value reported here.

A possible significant result of this work lies in the fact that the value of 1.33 for ϵ in the case of methane agrees within the limits of our precision with the value of 1.31 found for uranium hexafluoride. No conclusions can as yet be drawn regarding this agreement; however, further work is being undertaken to evaluate the self-diffusion coefficients of a number of gases, from which it is hoped that the true nature of ϵ may be established. An important case to be investigated is that of ammonia at room temperature, which has been shown by Watson and Woernley[4] to exhibit a reversal of the thermal diffusion effect and hence should have an $\epsilon \simeq 1.54$.

We wish to express our thanks to Professor A. O. C. Nier, of the University of Minnesota, for his kindness in supplying the sample of heavy methane used in this experiment.

[1] E. P. Ney and F. C. Armistead, Phys. Rev. **71**, 14 (1947).
[2] Rayleigh, Proc. Roy. Soc. **A66**, 68 (1900).
[3] S. Chapman and T. G. Cowling, *Mathematical Theory of Non-Uniform Gases* (The Macmillan Company, New York, 1939), p. 172.
[4] W. W. Watson and D. Woernley, Phys. Rev. **63**, 181 (1943).

Magnetic Dipole Fields in Unstrained Cubic Crystals

L. W. McKeehan
Sloane Physics Laboratory, Yale University, New Haven, Connecticut
June 6, 1947

LUTTINGER and Tisza[1] have recently made use of a few of the calculated values published some time since[2] under the above title. They mentioned discrepancies which tended to cast general doubt upon the accuracy of the earlier calculations. After correspondence, which clarified the exact character of these discrepancies, a check with the original work-sheets disclosed two misprints in Table II of the 1933 publication which now, therefore, requires the following corrections:

The numbers −2.13651 and 29.36734, appearing several times each in column 9 of Table II on page 916, should have been, respectively, −2.16351 and 29.36374.

This brings the values newly computed by Luttinger and Tisza into satisfactory agreement with what was done in 1933.

TABLE I. Additions to Table II of reference 2.

Column 1	*2*	*3*	*7*	*9*
(S)	100	1/4 1/4 0	4.18879	16.51841
			0	31.52037
			0	0
		0 1/4 1/4	4.18879	−20.47045
			0	0
			0	0
		1/4 1/4 1/2	4.18879	0.52690
			0	2.59919
			0	0
		1/2 1/4 1/4	4.18879	11.51257
			0	0
			0	0

A further computation has been made of the values of h_i at two points, not on the boundary of a dipole domain, which are of interest from the new viewpoint. In the notation of the 1933 paper these new values may be added to its Table II in the form given in Table I.

The components of a characteristic function $\mathbf{S}(\mathbf{r})$ in the notation of Luttinger and Tisza may be found by subtracting entries in column 7 from the corresponding entries in column 9. Care has to be taken to transpose the symbols in columns 2 and 3 and to change the order of entries in columns 7 and 9 to take care of the direction of dipole axes which may be assumed. Thus for dipoles parallel to the Z-axis, the newly computed entries give

$$S_x(0,\ 1/4,\ 1/4)=16.51841-4.18879=12.32962$$
$$S_y=(0,\ 1/4,\ 1/4)=31.52037-0=31.52037$$
$$S_y(1/2,\ 1/4,\ 1/4)=2.59919-0=2.59919.$$

While not affecting the most recent comparison of results, it is desirable to point out two further mistakes in the 1933 paper. In Eqs. (13)–(17) on page 919, a negative sign should precede each symbol h, e.g., h_{1111}. In the description of Fig. 1, on page 914, r_2 and r_3 should be transposed, so that the equations in the parentheses will read $r_1=r_3=-1$, $r_2=1$.

[1] J. M. Luttinger and L. Tisza, Phys. Rev. **70**, 954 (1946).
[2] L. W. McKeehan, Phys. Rev. **43**, 913 (1933).

Ultrasonic Absorption from 75 to 280 Mc/sec.*

Robert A. Rapuano
Research Laboratory of Electronics, Massachusetts Institute of Technology, Cambridge, Massachusetts
May 23, 1947

MEASUREMENTS of ultrasonic absorption in liquids at frequencies up to 100 Mc/sec. have been reported in the literature. The present note is a preliminary report of absorption measurements between 75 Mc/sec. and 280 Mc/sec. The pulse-echo method[1] has been adapted for this work by the use of a solid acoustic delay line.

Acoustic echoes are received from a reflector placed in the path of an ultrasonic beam set up in fluid which is contained in a tank. Attenuation is determined by measuring, with a calibrated attenuator, the amplitude of the received echo as a function of the separation of the reflector and transducer. The transducer is an x-cut quartz crystal

TABLE I. Ultrasonic absorption data for some liquids.

Substance	Frequency range (Mc/sec.)	Attenuation at highest frequency measured (db/cm)	T°C (approx)	$\alpha/f^2 \times 10^{17}$ cm^{-1} (average)	$\alpha/f^2 \times 10^{17}$ cm^{-1} (from literature)	T°C (approx)	Reference
Water	75–250	118	25	20.8(1±.01)	20.8	25	1
Methanol	75–250	170	21	31.2(1±.01)	37	19	2
Ethanol	75–220	230	22	53.7(1±.01)	23	2	2
1-Propanol	75–280	495	22	75.5(1±.02)	70	28	2
Carbon disulfide	75–105	1350	21	1400(1±.03)	3100	—	3
Carbon tetrachloride	75–105	520	24	560(1±.02)	533	24	2
Benzene	75–165	2100	25	900(1±.05)	800	22	2

[1] Fox and Rock. [2] Pellam and Galt, see reference 1 below. [3] L. Bergmann, *Der Ultraschall* (1942), p. 21, Table 22.

having a fundamental of 15 Mc/sec. Measurements are taken at the frequencies of the odd harmonics of the crystal. The attenuation is expressed as α/f^2 where α is the pressure attenuation coefficient in $P=P_0e^{-\alpha x}$. Plots of α/f^2 *vs.* f for some typical liquids are shown in Fig. 1. The constancy of α/f^2 is within the experimental error.

For attenuations above about 100 db/cm, the reflector must be placed very close to the transducer in order to obtain usable signal strength; hence the returned echo is often obscured by the transmitted pulse. This difficulty has been circumvented by using as an acoustic delay line, in place of the usual reflector, a rod of fused quartz with polished parallel end faces. Figure 2 is a schematic diagram

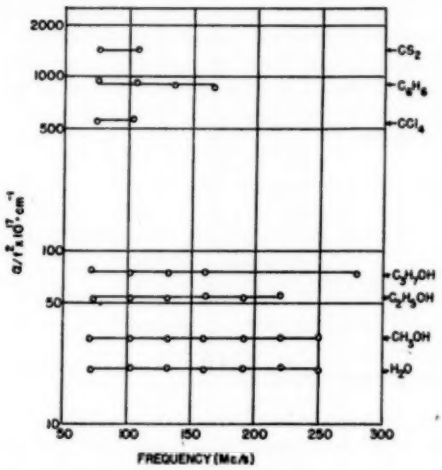

FIG. 1. The frequency dependence of α/f^2 for some liquids.

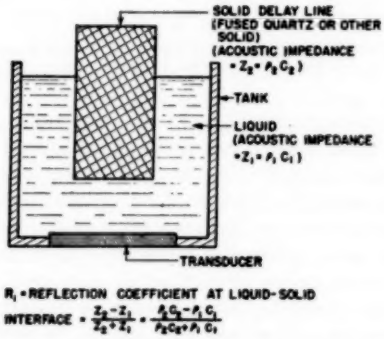
SOLID DELAY LINE (FUSED QUARTZ OR OTHER SOLID) (ACOUSTIC IMPEDANCE $=Z_2=\rho_2 C_2$)
TANK
LIQUID (ACOUSTIC IMPEDANCE $=Z_1=\rho_1 C_1$)
TRANSDUCER
R_i = REFLECTION COEFFICIENT AT LIQUID-SOLID INTERFACE $=\frac{Z_2-Z_1}{Z_2+Z_1}=\frac{\rho_2 C_2-\rho_1 C_1}{\rho_2 C_2+\rho_1 C_1}$

FIG. 2. Schematic diagram of the acoustic delay line.

of the arrangement. Measurements are taken in the usual fashion, using the echo resulting from sound which has penetrated into the quartz and has been reflected from the far end of the rod, the attenuation in the quartz being small. Thus, this echo is quite well removed in time from the transmitted pulse; in this way a liquid path down to 10^{-3} cm or less may be used. Table I gives some of the results obtained. The highest attenuation measured (2100 db/cm) is that of benzene at 165 Mc/sec. The highest frequency determination has been carried out on *n*-propyl alcohol. Attenuations as high as 20,000 db/cm can probably be measured; the limit is determined primarily by the mechanical precision of the tank.

Several echoes are observed on the indicator screen corresponding to sound which has been trapped inside the quartz rod by the acoustic mismatch. The acoustic absorption in solids can be measured from these successive echoes, since the reflection loss at the interfaces can be calculated fairly accurately from the acoustical properties of the solid and liquid. A rough measurement on fused quartz shows that the attenuation is still linear with frequency up to 200 Mc/sec. and has approximately the value given by Mason[2] for lower frequencies.

* This work has been supported by the joint Army-Navy Contract W-36-037 sc. 32037.

[1] J. R. Pellam and J. K. Galt, J. Chem. Phys. **14**, 608 (1946).
[2] W. P. Mason, J. Acous. Soc. Am. (to be published).

Rate of Sintering of Copper Powder

A. J. SHALER AND J. WULFF
Massachusetts Institute of Technology, Cambridge, Massachusetts
June 6, 1947

FRENKEL[1] has recently proposed a mechanism for the sintering of metal powders. He believes that surface tension is the driving force which accounts for a flow having the linear relationship between strain rate and stress characteristic of viscous fluids. Both Frenkel[1] and Kanter[2] have shown that the phenomenon of self-diffusion in metals entails the existence of such viscous flow. On that basis Frenkel[1] has calculated the coefficient of viscosity, the rate of contraction of a single pore in a mass of metal, and the rate of coalescence of two spheres.

By extending the analysis of Frenkel[1] it has been possible to derive expressions for the rate of shrinkage, at various temperatures, of powder aggregates containing many pores of uniform size. Equations were also derived to include the presence of foreign gases inside the pores and outside the aggregate.

The course of sintering predicted by these expressions is in qualitative accord with experimental results on the sintering of uniform spherical copper particles regularly packed and sintered both in argon at one atmosphere and in vacuum. If, however, we accept Samoilovich's[3] value of about 1200 dynes per centimeter for the surface tension of solid copper, then the experimental results indicate a much higher value for the viscosity coefficient than is predicted by Frenkel from the values of the self-diffusion constant reported in the literature.[4]

The viscosity coefficients calculated from the experiments are 2.4×10^{10} second per cubic centimeter at 850°C and 5×10^{9} second per cubic centimeter at 900°C, corresponding to a value for the heat of activation of self-diffusion of copper of over 85,000 calories instead of the 57,000–61,000 calories reported by Barrier.[4]

Further experiments are under way to see whether other metals exhibit the same phenomenon and to determine whether the discrepancy lies in the value of the surface tension, that of the self-diffusion constant, or in the mechanism of flow as analyzed by Frenkel.

If the process of sintering is as described above, it can be concluded that in the absence of entrapped gas, when the pores are of a range of sizes, the small pores disappear first and successively larger pores shrink at a later time, or at a higher temperature if the time of sintering is held constant. Ideally all pores eventually disappear at any temperature. In the practical case gas is always entrapped during the compression used to form powder metallurgy products. At first the smallest pores shrink, yet pores larger than a maximum size later expand rather than contract. In accordance with this analysis gas-containing aggregates were made to shrink, and, by varying the external pressure, were subsequently expanded.

[1] J. Frenkel, J. Phys. U.S.S.R. 9, 392 (1945).
[2] J. J. Kanter, Metals Technology 4, 8 (1937).
[3] A. Samoilovich, Acta Physicochimica U.R.S.S. 20, 97 (1945).
[4] R. M. Barrer, *Diffusion in and Through Solids* (MacMillan, London, 1941).

Ferromagnetic Resonance at Microwave Frequencies

W. A. Yager and R. M. Bozorth
Bell Telephone Laboratories, Murray Hill, New Jersey
May 24, 1947

Griffiths[1] has recently described a new resonance phenomenon in ferromagnetic materials, caused by the interaction of processing electrons with a magnetic field at microwave frequencies. Kittel[2] has shown that the resonance frequency is in close agreement with the Larmor frequency calculated for the fictitious field $(BH)^{\frac{1}{2}}$ and has given an expression for the complex permeability in the direction of the r-f magnetic field from which the apparent permeability, μ_r, can be derived. In this note we report experiments designed to test Kittel's theory and to evaluate the gyromagnetic ratio.

Experimental conditions have been chosen in accordance with the simplifying assumptions of the theory. The magnetic material used, Supermalloy,[3] has a very low magnetic crystal anisotropy and is probably the most

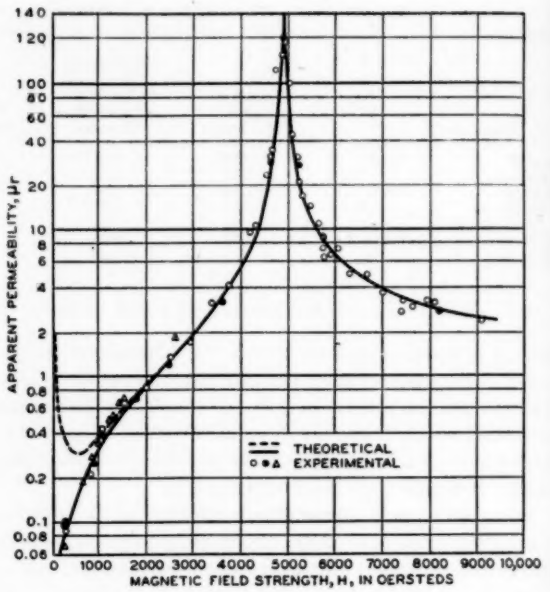

Fig. 1. Resonance curve on semi-log scale, showing points taken in different runs and theoretical curves for two kinds of assumed damping.

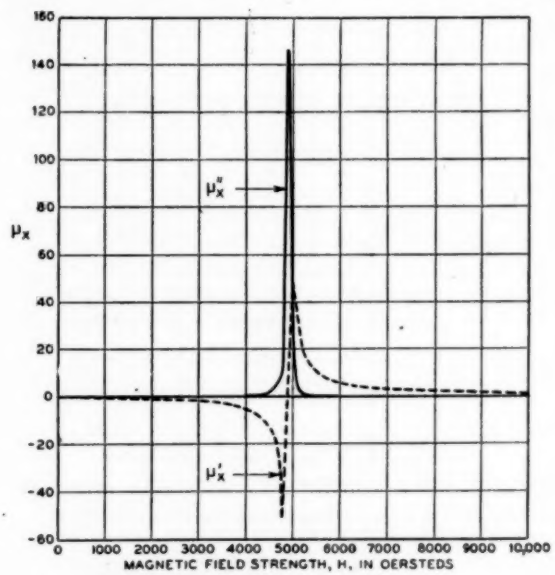

Fig. 2. Real (μ') and imaginary (μ'') components of complex permeability, plotted on linear scale.

easily saturable material known. By using thin foils and extending them beyond the walls of the cavity, the demagnetization factor in the direction of the static field is reduced to an estimated value of .30 oersteds when the material is magnetized to saturation ($B_s=7900$). A section of rectangular wave guide was terminated by a metal plate and a resonant cavity formed by the introduction of an asymmetrical inductive window of high susceptance one wave-length away from the end plate. The narrow sides of the cavity were milled off, and thin foils (0.004 in. thick)

of Supermalloy were soldered in place. The assembly was attached to the standing wave detector of a 1.25 cm heterodyne test set and placed between the pole pieces of an electromagnetic so that the static field was in the plane of the foils and at right angles to the r-f magnetic field. The resonance frequency of the cavity for the dominant mode of the wave guide was 24,050 megacycles.

A sharp resonance occurs at an applied field of 4950 oersteds corresponding to $H=4920$. According to Kittel's theory the numerical value of the Landé splitting factor, g, is thus found to be 2.17, which is considerably higher than the value 1.91 reported by Barnett[4] for an alloy of similar composition. A value of g greater than the electron spin value of 2 is not to be expected and suggests that a refinement of the theory may be necessary.

From the measured standing wave ratios, values of the unloaded Q of the cavity were determined using the procedure outlined by Slater,[5] and from these the values of μ_r of the Supermalloy were calculated and plotted (Fig. 1). Using a damping term of the form suggested by Kittel,[2] a good fit with experiment is obtained except below $H=1500$ (broken line). Using Frenkel's[6] form, good agreement is obtained over the whole range, as shown by the solid line of the figure, drawn for a relaxation time of 1.2×10^{-9} sec.

The low anisotropy and small demagnetizing field of the material apparently contribute to the sharpness of the resonance (Fig. 2).

We are indebted to Dr. C. Kittel and other members of the staff of the Electronics Laboratory of Massachusetts Institute of Technology for discussions of the theoretical and experimental aspects of the problem.

[1] J. H. E. Griffiths, Nature **158**, 670 (1946).
[2] C. Kittel, Phys. Rev. **71**, 270 (1947).
[3] O. L. Boothby and R. M. Bozorth, J. App. Phys. **18**, 173 (1947).
[4] S. J. Barnett, Phys. Rev. **66**, 224 (1944).
[5] J. C. Slater, Rev. Mod. Phys. **18**, 441 (1946).
[6] J. Frenkel, J. Phys. U.S.S.R. **9**, 299 (1945).

Stability and Spectrum in the Wave Mechanics of Lattices

AUREL WINTNER
The Johns Hopkins University, Baltimore, Maryland
June 4, 1947

CONSIDER a Schrödinger equation, say the one-dimensional wave equation,

$$\psi''+(E-U)\psi=0, \tag{1}$$

where $U=U(x)$ is given on the whole x-axis. The concept of the spectrum of (1) can then be approximated by qualitative considerations.[1] Such considerations do not lead, however, to a satisfactory definition of the set of E values to be called spectrum. If only the set of discrete eigenvalues (the "point spectrum") is involved, the situation is simple indeed. On the other hand, the qualitative considerations in question are known to have just an heuristic value in case of band spectra ("continuous spectra").

There seems to arise a simplification if the problem is that belonging to a lattice potential,[2] that is, if U is a periodic function of x, say $U(x)=U(x+1)$. Then, if the highly exceptional (and, as it turns out, immaterial) case of a secular term is disregarded, the general solution of (1) is of the form

$$\psi(x)=c_1e^{G(E)x}\pi_1(x)+c_2e^{-G(E)x}\pi_2(x), \tag{2}$$

where $\pi_1(x)$ and $\pi_2(x)$ are of period 1 and do not depend on the integration constants c_1, c_2, and the characteristic exponent, $G=G(E)$, is determined by the energy parameter E. (It is incidental that the actual determination of $G=G(E)$, where $-\infty<E<\infty$, depends, in general, on the machinery of infinite determinants or equivalent transcendental means.) The usual treatment of the spectrum of the lattice depends on the following statement: An energy level, E, is or is not in the spectrum according as the corresponding value of $G(E)$ is purely imaginary (including zero) or has a non-vanishing real part; that is, according as the general solution, (2), of (1) is or is not of stable type for both $x\to+\infty$ and $x\to-\infty$.

This specification of the spectrum agrees with the heuristic considerations, referred to above, but it cannot be accepted as a definition. For, if it could, the spectrum of a Schrödinger equation would be defined only for the case of a periodic potential. Consequently, it is necessary:

(a) to commence with a general definition of the spectrum of Eq. (1), in such a way as to take no account of the possible periodicity of $U(x)$;

(b) to prove that, if $U(x)$ happens to be periodic, then the set of those E values which are to be defined under (a) as the spectrum, turns out to be identical with the set of those E values for which $G(E)$ becomes of stable type.

There is nothing in the physical theory that could guarantee the latter desideratum. In fact, if the requirement of (b), instead of being provable for every periodic U, could be disproved, *on the basis of* (a), for some periodic U, all that would follow is that the heuristic approach, which is known to lead to incorrect results in certain cases, would have its limitations in the case of lattice potentials also.

For the sake of brevity, let a function be called of class (*) if it is defined and continuous at every point of the x-axis and is such that the square of its absolute value has a finite integral (over the full range, $-\infty<x<\infty$). For example, a value of the parameter E is a discrete eigenvalue of (1) if and only if there exists a solution $\psi(x)$ which is of class (*) and does not vanish identically. In particular, if $U(x)$ is periodic, then, whether $G(E)$ is or is not of stable type, it is clear from the periodicity of $\pi_1(x)$ and $\pi_2(x)$ that an arbitrary solution, (2), of (1) is of class (*) only if $c_1=c_2=0$; so that a lattice potential cannot produce a discrete eigenvalue.

Ad (a). The general definition of the spectrum of (1) is assigned by the theory of Hilbert's space. The difficulty contained in the possibility of "continuous eigenvalues" (which are not eigenvalues in the preceding sense) can then be avoided, by defining the spectrum on the basis of a negation, rather than by an existential requirement of a positive nature; *viz.*, as follows[3]:

An energy level, E, is said to be *not* in the spectrum of (1) if and only if the corresponding inhomogeneous equation

$$\chi''+(E-U)\chi=F \tag{3}$$

has[4] a solution, $\chi=\chi(x)$, of class (*) for *every* external disturbance, $F=F(x)$, of class (*).

Needless to say, the potential, $U=U(x)$, is not restricted to be of class (*); it is surely not of class (*) if it is a lattice potential.

Ad (b). Suppose that U is a lattice potential, say $U(x)=U(x+1)$. What must be proved is twofold:

(α) If E is such as to render the value of $G(E)$ purely imaginary (including zero), then there exists *some* $F=F(x)$ of class (*) with reference to which the inhomogeneous Eq. (3), belonging to the given value of E, fails to possess a solution of class (*).

(β) If the value $G(E)$, belonging to a given E, has a non-vanishing real part, then (3) admits a solution of class (*) for *every* $F(x)$ of class (*).

The verification of (α) and (β) involves quite an amount of mathematical drudgery. The proof of (α) depends on an appropriate application of a general lemma, recently proved with questions of this type in view.[5] The proof of (β) is of quite another nature; its basis is the "boundedness" of the case

$$K(s,t)=\exp(-|s-t|), \qquad -\infty<s,t<\infty,$$

(Weyl-Picard) of the integral analog of the Fourier "L-matrices" of Toeplitz.[6] Because of these general tools, the details of the proofs of (α) and (β) depend only on formal analysis, which will be carried out elsewhere.

[1] Cf. E. Schrödinger, Sitzber. Akad. Berlin, 668–682 (1929).
[2] R. de L. Kronig and W. G. Penney, Proc. Roy. Soc. **A130**, 499–513 (1930); cf. H. A. Kramers, Physica, **2**, 483–490 (1935).
[3] H. Weyl, Math. Ann. **68** 220–269 (1910); cf. A. Wintner, *Spektraltheorie der unendlichen Matrizen* (Leipzig, 1929), pp. 141–153 and 229–236.
[4] The solution in question is then unique. This seems to be at variance with a remark of Weyl, reference 3, p. 251. The contradiction disappears if it is observed that, in Weyl's case, the region is a half-line, the end of which carries a homogeneous boundary condition, whereas the present case is that of the whole line.
[5] A. Wintner, Am. J. Math. **69**, 10–12 (1947).
[6] O. Toeplitz, Gött. Nachr., 449–503 (1910).

Cobalt 61 Radioactivity

THOMAS J. PARMLEY AND BURTON J. MOYER
Radiation Laboratory, Department of Physics, University of California, Berkeley, California
May 17, 1947

TWO samples of nickel enriched, respectively, in isotopes 61 and 62 by the electromagnetic process (Calutron) were subjected to fast neutron bombardment near the target of the Crocker Laboratory 60-inch cyclotron. Among the activities produced was a prominent one having a 1.75±.05-hour half-life and associated most strongly with the Ni^{61} sample. Chemical extractions showed this activity to belong to cobalt, and most likely to Co^{61}.

In order to establish the mass assignment the following three experiments were performed:

(1) Electrolytic copper was bombarded with fast neutrons. The cobalt was extracted with a carrier and yielded a 1.75-hour half-life.

(2) Electrolytic copper was again bombarded with fast neutrons. The activated sample was analyzed with the Calutron and gave a 1.75-hour half-life in the mass 61 position. The reaction was evidently Cu^{65} $(n, \alpha n)$ Co^{61}.

(3) Isotopically normal nickel was given a 30-minute bombardment with 22-Mev deuterons in the Crocker cyclotron. A cobalt extraction followed by Calutron analysis again gave the 1.75-hour half-life at mass 61. This reaction was then Ni^{64} $(d, \alpha n)$ Co^{61}.

Following the assignment of the 1.75-hour activity to Co^{61}, additional corroborative evidence was obtained with the two following experiments performed with nickel enriched in isotope 64:

(1) The isotope was bombarded with 14-Mev protons from the 37-inch frequency-modulated cyclotron. The 1.75-hour half-life appeared in the cobalt extraction, presumably by the Ni^{64} (p, α) Co^{61} reaction.

(2) The isotope was given a 10-minute bombardment with 22-Mev deuterons in the Crocker cyclotron. The cobalt extraction yielded a 1.75-hour half-life, presumably by the reaction Ni^{64} (d, αn) Co^{61}.

Absorption measurements in aluminum give a maximum β^- energy of about 1.1 Mev as judged from an endpoint at 436 mg/cm² of Al plus 4 mg/cm² of air and counter window. There is no indication of a gamma-ray.

Recognition is due Robert Lilly and Dr. E. H. Huffman for the chemical extraction, and J. Beaufait for preparing the metallic samples of isotopic nickel. The Calutron analyses were done under the direction of Keith Pierce.

This problem was carried out under the auspices of the Atomic Energy Commission under Contract No. W-7405-Eng-48.

On Scattering Processes of Higher Order

OTTO HALPERN AND NORMAN M. KROLL
Physics Department, Columbia University, New York, New York
May 31, 1947

IN a recent paper by Eliezer,[1] to which our attention has just been drawn by an abstract in Science Abstracts, new results concerning scattering processes of higher order, in particular of the Compton type, have been enunciated. Since we have been independently working on a similar investigation which is near completion, we ask permission to comment on Eliezer's results.

Eliezer found, contrary to earlier results of Heitler and Nordheim,[2] that quantum theory leads to a large probability for the production of photon showers originated by quanta of relativistic energy, provided only that one of the quanta $h\nu''$ produced has a very small frequency. His expression for the cross section is of the type $d\nu''/\nu''$.

Our investigation has also led to certain clarifications and corrections of statements made by Heitler and Nordheim; we have equally obtained cross section expressions of the form given by Eliezer, although a direct comparison is not possible since Eliezer has not carried his expressions to numerical evaluation. But, as far as interpretation is concerned, we confirm the result of Heitler and Nordheim that quantum theory does not permit the prediction of photon showers, and we consider the analytical expression for the cross section as another manifestation of the infrared catastrophe.

Limiting ourselves for the moment to three quantum processes, the expressions obtained for the cross section by Eliezer and ourselves would lead to infinite values for

the total cross section of the double Compton process due to the behavior near $\nu''=0$. This physically absurd result makes it clear that the large cross section for low frequency ν'' is obviously caused by a faulty application of the theory.

The present case of infra-red catastrophe appears to us particularly interesting because it seems likely that the deviation from the Klein-Nishina formula due to multiple processes may be measurable for hard gamma-rays passing through matter of low atomic number. Although every higher step adds a factor of 137 in the denominator of the cross sections, still the numerical factors present seem to make an observable effect not unlikely once a proper cut-off frequency has been determined.

We hope to report on our calculations in detail in the near future.

[1] C. J. Eliezer, Proc. Roy. Soc. **A187**, 210 (1946).
[2] W. Heitler, *Quantum Theory of Radiation* (Oxford, 1936), paragraph 18.

Magnetic Fields of Astronomical Bodies

HORACE W. BABCOCK
Mount Wilson Observatory, Pasadena, California
June 7, 1947

ON the assumption that magnetic fields in stars of approximately equal mass are proportional to their rates of rotation, I predicted early in 1946 that fields of the order of 1500 gauss should occur in certain early-type stars, and that the integrated Zeeman effect resulting from such stellar fields should be observable under certain conditions. Observations of 78 Virginis beginning in April of the same year, have confirmed this prediction,[1] and fields of the same general order of magnitude have since been observed in other stars. The strongest field observed to date is that of the peculiar A-type star BD—18°3789 (HD 125248); measures from two plates give a polar field of 5500 gauss. The polarity is opposite to that of 78 Virginis. I have been able to show further that, within the uncertainties of the observations, *the magnetic dipole moments of the earth, sun, and 78 Virginis* (8×10^{25}, 8×10^{32}, and 4×10^{36} gauss cm^3, respectively) *are proportional to their angular momenta* and may be obtained by multiplying the angular momenta, in c.g.s. units, by 10^{-15} gauss cm sec. g^{-1}. A paper discussing this and some other aspects of magnetism in astronomical objects is in press.[2]

If the foregoing relationship is of real physical significance, it may possibly apply also to the galaxy, and this is of some interest, partly on account of the influence of magnetic fields on cosmic rays. Actually, it is easier to apply it to our nearest neighboring galaxy, the Andromeda Nebula (M31), which, converging evidence shows, is essentially a twin of our own, and for which the rotation and mass have been measured more directly by spectrographic observation.[3] From the same measurements, we know that the greater part of the mass of M31 lies far from its center, and that to a first approximation we may regard it as a rather thin disk of uniform density rotating with a nearly constant angular velocity of 2.5×10^{-15} rad/sec. Its mass, a major portion of which must be dark material, is calculated to be 1×10^{11} times that of the sun; and the effective radius, within which lies most of the mass, may be taken as 6000 parsecs. If M31 has a magnetic moment proportional to its angular momentum, then, using the coefficient 10^{-15} gauss cm sec. g^{-1}, the moment is computed to be of the order of 10^{39} gauss cm^3, corresponding to a field of about 10^{-8} gauss parallel to the axis. Within the uncertainties of our knowledge, this should apply almost as readily to our galaxy as to the Andromeda Nebula.

It is probably unnecessary to add that the computed result for M31 is meaningless unless it is granted that the proportionality of magnetic moment to spin is a universal law, and that it is applicable to an assemblage of stars and dust in revolution as well as to single stars in rotation. Chapman[4] has objected to the view that terrestrial and solar magnetism are fundamental on the ground that the magnetic axes are inclined to the axes of rotation by about 11½ degrees and 6 degrees, respectively, and that since at least a moderate component of the field seems not to be due to spin, it may be regarded as unlikely that any part of the field is due to a cause fundamentally related to gravitation.

[1] H. W. Babcock, Ap. J. **105**, 105 (1947).
[2] H. W. Babcock, Pub. Astro. Soc. Pac. **59**, 112 (June 1947).
[3] H. W. Babcock, Lick Observatory Bulletin **19**, 41 (1939).
[4] S. Chapman, Nature **124**, 19 (1929).

Method of Correcting Low Angle X-Ray Diffraction Curves for the Study of Small Particle Sizes

JESSE W. M. DUMOND
California Institute of Technology, Pasadena, California
May 26, 1947

A. GUINIER in France has had considerable success[1] in the study of small particle sizes (and even their shapes) by means of low angle x-ray diffraction utilizing the reflection-type focusing, curved crystal spectrometer to obtain a monochromatic convergent beam of x-rays. The sample whose diffraction pattern is to be studied is placed in the convergent beam about midway between the curved crystal and the focus; the geometry of the arrangement is shown in Fig. 1. In reality the convergent beam is focused

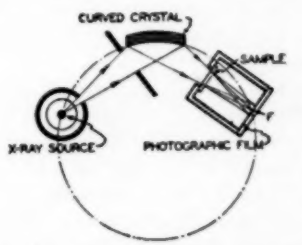

FIG. 1. Guinier's arrangement for the study of low angle x-ray diffraction.

only in the plane of the figure. The rays actually diverge in the direction normal to the plane of the figure so that in the absence of the sample a sharp spectral *line* is formed at *F*. With the sample in place a linear rather than a circular diffraction pattern is formed on the film.

It has occurred to the author, and possibly to others,[2]

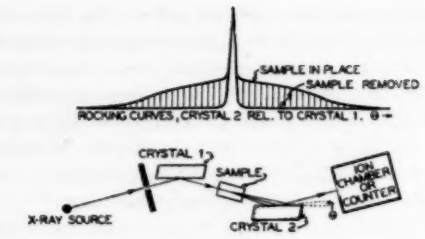

FIG. 2. Two-crystal spectrometer applied to the study of low angle x-ray diffraction.

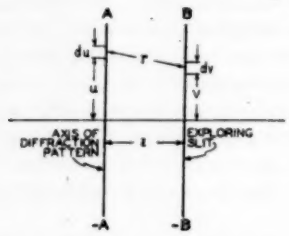

FIG. 3. Geometry of elongated diffraction patterns.

that another method of study of low angle x-ray diffraction utilizing the two-crystal spectrometer might also be successful. In Fig. 2, the arrangement is shown schematically. A "rocking curve" with the crystals in the "parallel position" is to be observed first *without*, then *with* the sample in place. The *difference* between the two curves should give the low angle x-ray diffraction pattern. Here again, however, the rays diverge in the direction normal to the figure.

The diffraction patterns obtained in both cases require a correction, as A. Guinier has pointed out,[3] in order to interpret them as the radial distribution of intensity or halo that the sample would give if the primary beam were a fine parallel pencil such as to form a sharp point in the center of the halo. Both the experimental arrangements described give instead of this an intensity distribution which is essentially a superposition of many such circular halos with their centers uniformly and continuously distributed along a straight line. The purpose of this note is to give a method for correcting the curves of the latter type so as to obtain the true radial intensity distribution which generated them.

In Fig. 3 the line $-AA$ is the line of centers along which the circular diffraction halos are considered to be uniformly spread. $-BB$ is the slit which explores across the resulting linear pattern spread to left and right of $-AA$. What is observed is the intensity $\Phi(z)$ integrated over the variables u and v, and plotted as a function of z. What is desired, is the radial intensity distribution $\phi(r)$ in an elementary circular halo. The problem is simplified by discussing it in terms of $F(z^2)$ and $f(r^2)$, where $F(z^2)=\Phi(z)$ and $f(r^2)=\phi(r)$. From Fig. 3, $r^2=z^2+(u-v)^2$. The situation is expressed as

$$F(z^2)=\int_{-A}^{A}\int_{-B}^{B} f[z^2+(u-v)^2]\,du\,dv. \qquad (1)$$

In this integral equation F is given and f is sought.[4] When the limits A and B are "infinite," that is to say when the height of the diffraction pattern and the exploring slit (or its equivalent) are each large compared to the width of the pattern along the z-axis,[5] the solution for (1) is

$$f(p)=-\frac{1}{2\pi B}\int_p^\infty F'(q)\frac{dq}{(q-p)^{\frac{1}{2}}}; \qquad p=z^2. \qquad (2)$$

(No method of solving this equation is known at present when the limits are finite.) The solution (2) involves operations all of which can be performed on observed diffraction curves F without the necessity for translating these into analytically expressed functions. The observed curve $\Phi(z)$ is replotted as $F(q)$, and its derivative $F'(q)$ is found by constructing tangents. A set of curves, each the product of $-F'(q)$ into the curve $(q-p)^{-\frac{1}{2}}$, is then formed for a series of appropriately selected values of p along the abscissa q, and the areas under each of these from p to ∞ (obtained by planimeter or otherwise) give the ordinates of $f(p)$. The author is much indebted to Dr. Robert Serber of the University of California for the method of inverting this integral equation.

[1] A. Guinier, Ann. de physique 12, 161 (1939).
[2] The author has heard indirectly that I. Fankuchen has been working on a similar method though its details are unknown to him.
[3] The correction for the special case of a Gaussian distribution, as Guinier has shown, amounts merely to a change in the normalizing factor, but no method heretofore was known for the general case.
[4] F and f do not have the same dimensions. f is the power per unit area in the diffraction pattern per unit length of line, $-AA$. F is the power per unit width of slit, $-BB$. Thus dimensionally $f=[\text{Power}\cdot L^{-2}]$; $F=[\text{Power}\cdot L^{-1}]$.
[5] These qualifications are inserted to minimize end effects due to changes in pattern intensity at the termini. This is best accomplished if B is less than A by an amount at least equal to the radius of the pattern $\phi(r)$ over which appreciable intensity is present.

First-Order Stark Effect in the Microwave Spectrum of Methyl Alcohol

B. P. DAILEY*
Harvard University, Cambridge, Massachusetts
May 24, 1947

HERSHBERGER and Turkevitch[1] report having found a series of five lines in the microwave absorption spectrum of methyl alcohol.

The methyl alcohol spectrum in this region has now been investigated in this laboratory using the microwave spectrograph recently described.[2] Twenty-four spectral lines have been observed. The Stark effect of these lines was observed using a square wave to modulate the absorption in the gas instead of the sine wave previously employed.[2] This modification was suggested and the amplifier used was constructed by Mr. Robert Karplus. Following this procedure the original spectral line and its resolved or unresolved Stark components, shifted in frequency by the field, were observed simultaneously on the oscilloscope screen. Frequency differences among components of the spectral pattern were measured by the method of Good and Coles.[3]

The Stark effect served to divide the spectral lines into two groups. The lines of series III were observed at a field level of only 30 volts/cm. The remaining lines required modulating fields of 300 volts/cm and higher. The series III lines had symmetric Stark patterns, and the Stark

TABLE I. Microwave spectrum of methyl alcohol.

Mc	Shape of Stark pattern	Minimum modulating voltage, v/cm	Series
20,898	unsym	300	I
20,989	unsym	300	I
21,551	unsym	300	I
22,095	unsym	300	I
23,033	unsym	300	I
25,385	unsym	300	I
24,040	unsym	300	II
24,081	unsym	300	II
24,317	unsym	300	II
25,050	unsym	300	II
24,928.8	unsym	30	III
24,954.6	sym	30	III
25,017.8	sym	30	III
25,132.0	sym	30	III
25,300.3	sym	30	III
25,546	sym	30	III
25,796	unsym	30	III
25,898	sym	30	III
26,310	sym	30	III
26,562	sym	30	III
23,121	unsym	300	—
23,415	unsym	300	—
23,450	unsym	300	—
23,861	sym	30	—

effect of the line at 25,126 Mc fitted the following formula

$$\Delta\nu = 0.084E,$$

where $\Delta\nu$ is the frequency separation of the unsplit line and one of its two shifted Stark components (or groups of unresolved components). The separation $\Delta\nu$ is in megacycles, and E is in volts/cm. The Stark patterns of the other lines were unsymmetric and for the line at 23,121.8 Mc $\Delta\nu$ was 3.84 Mc for a field of 504 volts/cm.

The experimental data are summarized in Table I. Frequencies given to six figures were obtained using lines of the $N^{14}H_3$ and $N^{15}H_3$ spectrum as secondary standards; other frequencies were obtained using a calibrated wavemeter and are good to ±5 Mc.

The rotational constants of methyl alcohol have been obtained from infra-red data by Borden and Barker.[4] They may be used with the appropriate selection rules to predict some of the features of the methanol spectrum in the microwave region. The transition $\Delta J=+1$, $\Delta K=0$, as pointed out by Hershberger and Turkevitch,[1] would give frequencies of 48,700 Mc and higher. For $\Delta J=0$, $\Delta K=+1$ we should expect frequencies in the far infra-red. For $\Delta J=\pm1$, $\Delta K=\pm1$ it is possible to place only two or three lines in this region of frequency, and their separations should be irregular. This is also true for transitions between the degenerate K levels split by the slight asymmetry of the molecule.

Koehler and Dennison[5] have calculated the energy levels for methyl alcohol considered as two coupled symmetric rotors whose mutual rotation is hindered by a potential function having a triple minimum. One or perhaps two transitions between the levels for $n=0$ (n=torsional vibration quantum number) should fall in the K-band. It seems likely that each of these transitions should be split by centrifugal distortion into one or more series of lines characterized by different values of J and K.

It seems unlikely that a fine structure due to free rotation is being observed, since the spacing of the levels is much too dense for the large values of the rotational constants of OH and CH_3 found by Borden and Barker.

I would like to thank Professor E. Bright Wilson, Jr. for his encouragement and many helpful suggestions during the course of this investigation.

* The research reported in this document was made possible through support extended Harvard University jointly by the Navy Department (Office of Naval Research) and the Signal Corps, U. S. Army, under Office of Naval Research contract N5ori-76.

[1] W. D. Hershberger and John Turkevitch, Phys. Rev. **71**, 554 (1947).
[2] Richard H. Hughes and E. Bright Wilson, Jr., Phys. Rev. **71**, 562 (1947).
[3] W. E. Good and D. K. Coles, Phys. Rev. **71**, 383 (1947).
[4] A. Borden and E. F. Barker, J. Chem. Phys. **6**, 553 (1938).
[5] J. S. Koehler and D. M. Dennison, Phys. Rev. **57**, 1006 (1940).

The 5.3 Day Isotope in Element 61

G. W. PARKER AND P. M. LANTZ,
Monsanto Chemical Company, Clinton Laboratories, Oak Ridge, Tennessee
AND
M. G. INGHRAM, D. C. HESS, JR., AND R. J. HAYDEN,
Argonne National Laboratory, Chicago, Illinois

June 6, 1947

A SAMPLE of element 61, formed by fission and shown by mass spectrographic analysis to be predominantly mass 147 (61 isotopes of other masses were present to less than one part in two thousand), was irradiated by slow neutrons in the Clinton Pile. After bombardment, a 5.3-day activity was found to be present in the element 61. The cross section for this reaction was approximately 60×10^{-24} cm².[3] The radiations from this sample, as determined by absorption curves, were a beta-ray of approximately 2.5 Mev, and a gamma-ray of approximately 0.8 Mev. This is probably the same activity observed by Law, Pool, Kurbatov, and Quill.[1,2] They observed it as formed by Nd(p, n), Nd(d, n), and Nd(α, p). The second of these reactions is incompatible with our determination of the mass of this isotope.

To verify that the reaction involved was actually (n, γ) and hence that the mass of the 5.3-day active isotope in element 61 was 148, a portion of the sample was analyzed by means of a mass spectrograph.[3] After separation, active isotopes were found at masses 147 and 148. To verify that the activity at mass 148 had a half-life of 5.3 days, the following technique was used: The photographic plate upon which the separated isotopes were deposited was placed successively against various parts of a larger photographic plate for times calculated to give equal intensity in the 148 position if its half-life were 5.3 days. Five exposures were taken for successive times of 33.2 hours, 40.7 hours, 52.3 hours, 72.3 hours, and 122 hours. Upon development this large plate showed equal blackening at mass 148 and increasing blackening for successive transfers at mass 147. Thus the active isotope in element 61 with a half-life of 5.3 days is at mass 148.

[1] H. B. Law, M. L. Pool, J. D. Kurbatov, and L. L. Quill, Phys. Rev. **59**, 936 (1941).
[2] J. D. Kurbatov and M. L. Pool, Phys. Rev. **63**, 463 (1943).
[3] M. G. Inghram and R. J. Hayden, Phys. Rev. **71**, 130 (1947).

Pressure Coefficient of Surface Tension and the Expansion Ratio of High Pressure Cloud Chambers*

THOMAS H. JOHNSON
Brookhaven National Laboratory, Patchogue, Long Island, New York
June 7, 1947

IN operating an argon-filled cloud chamber at 110 atmospheres Johnson, De Benedetti, and Shutt[1] found that good tracks were formed with an expansion ratio of 1.04, whereas with the same gas and vapor in a chamber at 1.5 atmospheres tracks were formed with an expansion ratio of 1.07. In both instances the vapor was a 50–50 mixture of water and *n*-propyl alcohol.

A reduction of the expansion ratio with increasing pressure can probably best be understood as an effect of the gas pressure on the surface tension of the droplets. According to the Kelvin theory[2] of charged droplets, the vapor density δ_r in equilibrium with a droplet of radius r is given by the equation

$$\delta_r=\delta_\infty \exp\left[(M/R\theta\rho)(2T/r-e^2/8\pi kr^4)\right], \quad (1)$$

where δ_∞ is the vapor density in equilibrium with a flat surface of the liquid, M is the molecular weight of the liquid, R is the gas constant, θ is the absolute temperature, ρ is the density of the liquid droplet, T is the surface tension, e is the electric charge on the droplet, and k is the dielectric constant of the surrounding gas. Before the expansion, when the temperature is θ_1 and the vapor density is $\delta_\infty(\theta_1)$, ion droplets grow to a radius r_1 where $\delta_{r1}(\theta_1)$ is equal to $\delta_\infty(\theta_1)$, i.e., $r_1=(e^2/16\pi kT)^{\frac{1}{2}}$. An adiabatic expansion of the chamber to a volume $(1+\epsilon)$ of the original volume reduces the vapor density to $\delta_\infty(\theta_1)/(1+\epsilon)$ and the temperature to

$$\theta_2=\theta_1(1+\epsilon)^{1-\gamma}, \quad (2)$$

and the droplet at its lower temperature grows until it is again in equilibrium with the surrounding vapor, a condition expressed by the equation

$$\delta_{r_2}(\theta_2)=\delta_\infty(\theta_1)/(1+\epsilon). \quad (3)$$

Here it is assumed that the time is long enough for the droplet to come into temperature equilibrium with the gas, but so short that no change other than that produced directly by the expansion occurs in the ambient vapor density. The radius of a droplet in equilibrium with the new conditions is found by solving Eq. (1) with the value of δ_r given by (3), and $\delta_\infty(\theta_2)$ equal to the vapor density in equilibrium with a flat surface at the temperature θ_2 of the expanded gas. Here it is convenient to represent the ratio of the saturated vapor densities at the two temperatures by the usual form of equation

$$\ln\left[\delta_\infty(\theta_1)/\delta_\infty(\theta_2)\right]=a(1/\theta_2-1/\theta_1),$$

and the resulting condition on r_2 may be written

$$2T/r_2-e^2/8\pi kr_2^4=(R\rho/M)\left[a(1-\theta_2/\theta_1)-\theta_2\ln(1+\epsilon)\right]. \quad (4)$$

If the value of r_2, thus determined, exceeds $r_{max}=e^2/4\pi kT$ at which δ_r in Eq. (1) has its maximum value, then the droplet can grow indefinitely and reach a visible size. With this value of r_2 inserted in (4) and expressing the temperatures in terms of the expansion ratio by (2), we find as the condition for the growth of large drops,

$$(1+\epsilon)^{1-\gamma}(a+\theta_1\ln(1+\epsilon))=a-(3M/R\rho)(\pi kT^4/2e^2)^{\frac{1}{2}}. \quad (5)$$

The constant a for water has the value 5330, that for *n*-propyl alcohol is 5700, and the constant for the mixture may be assumed to be about 5500. Consequently, the term in θ_1 is negligible, and ϵ is determined by

$$(1+\epsilon)^{1-\gamma}=1-(3M/R\rho a)(\pi kT^4/2e^2)^{\frac{1}{2}}. \quad (6)$$

With $M=39$ for the mixture, $\rho=0.9$, $\gamma=1.66$, and $k=1$, Eq. (6) gives values for T of 18.2 and 27.2 dynes per cm corresponding to the observed values 1.04 and 1.07 of $1+\epsilon$ at pressures of 110 and 1.5 atmospheres, respectively. The surface tension of *n*-propyl alcohol is given in the International Critical Tables as 23.8 at normal pressure and 20° C, but no data are given for this liquid when under high inert gas pressures. However, a lowering of surface tension by gas pressure of this order was found for ether and alcohol in atmospheres of air and hydrogen by Kundt.[3]

The understanding of this effect may lead to a better selection of gas and vapor for high pressure cloud chambers.

* This work was carried out at the Ballistic Research Laboratories, Aberdeen Proving Ground, Maryland.
[1] T. H. Johnson, S. De Benedetti, and R. P. Shutt, Rev. Sci. Inst. **14**, 265 (1943).
[2] Das Gupta and Ghosh, Rev. Mod. Phys. **18**, 225 (1946).
[3] A. Kundt, Ann. d. Physik **12**, 538 (1881).

Anomalous Values of Certain of the Fine Structure Lines in the Ammonia Microwave Spectrum

HARALD H. NIELSEN,
Mendenhall Laboratory of Physics, Ohio State University, Columbus, Ohio
AND
DAVID M. DENNISON
Randall Laboratory of Physics, University of Michigan, Ann Arbor, Michigan
June 4, 1947

RECENT measurements[1] have demonstrated that the fine structure lines in the ammonia microwave spectrum show certain anomalies. The lines arising from transitions between levels where $K=3$ are definitely displaced from the positions predicted for them by the empirical formula which has been constructed to fit the remainder of the lines. The lines arising when transitions occur between levels where $K=3$ and where J is an odd integer are displaced to the long wave-length side of the positions, while those due to transitions between levels where $K=3$ and where J is an even integer are displaced to the short wave-length side.

Qualitatively, the origin of this effect may readily be understood. It is well known that rotation levels where $K\neq 0$ are doubly degenerate. When $K\neq 0$, but is not a multiple of 3, these doubly degenerate levels belong to the mixed symmetry type[2] $\gamma\delta$ and they cannot be split apart by any perturbation possessing a threefold symmetry, that is, by any perturbation whose origin lies within the ammonia

molecule itself. When $K \neq 0$, and is a multiple of 3, the two originally superimposed levels belong to two symmetry classes[2,3] α and β. The first of these is symmetric for an interchange of two of the hydrogen nuclei, and the other is antisymmetric for such an interchange. The degeneracy of these levels may be removed by a perturbation which is threefold degenerate. Since the total wave function must be antisymmetric, and since the proton spin functions for three protons possesses no antisymmetric functions, of the two component rotation levels only one can actually occur. The order of the levels is inverted for the excited vibration level giving rise to the microwave spectrum. Thus, the line for $K=3$ will be displaced from its expected position. The direction in which the displacement takes place may be shown to depend upon the oddness or evenness of J.

We have examined the quantum-mechanical Hamiltonian for the ammonia molecule expanded in orders of magnitude and find that a splitting of the levels where $K=3$ occurs in the fourth order of approximation because of an interaction between the first-order Coriolis terms and first-order correction terms to the moments of inertia of the molecule. The constants which are involved are therefore only the usual potential constants together with the dimensions of the molecule and curiously enough do not depend to this approximation upon any anharmonicity in the motion. The displacements may be shown to be of the form

$$\Delta\nu = A F(J), \tag{1}$$

where A is a function of the molecular constants only, and $F(J)$ takes the values -1, 7, -28, 84, -210 for values of J from 3 to 7 inclusive. The numerical values may therefore be evaluated with an accuracy which we estimate to be of the order of 10 percent.

In Table I below are given, for various values of J, the shifts measured by Good and Coles of lines arising from transitions between levels where $K=3$ together with the values of these shifts predicted by the relation (1).

TABLE I. Measured and predicted values of the shifts of $K=3$ lines in the ammonia microwave spectrum.

J	K	Shifts as observed by Good and Coles (megacycles/second)	Predicted shifts (megacycles/second)
3	3	−0.30	−0.26
4	3	1.76	1.82
5	3	−7.17	−7.28
6	3	22.3	21.85
7	3	—	−54.62

The displacements where $K=6$ or higher are found to be exceedingly small. A full account of these calculations will appear in the near future.

[1] W. E. Good and D. K. Coles, Phys. Rev. 71, 383 (1947); M. W. P. Strandberg, R. Kyhl, T. Wentink, Jr., and R. E. Hilliger, Phys. Rev. 71, 639 (1947). We are also indebted to Dr. Good and Dr. Coles for a private communication giving numerical results which we shall quote in this letter.

[2] D. M. Dennison, Rev. Mod. Phys. 3, 280 (1931); see especially p. 341. These levels are also said to belong to the symmetry species E. See, for example, G. Herzberg, *Infrared and Raman Spectra* (D. Van Nostand Company, New York, 1945), p. 27.

[3] These levels are also said to belong to the symmetry species A_1 and A_2, respectively.

Propagation of U. H. F. Sound in Mercury

G. R. RINGO, J. W. FITZGERALD* AND B. G. HURDLE
U. S. Naval Research Laboratory, Washington, D. C.
May 16, 1947

MEASUREMENTS have been made of the velocity and attenuation of sound in Hg in the frequency range 100 to 1000 Mc/sec. The electroacoustic transducers used were two identical x-cut quartz crystal disks 0.038 cm thick and 2 cm in diameter. These crystal disks were each cemented on one face across the end of a 50-ohm coaxial line. They were then mounted facing each other in an Hg bath which served simultaneously as: (a) one electrode of each crystal, (b) an acoustic transmission medium, and (c) an electrical shield between the transmitting and receiving crystals.

By means of a micrometer adjustment the separation of the crystals could be varied. In order to obtain separations of the crystals as small as 0.05 cm, which was necessary at the two highest frequencies used, a grid of 0.025-cm diameter silver wires was placed between the crystals to prevent the Hg film from breaking and withdrawing from between the crystals. In addition, in order to insure that the Hg would wet the quartz crystals, the face of each crystal to be immersed in the Hg was coated with an evaporated film of silver before being placed in the bath. These precautions, of course, caused some contamination of the Hg, but the amount (less than 0.1 percent) probably did not affect the measurements.

Conventional transmitters of 50–100 watts power output were used to excite the transmitting crystal through its 50-ohm line, and conventional receivers were used to amplify the output of the receiving crystal. By use of modulated continuous-wave excitation, the band width of the receiving system was held to about 200 cycles/sec. The sound wave was detected by the familiar method of combining the output of the receiving crystal with a direct signal from the transmitter and then changing the separation of the crystals. This change in the separation changed the phase of the acoustic wave incident on the receiving crystal and gave rise to variations in the output of the receiver which approximately repeated as the separation of the crystals was changed by multiples of the acoustic wave-length in Hg. In order to detect sound at the highest frequency used, it was necessary to record the output of the receiver on a recorder driven synchronously with the micrometer controlling the crystal separation.

The attenuation was measured by noting the change in the amplitude of the variations of the receiver output as

TABLE I. Data on propagation of sound in Hg.

Frequency in Mc/sec.	Velocity $\times 10^{-5}$ in cm/sec.	Frequency-free pressure absorption coefficient $\times 10^{17}$ in sec.^{2}/cm	Temperature °C
0.50[1]	1.451		20
21.5[2]		6.3	24.3
54.0[2]		6.4	24.3
152	1.449 ±0.002	5.8 ±0.5	23.8
291	1.451 ±0.002	5.5 ±0.5	24.0
390	1.450 ±0.002	5.7 ±0.5	28.2
774	1.47 ±0.02	4.7 ±1.0	27.2
996	1.44 ±0.05	6.0 ±1.0	26.9

the separation of the crystals was changed by many acoustic wave-lengths. In these attenuation measurements the direct signal from the transmitter was kept constant at a level above that of the highest output of the receiving crystal. Standing wave effects were not important in these measurements because the sound absorption was so high at the frequencies used.

The results of these measurements are summarized in Table I, which also shows some of the results obtained by earlier workers. Attenuation is ascribed entirely to absorption, largely on the grounds that the frequency-free attenuation coefficient (i.e., the attenuation coefficient divided by the square of the frequency) is very near the value of the frequency-free absorption coefficient given by the Stokes–Kirchoff formula, which is 5.1 for Hg. The data show no significant change in velocity or frequency-free absorption coefficient with frequency.

It is planned to extend this work to higher frequencies and to fluids other than Hg.

* Now at Engineering Research Associates, Inc., Washington, D. C.
[1] J. C. Hubbard and A. L. Loomis, Phil. Mag. **5**, 1177 (1928).
[2] P. Rieckmann, Physik. Zeits. **40**, 582 (1939).

The Fission Cross Section of Np^{237}*

ERNEST D. KLEMA[1]
University of California, Los Alamos Scientific Laboratory, Santa Fe, New Mexico
May 28, 1947

THE fission cross section of Np^{237} has been measured for neutrons of energies from near thermal to 3 Mev by counting simultaneously the fissions from known foils of Np^{237} and U^{235}, placed back to back in a parallel-plate comparison chamber filled with pure argon.[2]

The source of monoenergetic neutrons in the energy range from near thermal to 1.67 Mev was the Wisconsin electrostatic generator, using the $Li^7(p, n)Be^7$ reaction with a Li target 60 kev thick. The 2.5-Mev and 3.0-Mev points were taken with the Illinois Cockcroft-Walton set, using the $D-D$ reaction with a thick heavy-ice target and an accelerating voltage of 200 kev.

The Np^{237} foil was prepared from material purified and analyzed by the Chicago Metallurgical Laboratory groups. According to the analysis furnished us, the 1N sulfuric acid solution contained 100 micrograms of Np^{237} metal, about 0.05 microgram of Pu^{239} metal, and 50 micrograms of potassium as bisulfate. The solution was deposited in drops on a platinum foil by means of a micropipette and evaporated. Care was taken to transfer all the material in the solution to the foil, and the Np^{237} mass was taken as 100 micrograms.

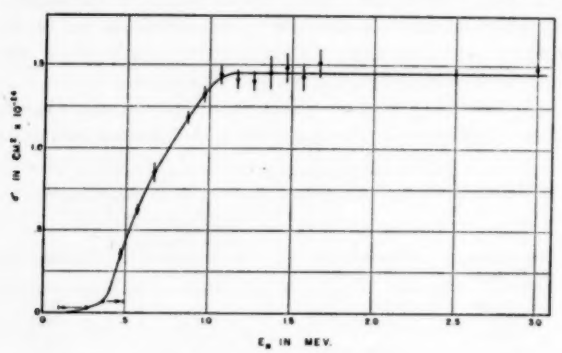

FIG. 1. The fission cross section of Np^{237} as a function of the incident neutron energy. The errors given are the statistical errors of counting. Because the errors of the two lowest energy points are so small, they have been drawn to the side and are the vertical lines at the heads of the horizontal arrows.

Figure 1 gives the fission cross section of Np^{237} as a function of the incident neutron energy. For each point the statistical error of counting is given. For the points obtained with the electrostatic generator, the cross sections are given for the average neutron energy in each case. A correction was made for the Pu^{239} in the Np^{237} foil for the 270- and 370-kev points.

A point was taken with the electrostatic generator with a maximum primary neutron energy of 150 kev and a block of paraffin about $1\frac{1}{4}$ inch thick between the target and the comparison chamber. Using the ratio of cross sections of U^{235} and Pu^{239} at near thermal energy, and assuming the Np^{237} foil to contain 0.05 percent Pu^{239} by weight, the fissions from the Np^{237} foil obtained by this means can be more than accounted for by the fission of Pu^{239} in this foil. Thus no thermal fission was observed in Np^{237} within the accuracy of this experiment.

The cross sections given here for Np^{237} are based on the fission cross sections of U^{235}, U^{238}, and Pu^{239} as measured at Los Alamos.

* This paper is based on work performed under Contract No. W-7405-Eng-36 with the Manhattan Project at the Los Alamos Scientific Laboratory of the University of California.
[1] Now at the University of Illinois.
[2] Work on the relative cross section as a function of energy was carried out at Los Alamos by D. H. Frisch and K. Greisen prior to the measurements reported here.

Solar Magnetic Field and Diurnal Variation of Cosmic Radiation

H. ALFVÉN
Department of Electronics, The Royal Institute of Technology, Stockholm, Sweden
June 4, 1947

THE effect of the solar magnetic field on the cosmic radiation, according to the Störmer theory, is that particles below a certain momentum $P_1=(a/r^2)(3-2\sqrt{2})$ (a = sun's moment, r = distance sun-earth) cannot reach the earth at all, whereas particles above a certain momentum $P_2=a/r^2$ can reach it from any direction. For momenta between P_1 and P_2 some orbits intersecting the earth's surface come from infinity, whereas others are periodic (or quasi-periodic) in the solar magnetic field. In the theory of the influence of the solar magnetic field on cosmic radiation proposed by Jánossy[1] and further developed by Vallarta,[2] Epstein,[3] and Rossi,[4] it is tacitly assumed that the asymptotic orbits possess full intensity whereas no particles move in periodic orbits.

This is not certain, however, because particles may be *scattered* from the asymptotic into the periodic orbits. Interplanetary dust, and also the electric fields associated with magnetic disturbances,[5] may produce scattering, but

probably the most effective source is the magnetic field of the earth. In order to be scattered considerably a particle must approach the earth so closely that its radius of curvature, ρ, in the terrestrial magnetic field, H, is of the same order as the distance R to the earth's magnetic dipole (moment $=A$). If P is the momentum of the particle we have

$$R \approx \rho = P/H \approx PR^3/A,$$

or

$$R^2 \approx A/P.$$

For $P=10^7$ gauss-cm (corresponding to $3\cdot10^9$ ev for electrons), and with $A=8\cdot10^{25}$ gauss-cm^3, we find for the scattering cross sections of the terrestrial magnetic field

$$S=\pi R^2=2.5\cdot10^{19}\ \text{cm}^2.$$

If cosmic radiation is leaking with the velocity c through this "hole" in the screen of the solar magnetic field, the volume τ inside the "screen" will be filled after the time

$$T=\tau/Sc.$$

Putting $\tau \approx r^3$ (r = orbital radius of the earth) we find

$$T=0.5\cdot10^{10}\ \text{sec}.$$

The number of particles in the periodic orbits is determined by the absorption in interplanetary matter during this time. If the density is ρ g/cm^3, the matter which the radiation passes in the time T is $D=cT\rho=1.5\cdot10^{20}\ \rho$ g/cm^2. According to Baumbach[6] the density in the outer corona is $\sim10^{-19}$ g/cm^3, and in interplanetary space the density must be much less. Consequently D is probably less than 1 g/cm^2, so that the absorption is small.

This seems to indicate that for momenta above P_1 cosmic rays reach the earth from all directions. Below P_1 all directions are forbidden unless scattering by the outer planets or other causes cause some of the weaker radiation to leak in.

Hence theoretically the solar magnetic field is not likely to produce a diurnal variation. Through a study of the trajectories, Malmfors[7] has shown that the observed solar time variations cannot be due to the solar magnetic field.

[1] L. Jánossy, Zeits f. Physik **104**, 430 (1937).
[2] M. S. Vallarta, Nature **139**, 839 (1937).
[3] P. S. Epstein, Phys. Rev. **53**, 862 (1938).
[4] B. Rossi, Cosmic Ray Conference, New York, April 10, 1947.
[5] H. Alfvén, Nature **158**, 618 (1946).
[6] S. Baumbach, Astro. Nachr. **263**, 121 (1937).
[7] K. G. Malmfors, Ark. f. mat., astr. o. fysik **32** [A], No. 8 (1945).

The Magnetic Threshold Curves of Superconductors

JOHN G. DAUNT
Mendenhall Laboratory of Physics, Ohio State University, Columbus, Ohio
May 24, 1947

IN a recent letter Stout[1] has ably summed up the evidence in favor of assuming that the magnetic threshold curves of superconductors are approximately parabolic functions of temperature, a suggestion that was put forward by Kok.[2] He has pointed out that a three-halves power function, as has been suggested recently by Sienko and Ogg,[3] cannot be supported by known magnetic or calorimetric data.

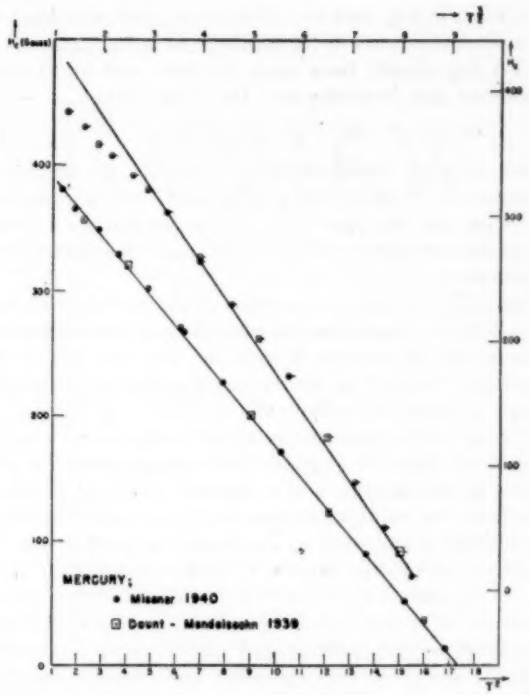

FIG. 1. The variation with temperature of the magnetic threshold of mercury.

As is well known, the magnetic transition of a superconductor is strongly dependent on small chemical or physical impurities. The significance of the latter effect has been emphasized recently by the experiments of Lasarew and Galkin[4] on tin specimens subjected to anisotropic stress. In view of these impurity effects, considerable care must be taken in assessing the magnetic measurements on various superconductors. Probably the material with the highest purity and smallest strain is mercury, as measured by Daunt and Mendelssohn[5] and by Misener,[6] the magnetic transition of which was found by these independent workers to agree within one percent. The temperature variation of the magnetic threshold field, H_c, in mercury, therefore, is given in Fig. 1. The lower curve plots H_c against T^2, which for a parabolic function should be a straight line. It will be seen that the measured points do not deviate from the straight line by more than ±4 gausses, a variation which, for the higher fields, is probably covered by the experimental error. The upper curve shows H_c plotted against $T^{\frac{1}{2}}$, which according to Sienko and Ogg[3] should be a straight line. It will readily be seen that the deviations of the measured points from a straight line are too systematic and too large to be covered by experimental error.

Similar curves have also been drawn up for other superconductors and all show that the $T^{\frac{1}{2}}$ function is the more unsatisfactory.

The immediate significance that can be attached to an exact formulation of the magnetic threshold curve is two-

fold. First, it may lead to a satisfactory generalization for all superconductors. For the parabolic form, such a generalization has already been made by Kok[2] and by Daunt, Horseman, and Mendelssohn.[7] The result is that

$$H_0/T_c\gamma^{\frac{1}{2}}=(2\pi/V)^{\frac{1}{2}}, \tag{1}$$

where H_0 is the threshold field at $T=0$, T_c the transition temperature, V the atomic volume, and γ the Sommerfeld electronic specific heat term[8] of the normal state. This generalization seems to be in satisfactory agreement with experiment.

Secondly, an exact formulation of the threshold curves may lead to a method of assessing the variation with temperature of the number of electrons that can partake in superflow. Although in the absence of a satisfactory atomic theory of superconductivity the method to be adopted is not clear, some comment on recent experimental results may be of value. H. London,[9] from measurements on the depth on penetration, δ, of a magnetic field into a superconductor and on high frequency resistance, concluded that the number of electrons, n_s, partaking in superflow may be expressed as a power series in T, with a predominant term in T^2. The variation of n_s with T, as calculated from measurements of δ, however, is very sensitive to the assumed magnitude of δ at absolute zero; and, since the latter can only be estimated with difficulty, these results must be taken with reserve. Recent measurements by Désirant and Shoenberg[10] on δ for mercury allow a new evaluation of n_s to be made, if the relation between n_s and δ as given by the theory of F. and H. London[11] is assumed. Such an evaluation has been made by the writer, yielding a function in T^3, i.e.,

$$n_s=n_0[1-(T/T_c)^3], \tag{2}$$

where T_c is the transition temperature.

Owing to the divergent results quoted above, and to the somewhat arbitrary nature of the assumptions by which they have been deduced, one may conclude that more data are required. It has been pointed out elsewhere[12] that the threshold curves, giving the maximum current density permissible at any given temperature on the surface of a superconductor, are analogous to the rate-of-flow curve for superflow in helium II[13], and the hypothesis was put forward that they both represent the variation in the number of particles partaking in superflow. Such a hypothesis has received some support on theoretical grounds,[14] and in the case of helium II the recent measurement by Andronikashvilli[15] on the number of superfluid particles gives direct experimental support to it. It would be of value to have similar detailed experimental evidence for superconductivity.

[1] J. W. Stout, Phys. Rev. **71**, 741 (1947).
[2] J. A. Kok, Physica **1**, 1103 (1934).
[3] M. J. Sienko and R. A. Ogg, Phys. Rev. **71**, 319 (1947).
[4] B. Lasarew and A. Galkin, J. Phys. U.S.S.R. **8**, 376 (1944).
[5] J. G. Daunt and K. Mendelssohn, Proc. Roy. Soc. **A160**, 127 (1937).
[6] A. D. Misener, Proc. Roy. Soc. **A174**, 262 (1940).
[7] J. G. Daunt, A. Horseman, and K. Mendelssohn, Phil. Mag. **27**, 754 (1939).
[8] A. Sommerfeld, Zeits. f. Physik. **47**, 1 (1928).
[9] H. London, Proc. Roy. Soc. **A176**, 522 (1940); see also E. T. S. Appleyard, J. R. Briston, H. London, and A. D. Misener, Proc. Roy. Soc. **A172**, 540 (1939).
[10] M. Désirant and D. Shoenberg, Nature **159**, 201 (1947).
[11] F. London and H. London, Proc. Roy. Soc. **A149**, 71 (1935).
[12] J. G. Daunt and K. Mendelssohn, Nature **150**, 604 (1942).
[13] J. G. Daunt and K. Mendelssohn, Proc. Roy. Soc. **A170**, 439 (1939).
[14] F. London, Rev. Mod. Phys. **17**, 310 (1945); K. Mendelssohn, Proc. Phys. Soc. **57**, 371 (1945); J. G. Daunt and K. Mendelssohn, Phys. Rev. **69**, 126 (1946).
[15] E. Andronikashvilli, J. Phys. U.S.S.R. **10**, 201 (1946).